Standard Manoeuvres Simulation of a Fishing Vessel

Krzysztof Patalong

Master Thesis

presented in partial fulfillment
of the requirements for the double degree:
"Advanced Master in Naval Architecture" conferred by University of Liège
"Master of Sciences in Applied Mechanics, specialization in Hydrodynamics,
Energetics and Propulsion" conferred by Ecole Centrale de Nantes

developed at "Dunărea de Jos" University, Galaţi
in the framework of the

"EMSHIP"
Erasmus Mundus Master Course
in "Integrated Advanced Ship Design"

Ref. 159652-1-2009-1-BE-ERA MUNDUS-EMMC

Supervisor: Prof. Dr. Ing. Dan Obreja

Reviewer: Prof. Dr. Ing. Marco Ferrando

Galaţi, February 2012

This page intentionally left blank

ABSTRACT

Standard Manoeuvres Simulation of a Fishing Vessel

By **Krzysztof Patalong**

Fishing at sea has been known for many years as one of the most dangerous occupations in the world. According to IMO statistical data (1999), over 24,000 lives are lost world-wide every year during fishing operation as the vessels would often operate in the most harsh conditions in the open sea. For this reason, the safety of their operation and performance should be circumstantially examined.

In this thesis, the manoeuvring performance of a typical Mediterranean Sea fishing vessel is investigated. The obtained results should provide some new valuable hydrodynamic information into the common database of existing hullforms, since a rather complex and uncommon hull shape with a double hard chine and inclined bar keel puts this vessel out of the range of typical forms. Additionally, due to her moderately small length, the vessel operates at fairly high Froude number, making the investigation even more challenging.

The main steps undertaken in order to achieve the goal of the thesis consist of: design of a rudder geometry, estimation of the hydrodynamic forces and moments generated on the rudder in order to determine the position and diameter of the rudder stock, preliminary checking of the rudder cavitation and estimation of the manoeuvring performance by means of the preliminary methods (based on regression formulas and linear hydrodynamic models) as well as simulation codes based on non-linear hydrodynamic models.

In order to resolve above-mentioned problems, the following investigation methods are used:

- Voitkounsky method (1985), in correspondence with PHP Galati University program (Preliminary Hydrodynamics Performance), to preliminary estimate the hydrodynamic forces and moments on the rudder as well as the position of the rudder stock;
- CFD methods and ShipFlow code, with non-zero drift angles and rudder deflection applied, to determine the hydrodynamic forces and moments acting on the hull and on the rudder;
- Brix method (1993) to verify the rudder cavitation (with the use of PHP code);
- Clarke (1982) regression empirical formulae and linear mathematical models in correspondence with MPP Michigan University program, to estimate the characteristics of the turning circle and the dynamic stability parameter;
- Non-linear mathematical models applied in the PHP code (Abkowitz model, 1964) and TRIBON commercial software, in order to simulate the standard manoeuvres in time-domain (turning circle, zig-zag test and spiral manoeuvre) and to determine the vessel's manoeuvring performance.

Finally, the similarities between obtained numerical and provided experimental results are examined with the following observations and conclusions derived:

- Existing preliminary codes based on empirical formulas and linear mathematical models should be used, with fair attention paid to, only in the initial design stage of a vessel;
- Time-domain simulation codes based on non-linear mathematical models, hence providing more accurate manoeuvring performance characteristics, can be used in the basic design stage, simultaneously with the CFD codes and/or experimental tests, in order to determine the hydrodynamic derivatives of a given vessel.

ACKNOWLEDGEMENTS

First of all, I would like to express my sincere appreciation and gratitude to my Mum and Dad for their love and support, not only during this Master Course, but throughout my whole life. I am so lucky to be their son and to them I dedicate this thesis.

Secondly, my heartfelt thanks go to M.M. Without her love, patience, understanding and constant support, it would have been impossible to finish this Course.

I am also grateful indeed to my supervisor, prof. Dan Obreja (from UGAL), for welcoming me in any occasion in his office and guiding through the challenging, but compelling aspects of ship hydrodynamics and manoeuvring.

I am also obliged to prof. Adrian Lungu, Florin Pacuraru, Oana Marcu and all the academic and PhD staff at the Naval Faculty of UGAL for their constant assistance and support in my first steps in Computational Fluid Dynamics. It was a real pleasure to work with them.

Additionally, I owe a great deal to prof. Lungu (the Dean of the Naval Faculty at UGAL) for providing me with excellent working environment.

Many thanks to the EMSHIP Consortium for giving me the opportunity to participate in the Course.

Special thanks to Audrey Mélotte (from the International Office of ULg) for welcoming me anytime and helping in every situation during my studies.

Finally, I would like to express my gratefulness to my colleagues of the EMSHIP Course. It was an honor for me to meet them and I am really thankful for their help, support as well as the good times we had together during the Course. They are all very special to me and I hope we would stay in touch throughout all our lives.

TABLE OF CONTENTS:

List of Figures:

List of Tables:

Declaration of Authorship

I declare that this thesis and the work presented in it are my own and have been generated by me as the result of my own original research.

Where I have consulted the published work of others, this is always clearly attributed.

Where I have quoted from the work of others, the source is always given. With the exception of such quotations, this thesis is entirely my own work.

I have acknowledged all main sources of help.
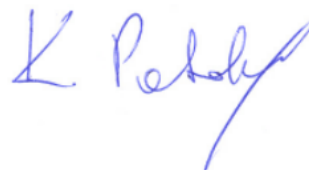
Where the thesis is based on work done by myself jointly with others, I have made clear exactly what was done by others and what I have contributed myself.

This thesis contains no material that has been submitted previously, in whole or in part, for the award of any other academic degree or diploma.

I cede copyright of the thesis in favour of the "Dunărea de Jos" University of Galati, University of Liège and Ecole Centrale de Nantes

24.02.2012　　　　*Krzysztof Patalong*

1. INTRODUCTION

Fisheries sector contributes significantly to the economy of many countries and provides employment opportunities to thousands of people. FAO[1] statistics (2004) reveal that roughly 30 million fishers are working aboard 4 million fishing vessels operating in capture fisheries, 1.3 million decked and 2.7 million undecked vessels. For this reason, designing a ship with a good hydrodynamic performance that would allow the safe operation in a given environmental condition should be the main aim of the naval architect.

For conventional ships (including the fishing vessels), the course-keeping and manoeuvring characteristics often tend to work against each other: an easy-turning ship would be difficult to keep on course whereas course-stable ship might be hard to turn. However, a practical compromise between those two features is usually possible to be applied. But before it could be implemented, it first needs to be found.

There exist several different techniques and tools allowing the naval architect to design a ship with an optimum hydrodynamic performance allowing safe operations in a certain environmental conditions. Since designing a ship is a long-lasting iterative process, it is very important for the designer to use the powerful and reliable hydrodynamic tools allowing the investigation of the ship performance at sea from the initial design stage.

Some of the tools are based on comparison of the vessel's characteristics with the earlier successful designs. They can be referred to as statistical methods. Other methods may consist of experimental techniques, theoretical analyses, simple empirical or semi-empirical formulas up to complex manoeuvring simulation models containing sets of non-linear differential equations covering three (or more) degrees of motion freedom. Additionally, the CFD-based simulation codes are becoming more polular and widely-used.

In general, use of data bases would be reliable only for a standard forms of the hull, stern-propeller-rudder configurations, size of rudder etc., and could not be extrapolated to a new design concepts. The empirical relations, derived by means of regression analysis which correlated the manoevrability performance of the existing ships with their main dimensions [Lyster, 1979; Norrby, 1972], result to be highly imprecise, especially for the new and unusual hullforms. On the other hand, model tests are inappropriate

---

[1] The Food and Agriculture Organization of the United Nations (FAO) – a specialized agency of the United Nations leading the international efforts to defeat hunger among people all over the world.

at the initial stages of design due to the high cost of preparation of the model as well as long time of execution of the tests. Additionally, since usually an extensive number of conditions have to be tested with large number of hull concepts, the model tests become even more costly and time consuming. To add to this, scaling relations are often not precisely known or are based upon very limited data. For all the above reasons, the initial computer simulations should be performed in order to establish the optimal dimensions of the designed concept and to avoid running the tests with undesirable model configurations. Moreover, when providing reliable results, simulations can be complementary used by the governmental authorities (e.g. IMO) for the judgment of the ship's safety, by harbor authorities while verifying the port design, operations, traffic system and scope of manoeuvrability in the confined areas, as well as training tool for the sea-going crew.

The main goal of this thesis is to investigate the manoeuvring performance of a typical Mediterranean Sea fishing vessel. To do so, three standard manoeuvres (turning circle, zig-zag manouvre and spiral test) are simulated using both commercial and university-developed simulation programs. Subsequently, the accuracy and reliability of these programs is evaluated by comparing the numerical results with the data obtained during the experimental campaign (Obreja, 2001). Additionally, the optimum geometry of the rudder is designed, together with the calculation and selection of a steering gear, as well as verification of the proposed rudder cavitation risk.

In the final part of the thesis the CFD techniques are applied to estimate the hydrodynamic forces and moments acting on the hull as well as on the designed rudder.

The detailed structure of the thesis can be described as follows:

Chapter 1 highlights the main goal of the thesis and the main steps undertaken to accomplish this objective.

Chapter 2 introduces the mathematical models applied in ship manoeuvring performance estimation as well as explains the theoretical preliminary methods of hydrodynamic derivatives prediction.

Chapter 3 presents the standard manoeuvres of the vessel as well as describes the main methods of estimating the standard manoeuvring parameters and correlated with them IMO requirements and limits.

Chapter 4 consists of theoretical explanation of hydrodynamic behavior of a passive control surface.

In Chapter 5 the main characteristics of the investigated vessel are presented. Additionally, the design of the rudder and the analysis of its hydrodynamic performance and cavitation risk are performed. Finally, the optimal steering device for the proposed rudder is chosen from the commercial catalogue.

Chapter 6 refers to the hydrostatic verification of the given loading condition.

The aim of Chapter 7 is to estimate the manoeuvrability performance of the ship in the initial design stage by means of tools commonly used by naval architects. The accuracy and reliability of these tools for hydrodynamic prediction of the unusual hullforms is subsequently evaluated.

Chapter 8 presents the standard manoeuvres results obtained with a use of a time-domain simulation code. The main numerical parameters of these manoeuvres are then compared with the experimental data and results obtained with the initial design programs. Additionally, the hydrodynamic derivatives of the fishing vessel are estimated and the verification of their influence on the standard manoeuvres parameters is subsequently analyzed.

The computation of the hydrodynamic forces based on the CFD techniques is presented in Chapter 9. The vessel's resistance computation, subsequently compared with experimental data and results obtained by means of commonly-used empirical formulas, is performed on the basis of potential flow theory. The hydrodynamic forces in oblique flow are computed by use of the Reynolds-averaged Navier-Stokes equations. Different drift and rudder deflection angles are applied in these simulations, resulting in a total number of 21 computational cases.

Chapter 10 consists of a final conclusions on different aspects of the manoeuvrability prediction of the investigated fishing vessel.

Additionally, two appendices are attached to the thesis. Appendix 1 provides an extensive description of the steering gear selected from a commercial catalogue, whereas Appendix 2 presents a detailed parameters of the standard manoeuvres obtained by means of the university-developed simulation code.

2. NONLINEAR MATHEMATICAL MODEL OF THE SHIP MANOEUVRABILITY

2.1. ABKOWITZ'S MODEL

2.1.1. Equations of Motion for a Body Moving with Six Degrees of Freedom

Thanks to many researchers of the past decades, the hydrodynamic phenomena of ship motion as well as forces and moments acting on the vessel when performing maneuvers can be represented these days by a suitable mathematical models.

Mathematical models are very common and widely used in many disciplines, including, but not limited to, natural and social sciences, engineering disciplines etc., and can take various forms. These models simply describe a certain system by means of mathematical concepts and language. Eykhoff (1974) defined a mathematical model as "a representation of the essential aspects of an existing system (or a system to be constructed) which presents knowledge of that system in usable form".

The assessment of the manoeuvrability performance at the initial design stage of the vessel requires a reliable mathematical description of the manoeuvring motion of the ship. For this reason, many mathematical models have been developed in the recent decades. One of them, commonly used to simulate the standard manoeuvres of a vessel, has been proposed by a former professor and director of MIT Ship Model Towing Tank, as well as a Life Member of SNAME and regular participant in the ITTC, prof. dr. M.A. Abkowitz.

In this model, providing the equations of motion for a moving body with six degrees of freedom, the following conventions have been applied:

- right-handed earth-located coordinate system $O_0x_0y_0z_0$;
- right-handed coordinate system $Oxyz$ fixed on the moving rigid body;
- the origin of the coordinate system placed on the midship section;
- the longitudinal *x-axis*, positive forward, coincides with the centerline plane and is parallel to the keel and/or still water plane;
- the transverse *y-axis*, positive to starboard, is perpendicular to the plane of symmetry;
- the vertical *z-axis*, positive downwards, is perpendicular to the still water plane;
- the heading angle (yaw angle) ψ between the ship's centerline and x_0-*axis*;

- the drift angle (angle of attack) β between the ship's centerline and the velocity vector;

- the angle of the rudder deflection (rudder angle) δ;

- the velocity vector $\overline{v_0}$ tangential to the CG path of the ship in the origin.

Having the coordinate systems established [Fig. 1], one can define the ship's rotation motions as follows (looking forward from the ship bridge):

- roll motion about the *x-axis* is considered positive clockwise;

- pitch motion about the *y-axis* is considered positive bow-up;

- yaw motion about the *z-axis* is considered positive turning-starboard.
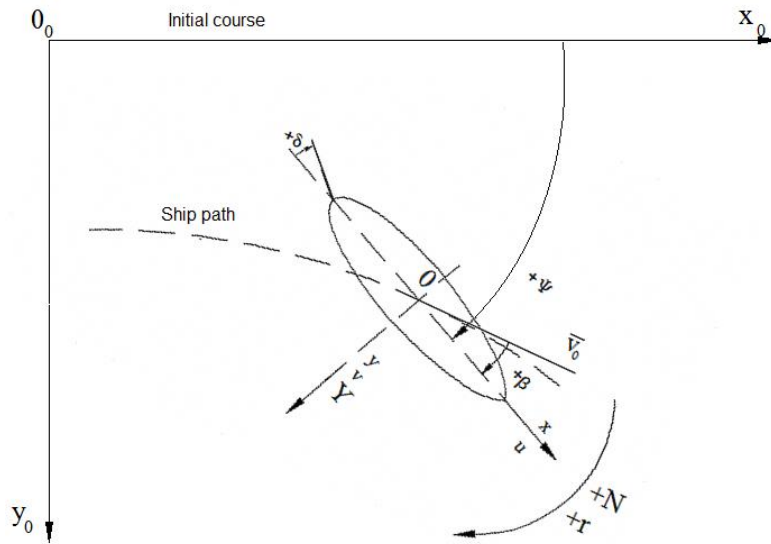
Fig. 1. Adopted axial systems

Additionally, the following notation complying with SNAME [1950] have been introduced [Table 1]:

Table 1. The notation of SNAME for marine vessels

DOF		Force / Moment	Linear/Angular velocity	Position / Eulers angles
1	surge	X	u	x
2	sway	Y	v	y
3	heave	Z	w	z
4	roll	K	p	ϕ
5	pitch	M	q	θ
6	yaw	N	r	ψ

A rigid body dynamics with six degrees of freedom is based on two fundamental theorem: the linear momentum and the angular momentum [9].

The linear momentum theorem states that:

$$\sum_{i=1}^{N} \overline{F_i} = \sum_{i=1}^{N} \frac{d}{dt}\left(m_i \cdot \overline{v_i}\right) \tag{1}$$

with m_i being the mass of a small particle; $\overline{v_i}$ the speed and $\overline{F_i}$ the external force acting on the particle.

Accordingly, the angular momentum theorem implies that:

$$\sum_{i=1}^{N}\left(\overline{M}_i + \overline{r_i} \times \overline{F_i}\right) = \sum_{i=1}^{N} \overline{r_i} \times \frac{d}{dt}\left(m_i \cdot \overline{v_i}\right) \tag{2}$$

where $\overline{M}_i$ is the external moment acting on the particle i and $\overline{r_i}$ is the body-referenced radius vector.

Indicating $\overline{v_0}$ as the ship speed in the origin of the coordinate system and $\overline{\omega}$ as the angular speed, the total speed of the vessel can be expressed as:

$$\overline{v_i} = \overline{v_0} + \overline{\omega} \times \overline{r_i} \tag{3}$$

Using the above relation (3), equation (1) can be written as:

$$\sum_{i=1}^{N} F_i = \sum_{i=1}^{N} \frac{d}{dt}\left[m_i \cdot \left(\overline{v_0} + \overline{\omega} \times \overline{r_i}\right)\right] = m \cdot \frac{\partial \overline{v_0}}{\partial t} + \frac{d}{dt}\left(\overline{\omega} \times \sum_{i=1}^{N} m_i \cdot \overline{r_i}\right) \tag{4}$$

where $m = \sum_{i=1}^{N} m_i$ is the total mass of the ship.

Subsequently, defining the center of gravity vector $\overline{r_G}$ as:

$$m \cdot \overline{r_G} = \sum_{i=1}^{N}\left(m_i \cdot \overline{r_i}\right) \tag{5}$$

and accepting the following conventions:

$$\overline{r}_G = x_G \cdot \overline{i} + y_G \cdot \overline{j} + z_G \cdot \overline{k}$$
$$\overline{v}_0 = u \cdot \overline{i} + v \cdot \overline{j} + w \cdot \overline{k}$$
$$\overline{\omega} = p \cdot \overline{i} + q \cdot \overline{j} + r \cdot \overline{k} \qquad (6)$$
$$\overline{F} = X \cdot \overline{i} + Y \cdot \overline{j} + Z \cdot \overline{k}$$

one can continue the development of the equations obtaining finally three linear momentum equations (with $\overline{r}_G \neq 0$):

$$X = m \cdot \left[\frac{\partial u}{\partial t} + qw - rv + \frac{dq}{dt} z_G - \frac{dr}{dt} y_G + (qy_G + rz_G) p - (q^2 + r^2) x_G \right]$$

$$Y = m \cdot \left[\frac{\partial v}{\partial t} + ru - pw + \frac{dr}{dt} x_G - \frac{dp}{dt} z_G + (rz_G + px_G) q - (r^2 + p^2) y_G \right] \qquad (7)$$

$$Z = m \cdot \left[\frac{\partial w}{\partial t} + pv - qu + \frac{dp}{dt} y_G - \frac{dq}{dt} x_G + (px_G + qy_G) r - (p^2 + q^2) z_G \right]$$

Similar development of equations can be performed for the angular momentum theorem. Employing the definitions of moments of inertia:

$$I = \begin{vmatrix} I_{xx} & I_{xy} & I_{xz} \\ I_{yx} & I_{yy} & I_{yz} \\ I_{zx} & I_{zy} & I_{zz} \end{vmatrix} \qquad (8)$$

$$I_{xx} = \sum_{i=1}^{N} m_i \left(y_i^2 + z_i^2 \right)$$

$$I_{yy} = \sum_{i=1}^{N} m_i \left(x_i^2 + z_i^2 \right)$$

$$I_{zz} = \sum_{i=1}^{N} m_i \left(x_i^2 + y_i^2 \right)$$

$$I_{xy} = I_{yx} = -\sum_{i=1}^{N} m_i x_i y_i$$

$$I_{xz} = I_{zx} = -\sum_{i=1}^{N} m_i x_i z_i$$

$$I_{yz} = I_{zy} = -\sum_{i=1}^{N} m_i y_i z_i$$

and performing some logical transformations of equations, the complete momentum equations can be obtained as follows:

$$
\begin{aligned}
K = {} & \frac{\partial p}{\partial t} I_{xx} + \frac{\partial q}{\partial t} I_{xy} + \frac{\partial r}{\partial t} I_{xz} + \\
& + rq\left(I_{zz} - I_{yy}\right) + \left(q^2 - r^2\right) I_{yz} + pqI_{xz} - prI_{xy} + \\
& + m\left[y_G\left(\frac{\partial w}{\partial t} + pv - qu\right) - z_G\left(\frac{\partial v}{\partial t} + ru - pw\right)\right]
\end{aligned}
$$

$$
\begin{aligned}
M = {} & \frac{\partial p}{\partial t} I_{yx} + \frac{\partial q}{\partial t} I_{yy} + \frac{\partial r}{\partial t} I_{yz} + \\
& + pr\left(I_{xx} - I_{zz}\right) + \left(r^2 - p^2\right) I_{xz} + qrI_{xy} - qpI_{yz} + \\
& + m\left[z_G\left(\frac{\partial u}{\partial t} + qw - rv\right) - x_G\left(\frac{\partial w}{\partial t} + pv - qu\right)\right]
\end{aligned} \tag{9}
$$

$$
\begin{aligned}
N = {} & \frac{\partial p}{\partial t} I_{zx} + \frac{\partial q}{\partial t} I_{zy} + \frac{\partial r}{\partial t} I_{zz} + \\
& + pq\left(I_{yy} - I_{xx}\right) + \left(p^2 - q^2\right) I_{xy} + prI_{yz} - qrI_{xz} + \\
& + m\left[x_G\left(\frac{\partial v}{\partial t} + ru - pw\right) - y_G\left(\frac{\partial u}{\partial t} + qw - rv\right)\right]
\end{aligned}
$$

Finally, neglecting the cross-inertia terms and considering $\overline{r_G} = 0$, equations (7) and (9) become:

$$
X = m\left(\frac{\partial u}{\partial t} + qw - rv\right)
$$

$$
Y = m\left(\frac{\partial v}{\partial t} + ru - pw\right) \tag{10}
$$

$$
Z = m\left(\frac{\partial w}{\partial t} + pv - qu\right)
$$

$$
K = \frac{\partial p}{\partial t} I_{xx} + rq\left(I_{zz} - I_{yy}\right)
$$

$$
M = \frac{\partial q}{\partial t} I_{yy} + pr\left(I_{zz} - I_{zz}\right) \tag{11}
$$

$$
N = \frac{\partial r}{\partial t} I_{zz} + pq\left(I_{yy} - I_{xx}\right)
$$

However, as most of the ships can be assumed to be symmetric about the *x-z plane*, then:

$$y_G = 0$$

$$w = 0 \qquad (12)$$

$$q = 0$$

Further, neglecting the influence of the roll motion ($p = 0$, $K = 0$), the system of the differential equations of motion in the horizontal plane finally becomes:

$$X = m\left(\frac{\partial u}{\partial t} - rv - r^2 x_G\right)$$

$$Y = m\left(\frac{\partial v}{\partial t} + ru + \frac{dr}{dt}x_G\right) \qquad (13)$$

$$N = \frac{\partial r}{\partial t}I_{zz} + mx_G\left(\frac{\partial v}{\partial t} + ru\right)$$

in which *X* and *Y* are the longitudinal and transverse components of the hydrodynamic forces, *N* is the vertical component of the hydrodynamic moment, *m* is the mass of the ship, I_{zz} symbolizes the ship's yaw moment of inertia, $\overline{V_0}(u, v, 0)$ is the speed of the ship in the origin of the coordinate system, $\overline{\omega}(0, 0, r)$ is the angular speed and *(xG,0,zG)* are the coordinates of the ship's center of gravity placed on the symmetry plane.

2.1.2. *Hydrodynamic Forces and Moments Acting on the Ship*

The hydrodynamic forces and moments acting on a ship depend on such factors as: properties of the hull (e.g. body lines, main dimensions, CG, mass, inertia moments etc.), ship motions, properties of the fluid and surface control parameters (angle of incidence, speed and acceleration of the rudder deflection).

To ease the notation of the derivative equations, the following convention will be introduced into the equations from now on:

$$\frac{\partial A}{\partial \alpha} = A_\alpha \tag{14}$$

By the use of Taylor's series expansion method, one can obtain a simplified formulations of the above-mentioned equations of motion where only the first order terms are taken into account. If the initial condition of the ship is considered to be a straight ahead motion in horizontal plane at a constant speed *(u=U)*, the linear form of the differential set of equations (13) is given by:

$$
\begin{aligned}
&X_e + X_u u + X_{\dot{u}} \dot{u} = m\dot{u} \\
&Y_e + Y_v v + Y_r r + Y_{\dot{v}} \dot{v} + Y_{\dot{r}} \dot{r} = m\left(\dot{v} + rU + \dot{r}x_G\right) \\
&N_e + N_v v + N_r r + N_{\dot{v}} \dot{v} + N_{\dot{r}} \dot{r} = I_{zz}\dot{r} + mx_G\left(\dot{v} + rU\right)
\end{aligned} \tag{15}
$$

with X_e, Y_e and N_e being the components of the external forces and moments acting on the ship due to the rudder-propeller system and the thrusters.

The terms $X_u, X_{\dot{u}}, Y_v, Y_{\dot{v}}, Y_r, Y_{\dot{r}}, N_v, N_{\dot{v}}, N_r, N_{\dot{r}}$ are called hydrodynamic derivatives and represent the action of the fluid motion on the ship.

As far as the ship motions in the horizontal plane only are concerned, equations (15) can be presented under the following equivalent form:

$$
\begin{aligned}
&\left(m - X_{\dot{u}}\right)\dot{u} = X_u u + X_e \\
&\left(m - Y_{\dot{v}}\right)\dot{v} + \left(mx_G - Y_{\dot{r}}\right)\dot{r} = Y_v v + \left(Y_r - mU\right)r + Y_e \\
&\left(mx_G - N_{\dot{v}}\right)\dot{v} + \left(I_{zz} - N_{\dot{r}}\right)\dot{r} = N_v v + \left(N_r - mx_G U\right)r + N_e
\end{aligned} \tag{16}
$$

It can be observed that the surge equation (of the ship motion along the *x-axis*) is independent of the sway and yaw motion ones.

2.1.3. Stability of the Ship in Straight Ahead Motion

Directional stability of the ship, also called the dynamic stability or course-keeping stability, is a feature of a vessel to take up a new straight line after she has been disturbed from her initial straight path. Directional stability in usually referred to as controls-fixed

directional stability where rudder and any other control surfaces are fixed amidships and no control forces are being applied.

Assessing whether the vessel is stable (or not) only by looking at her body lines plan is an impossible task. For this reason, the designer can use such called ship stability parameter, C, which depends on the magnitude and sign of the derivative N_v. For a ship to be stable, to following relation must be achieved:

$$C = Y_v N_r + N_v \left(mU - Y_r \right) > 0 \tag{17}$$

If the assumption $x_G \neq 0$ needs to be considered, the stability condition (17) becomes:

$$C = Y_v \left(N_r - mx_G U \right) + N_v \left(mU - Y_r \right) > 0 \tag{18}$$

Generally, one can expect the ships with large skegs aft and with well-rounded forefoot to be more directionally stable than a similar ship without these features. Also, a long slender hull would be more directionally stable than a short tubby form [8].

Two main solutions exist to increase the course-keeping stability of the vessel: adding more lateral surface area in the aft part of a ship and/or moving the longitudinal center of gravity forward. In the latter case the attention needs to be paid not to introduce a negative trim. However, if no hull modifications could be applied, the dynamically unstable ship can maintain the linear course only by continuous use of the rudder deflection.

2.1.4. Ship Response to the Action of the Control Surface and Moments

The manoeuvring systems generates the forces and moments capable of controlling the ship trajectory. In this case, the most important components of the ships velocities would be: v = sway velocity and r = yaw velocity, which can be described with the following formulas:

$$v = \frac{\delta}{C} \left[\left(mx_G U - N_r \right) Y_\delta + \left(Y_r - mU \right) N_\delta \right] \tag{19}$$

$$r = \frac{\delta}{C} \left(N_v Y_\delta - Y_v N_\delta \right)$$

where C is the stability parameter.

Neglecting the expression $N_v Y_\delta$, the steady turning rate can be approximated by:

$$r = -\frac{\delta}{C} Y_v N_\delta \tag{20}$$

It should be noted that for a stable ship ($C > 0$) the steady-state yaw rate is negative for a positive rudder deflection ($\delta > 0$).

The turning radius, R, can be estimated with the following relations:

$$R = \frac{U}{r} = \frac{UC}{\delta \left(N_v Y_\delta - Y_v N_\delta \right)} \tag{21}$$

or

$$R = \frac{UC}{-\delta Y_v N_\delta} \tag{22}$$

It can be observed that the radius increases with the increase of the stability coefficient, C. That means that a very stable ship would certainly have a poor turning performance. However, increasing the rudder area would cause the N_δ to increase, which in turn would decrease the turning radius.

The drift angle, β, can be calculated with the relation:

$$v = -U \cdot tg\,\beta \tag{23}$$

where for small drift angles ($tg\beta \approx \beta$) one can use the following estimation:

$$\beta = -\frac{v}{U} = -\frac{\delta}{UC} \left[\left(mx_G U - N_r \right) Y_\delta + \left(Y_r - mU \right) N_\delta \right] \tag{24}$$

which shows that increasing the rudder deflection causes the increase of the drift angle.

2.1.5. Solution of the Nonlinear Equations of Motion

Due to its complexity, the realistic prediction of the ship manoeuvers at high rudder deflection angles requires the development of the nonlinear mathematical model, including higher order terms of Taylor's series expansion of the hydrodynamic forces and moments.

One of such models (with terms up to the third order) have been proposed by Strom-Tejsen [19], employing the following assumptions due to the nature of the acceleration forces (Abkowitz, 1964; Chislett and Strom-Tejsen, 1965):

- the second and higher order terms of acceleration can be neglected;
- the cross-coupling terms between acceleration and velocity parameters can be neglected;
- as a consequence of the symmetry of the body, the following terms are considered to be equal to zero:

$$Y_u = Y_{uu} = Y_{uuu} = Y_{\dot{u}} = N_u = N_{uu} = N_{uuu} = N_{\dot{u}} = 0 \qquad (25)$$

Taking the above assumptions into account, the nonlinear mathematical model of the ship manoeuvring can be written under the form:

$$(m - X_{\dot{u}})\dot{u} = X_u u + X_e + f_1(u, v, r, \delta)$$

$$(m - Y_{\dot{v}})\dot{v} + (m x_G - Y_{\dot{r}})\dot{r} = Y_v v + (Y_r - mU)r + Y_e + f_2(u, v, r, \delta) \qquad (26)$$

$$(m x_G - N_{\dot{v}})\dot{v} + (I_{zz} - N_{\dot{r}})\dot{r} = N_v v + (N_r - m x_G U)r + N_e + f_3(u, v, r, \delta)$$

with

$$f_1(u, v, r, \delta) = \frac{1}{2}\left(X_{uu}u^2 + X_{vv}v^2 + X_{\delta\delta}\delta^2\right) + \left(\frac{1}{2}X_{rr} + m x_G\right)r^2 +$$

$$+ X_{v\delta}v\delta + X_{r\delta}r\delta + (X_{vr} + m)vr + \frac{1}{6}X_{uuu}u^3 + \qquad (27)$$

$$+ \frac{1}{2}\left(X_{vvu}v^2 u + X_{rru}r^2 u + X_{\delta\delta u}\delta^2 u\right) + \left(X_{vru}vru + X_{v\delta u}v\delta u + X_{r\delta u}r\delta u\right)$$

$$f_2(u, v, r, \delta) = Y_u' u + Y_{uu}' u^2 + Y_\delta \delta + \left(Y_{vu}vu + Y_{ru}ru + Y_{\delta u}\delta u\right) +$$

$$+ \frac{1}{6}\left(Y_{vvv}v^3 + Y_{rrr}r^3 + Y_{\delta\delta\delta}\delta^3\right) +$$

$$+ \frac{1}{2}\left(Y_{vrr}vr^2 + Y_{rvv}rv^2 + Y_{\delta vv}\delta v^2 + Y_{v\delta\delta}v\delta^2 + Y_{r\delta\delta}r\delta^2\right) + \qquad (28)$$

$$+ \frac{1}{2}\left(Y_{\delta rr}\delta r^2 + Y_{vuu}vu^2 + Y_{ruu}ru^2 + Y_{\delta uu}\delta u^2\right) + Y_{vr\delta}vr\delta$$

$$f_3(u,v,r,\delta) = N_u' u + N_{uu}' u^2 + N_\delta \delta + (N_{vu} vu + N_{ru} ru + N_{\delta u} \delta u) +$$
$$+\frac{1}{6}(N_{vvv} v^3 + N_{rrr} r^3 + N_{\delta\delta\delta} \delta^3) +$$
$$+\frac{1}{2}(N_{vrr} vr^2 + N_{rvv} rv^2 + N_{\delta vv} \delta v^2 + N_{v\delta\delta} v\delta^2 + N_{r\delta\delta} r\delta^2) +$$
$$+\frac{1}{2}(N_{\delta rr} \delta r^2 + N_{vuu} vu^2 + N_{ruu} ru^2 + N_{\delta uu} \delta u^2) + N_{vr\delta} vr\delta$$

(29)

Considering the new functions as:

$$f_1'(u,v,r,\delta) = X_u u + X_e + f_1(u,v,r,\delta)$$
$$f_2'(u,v,r,\delta) = Y_v v + (Y_r - mU)r + Y_e + f_2(u,v,r,\delta)$$
$$f_3'(u,v,r,\delta) = N_v v - (N_r - mx_G U)r + N_e + f_3(u,v,r,\delta)$$

(30)

the nonlinear equations become:

$$(m - X_{\dot{u}})\dot{u} = f_1'(u,v,r,\delta)$$
$$(m - Y_{\dot{v}})\dot{v} + (mx_G - Y_{\dot{r}})\dot{r} = f_2'(u,v,r,\delta)$$
$$(mx_G - N_{\dot{v}})\dot{v} + (I_{zz} - N_{\dot{r}})\dot{r} = f_3'(u,v,r,\delta)$$

(31)

An approximate numerical solution of the equations (31) can be obtained calculating the unknown velocity components u, v and r at the time step $(t+\Delta t)$ if the values of u, v and r at the time t are known:

$$u(t + \Delta t) = u(t) + \Delta t \cdot \dot{u}(t)$$
$$v(t + \Delta t) = v(t) + \Delta t \cdot \dot{v}(t)$$
$$r(t + \Delta t) = r(t) + \Delta t \cdot \dot{r}(t)$$

(32)

This method is known to give an accurate results due to the fact that the acceleration terms vary fairly slowly with time, mostly because of the large mass and inertia of a ship compared to the relatively small forces and moments developed by its control surfaces.

However, to obtain the solution of (32) one needs to know the values of $u(0)$, $v(0)$, $r(0)$ at the time $t = 0$. Subsequently, one can determine the instantaneous values of:

- the heading angle:

$$\psi\left(t+\Delta t\right)=\psi(t)+\Delta t\cdot r(t) \tag{33}$$

- the trajectory of the ship in an earth-located coordinate system $0_0 x_0 y_0 z_0$:

$$
\begin{aligned}
x_0\left(t+\Delta t\right) &= x_0(t)+\Delta t\left[u(t)\cos\psi(t)-v(t)\sin\psi(t)\right] \\
y_0\left(t+\Delta t\right) &= y_0(t)+\Delta t\left[u(t)\sin\psi(t)+v(t)\cos\psi(t)\right]
\end{aligned} \tag{34}
$$

- the radius of the trajectory:

$$R(t)=\frac{\sqrt{u^2(t)+v^2(t)}}{r(t)} \tag{35}$$

- the drift angle:

$$\beta(t)=-arctg\,\frac{v(t)}{U} \tag{36}$$

It just has to be added that the accuracy of the above solutions depends strongly on the time step Δt.

In order to practically resolve the ship manoeuvring equations it is necessary to know the hydrodynamic derivatives, which can be determined using both theoretical and/or experimental methods.

2.2. Preliminary Theoretical Prediction of the Hydrodynamic Derivatives

In the theoretical prediction of the hydrodynamic derivatives, the linear equations of motion (16) for the horizontal sway-yaw problem can re-written as:

$$
\begin{aligned}
\left(m-Y_{\dot{v}}\right)\dot{v}-Y_v v+\left(mU-Y_r\right)r+\left(mx_G-Y_{\dot{r}}\right)\dot{r} &= Y_e \\
\left(I_{zz}-N_{\dot{r}}\right)\dot{r}+\left(mx_G U-N_r\right)r+\left(mx_G-N_{\dot{v}}\right)\dot{v}-N_v v &= N_e
\end{aligned} \tag{37}
$$

Using a standard nondimensionalizing procedure (by means of the quantities: ship length L, ship speed U and water density ρ), the above (37) can be written under the form:

$$\left(m'-Y_{\dot{v}}'\right)\dot{v}'-Y_{v}'v'+\left(m'U'-Y_{r}'\right)r'+\left(m'x_{G}'-Y_{\dot{r}}'\right)\dot{r}'=Y_{e}'$$
$$\left(I_{zz}'-N_{\dot{r}}'\right)\dot{r}'+\left(m'x_{G}'U'-N'r'\right)r'+\left(m'x_{G}'-N_{\dot{v}}'\right)\dot{v}'-N_{v}'v'=N_{e}'$$

(38)

The linear nondimensional derivatives from (38) can be approximated with the regression formulae developed by Clarke, Gedling and Hine (1982). This formulae is valid only for the ships on even keel:

$$Y_{\dot{v}}'=-\pi\left(T/L\right)^{2}\left[1+0.16C_{B}\left(B/T\right)-5.1\left(B/L\right)^{2}\right]$$
$$Y_{v}'=-\pi\left(T/L\right)^{2}\left[1+0.4C_{B}\left(B/T\right)\right]$$
$$Y_{\dot{r}}'=-\pi\left(T/L\right)^{2}\left[0.67\left(B/L\right)-0.0033\left(B/T\right)^{2}\right]$$
$$Y_{r}'=-\pi\left(T/L\right)^{2}\left[-0.5+2.2\left(B/L\right)-0.08\left(B/T\right)\right]$$
$$N_{\dot{v}}'=-\pi\left(T/L\right)^{2}\left[1.1\left(B/L\right)-0.041\left(B/T\right)\right]$$
$$N_{v}'=-\pi\left(T/L\right)^{2}\left[0.5+2.4\left(T/L\right)\right]$$
$$N_{\dot{r}}'=-\pi\left(T/L\right)^{2}\left[1/12+0.017C_{B}\left(B/T\right)-0.33\left(B/L\right)\right]$$
$$N_{r}'=-\pi\left(T/L\right)^{2}\left[0.25+0.039\left(B/T\right)-0.56\left(B/L\right)\right]$$

(39)

To obtain the speed derivatives for a vessel with draft difference:

$$t=T_{AP}-T_{FP}$$

(40)

the below stated formulas can be used (*T* being the mean draft):

$$Y_{v}'(t)=Y_{v}'\left[1+0.67(t/T)\right]$$
$$Y_{r}'(t)=Y_{r}'\left[1+0.8(t/T)\right]$$
$$N_{v}'(t)=N_{v}'\left[1-0.27(t/T)\left(Y_{v}'/N_{v}'\right)\right]$$
$$N_{r}'(t)=N_{r}'\left[1+0.3(t/T)\right]$$

(41)

The experimental investigation of the hydrodynamic derivatives can be performed using the following methods:

- captive model in a towing tank with a Planar Motion Mechanism (PMM);
- captive model tests with rotating-arm-system in a circular tank.

3. STANDARD MANOEUVRES OF THE SHIP

3.1. Measures and Criteria of Manoeuvrability

3.1.1. Manoeuvring Prediction Methods

There are many possible ways to predict the key parameters as well as the trajectories of the standard manoeuvres of the ship, as illustrated on Fig. 2.
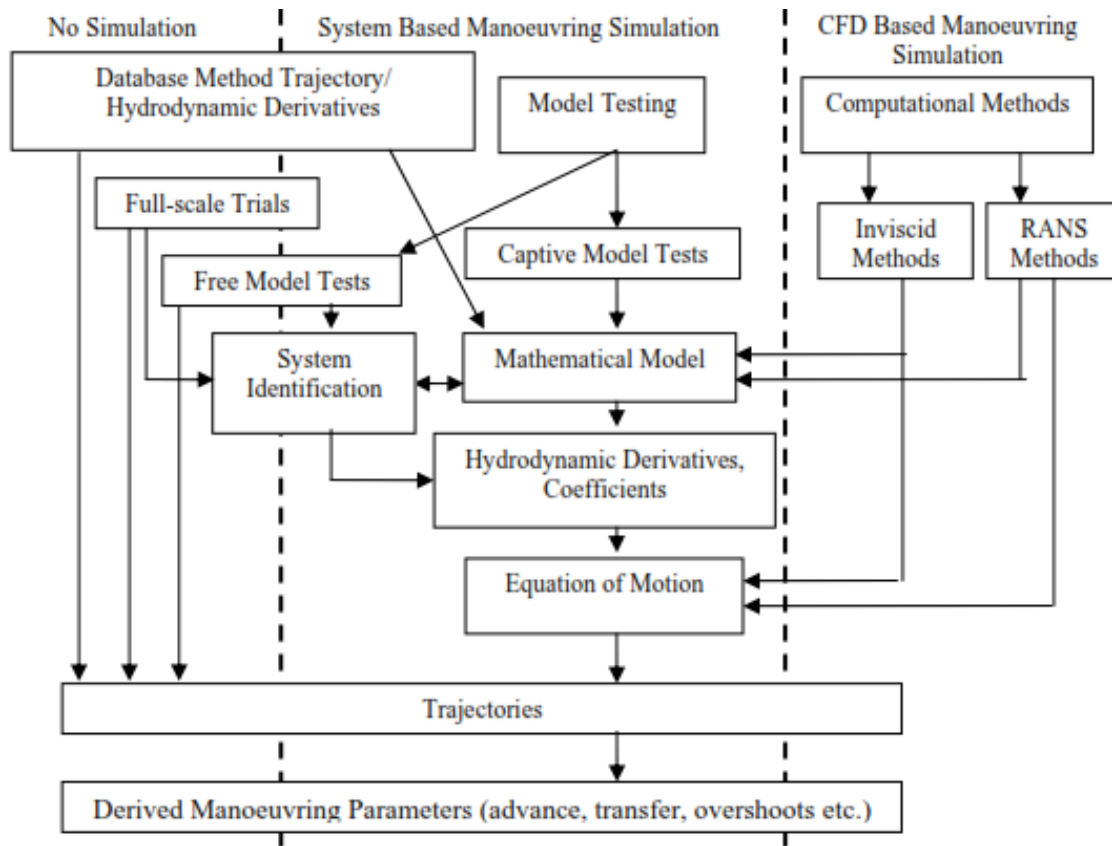
Fig. 2. Manoeuvring prediction methods
Source: 24th ITTC Manoeuvring Committee Report, 2005, p. 2

The "no simulation" methods are based on the existing database of manoeuvring parameters derived from a wide spectrum of full-scale trials and free model tests. They can indeed serve as a useful tool, especially at the very initial design stage, where the simple formulas for hydrodynamic coefficients can be applied (Abkowitz, 1964; Clarke, 1982; Voitkounsky, 1985). However, these methods would only be reasonable for a usual shapes of the hull with a wide range of data to be investigated. If this is not provided, the free

model tests are necessary to be performed with the scale effects on the trajectories carefully taken into account.

If the manoeuvring parameters are not available in the database, the simulation methods are necessary to be used. This requires the hydrodynamic forces and derivatives to be provided, either from the hydrodynamics database or by means of captive model tests. With the required input data possessed, the simulations, based on the developed mathematical models (e.g. Abkowitz non-linear model, 1964), can be run with reasonably accurate results delivered, which makes these methods useful in the basic design stage.

However, the unsteady character of the hydrodynamic forces makes the above-mentioned methods sometimes hard to be correctly applied. In this case, the CFD simulations allowing the user to calculate the complex hydrodynamic forces for both steady and unsteady cases should be seriously considered. Although still under development, they seem to become a very useful and commonly-used tools in the nearest future. Especially codes employing the RANS methods have been found to provide satisfactory agreements between numerical and experimental results for most of the investigated cases [14].

3.1.2. IMO Requirements

Professors Amin and Hasegawa (2010) from the Osaka University define the manoeuvrability of the ship as "predictability and controllability of the motion of ships at different situations at sea conditions". Since navigating the ship is a complex problem in terms of ship manoeuvrability, the International Maritime Organization (IMO) adopted a set of detailed manoeuvring criteria and standards to evaluate its performance. These criteria are considered as a valuable tool to ensure the minimum manoeuvrability and enhanced controllability ensuring at the same time the operational safety of the ship.

The following recommendations related to manoeuvrability of ships have been adopted by IMO:

1. Interim Guidelines for Estimating Manoeuvring Performance in Ship Design, adopted by MSC/Circ. 389, 10 January 1985;

2. Provision and Display of Manoeuvring Information on Board Ships, adopted by Resolution A.601 (15) on 19 November 1987;

3. Interim Standards for Ship Manoeuvrability, adopted by Resolution A.751 (18) on 4 November 1993;

4. Explanatory Notes to the Interim Standards for Ship Manoeuvrability, adopted by MSC/Circ.644 on 6 June 1994.

MSC/Circ. 389 provides the specific manoeuvring characteristics and recommends the estimation of them during design process both for the fully loaded ship and test condition in deep water. It also outlines the list of the full-scale tests to be performed in order to estimate the manoeuvring performance of a ship. The list includes:

- Turning circle test;
- Yaw checking ability (zig-zag test);
- Initial turning test;
- Course keeping information test:
    - The pull-out test,
    - The direct spiral test,
    - The reverse spiral test;
- Stopping test.

Resolution A.601 (15) requires that the manoeuvring information such as: pilot card, wheelhouse poster and manoeuvring booklet are kept onboard and available to navigators.

Resolution A.751 (18) recommends application of the interim standards for ships longer than 100 meters and for all gas carriers and chemical tankers. The standards comprise: turning ability, initial turning ability, yaw checking and course keeping abilities as well as stopping ability.

MSC/Circ. 644 is intended to provide Administrations with specific guidance on unified interpretation, application and consistent evaluation of the standards for ship manoeuvrability adopted by Resolution A.751 (18).

3.2. Turning Circle Manoeuvre

The turning circle, measured on model-scale, full-scale trials or numerically simulated, is used to evaluate the turning ability of the ship as well as the efficiency of the rudder. Starting from a steady course at a constant speed the rudder is put over to a specified angle δ (usually max. rudder angle) and held on this position until the ship completes the circle. The manoeuvre should be performed for both port and starboard side. Additionally, for a ship to turn, the drift angle, β, must be different from zero. Based on empirical data, β, in degrees, generally falls within the following range of values: $\beta = 22.5\ L/R + 1.45$ and $\beta = 18\ L/R$ [4].

The response of the ship to the deflection of the rudder as well as the forces and moments resulting from this action can be divided into two groups [4]:

- an initial transient one in which significant surge, sway and yaw accelerations occur ($\dot{u}, \dot{v}, \dot{r} \neq 0$);

- a steady turning one in which the rate of turn and forward speed are constant and the path of the ship is circular ($V, r, R = const.$, $\dot{u}, \dot{v}, \dot{r} = 0$).

Fig. 3 represents a diagram for turns of any diameter, which primarily consist of three phases, whereas the Fig. 4 illustrates the detailed characteristics of each phase. The first phase starts at the very moment of the initial rudder deflection and may be completed by the time the rudder reaches its desired deflection angle. During this period, the rudder force, $Y_\delta \delta_R$, and the rudder moment, $N_\delta \delta_R$, develop the accelerations, which are opposed only by the inertial reaction of the ship because no hydrodynamic forces has been developed yet. The values of these accelerations, $\dot{v}$ and $\dot{r}$, can be obtained from the following linearized equations of motion in the first phase of turning:

$$(\Delta - Y_{\dot{v}})\dot{v} - Y_{\dot{r}}\dot{r} = Y_\delta \delta_R$$
$$(I_z - N_{\dot{r}})\dot{r} - N_{\dot{v}}\dot{v} = N_\delta \delta_R$$

(42)

As it is can be observed on figures below, the transverse acceleration, $\dot{v}$, is directed to port in the first phase of the manoeuvre, whereas the turn will eventually be performed to starboard. This happens because the rudder force, $Y_\delta \delta_R$, is directed to port for a starboard turn. The same accelerations soon develop the drift angle, β, and a rotation, r, and the vessel enters into the second phase of the turn. During this phase, the acceleration,

$\dot{v}$, stops growing (to port) and eventually is reduced to zero as the inwardly directed $Y_v v$ force comes into balance with the outwardly directed centrifugal force. With the establishment of the final equilibrium of forces, the vessel finally enters it the third, steady phase of turn, continuing its circle trajectory with a constant radius. In this phase, the r and v speed components have nonzero values, whereas $\dot{v}$ and $\dot{r}$ are equal to zero. The linearized equations of motion in a steady state can then be written under the following form:

$$
\begin{aligned}
-Y_v v - (Y_r - \Delta' u_1) r &= Y_\delta \delta_R \\
-N_v v - N_r r &= N_\delta \delta_R
\end{aligned}
\tag{43}
$$

with u_1 being the initial equilibrium value of velocity component along the x-axis.

Generally, the turning performance of a ship is characterized by four numerical values: advance, transfer, tactical diameter and steady turning radius [Fig. 3]. The advance is the distance from the origin at the very first execute of the rudder to the x-axis of the ship when performed a 90 degrees turn. The transfer is defined as the distance from the original approach course to the origin of the ship when her x-axis has turned 90 deg. The tactical diameter is the distance from the approach course to the ship's x-axis when that axis has turned 180 deg [4].

IMO requires the tactical diameter to be less than 5 ship lengths and the advance to be less than 4.5 ship lengths [IMO, 2002a]. Additionally, the speed lost during the turn and maximum heel angle ψ, as well as the peak and final yaw rates, should be recorded.

Another interesting characteristic of a steady turn is a "pivot" point, also presented in Fig. 3. At this point, because of the combination of the drift angle on the ship and the rotation of the ship, the flow of water past the hull is parallel to the x-axis of the ship. Forward of this point, for a starboard turn, the flow approaches from off the starboard side whereas aft of this point the flow comes from the portside. For most of the ship, the pivot point would be located somewhere between the bow and about $1/5\ L$ aft of the bow (Mandel, 1953).
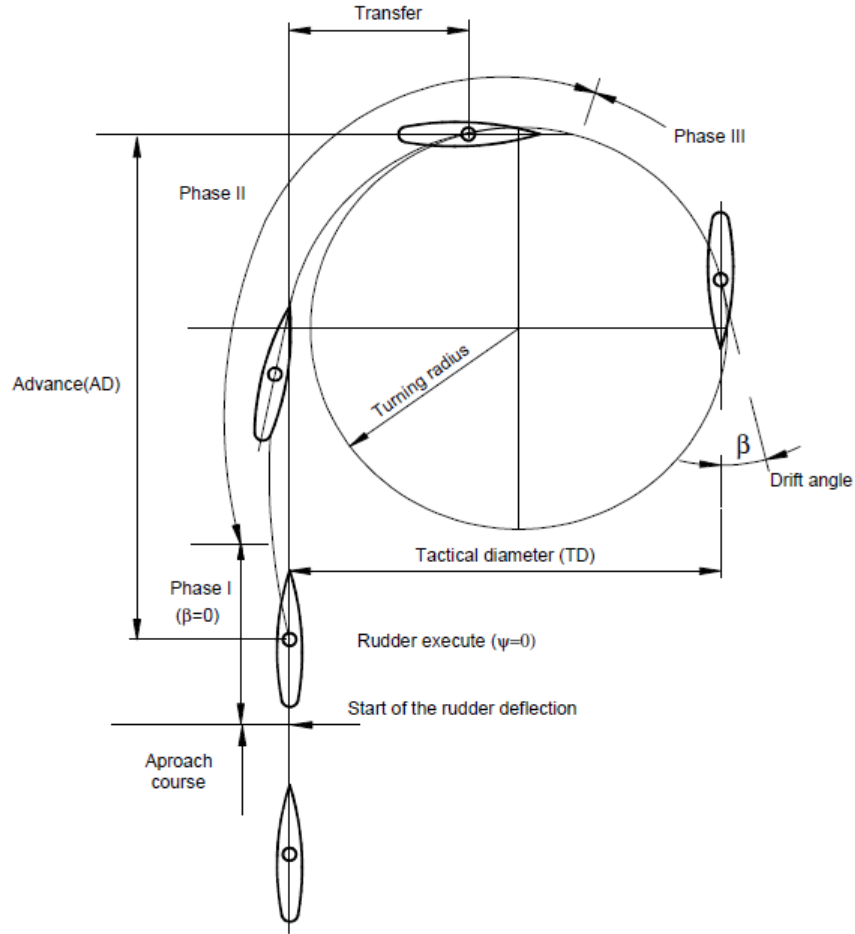
Fig. 3. Definitions used in turning circle
Source: Ship Maneuvering and Control, Ed. SNAME, 1977
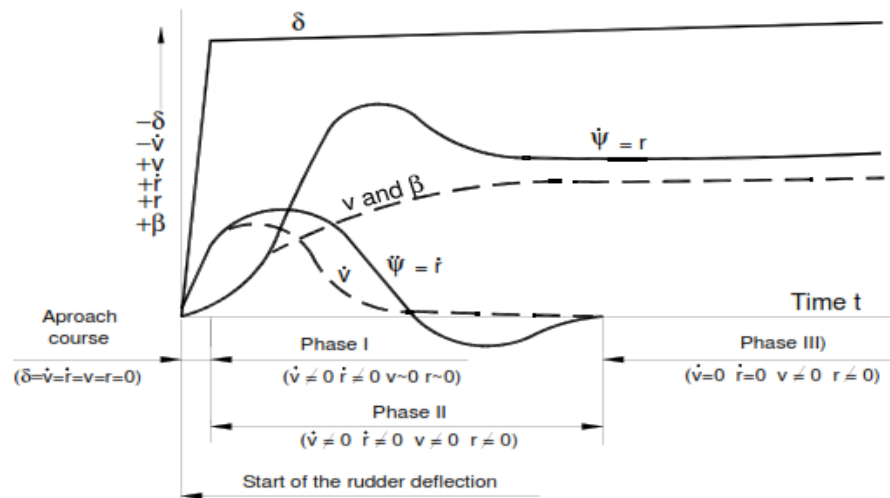
Fig. 4. Characteristics of the turning manoeuvre phases
Source: Ship Maneuvering and Control, Ed. SNAME, 1977

The additional phenomena to be observed during the turning circle manoeuvre is that the ship would heel to both sides while performing one circle. The heel results from the vertical disposition of the forces applied both on the rudder and hull [Fig. 5]. As the fluid forces act below the waterline, but the center of gravity of the ship is usually situated near or above the waterline, the heeling moment occurs.
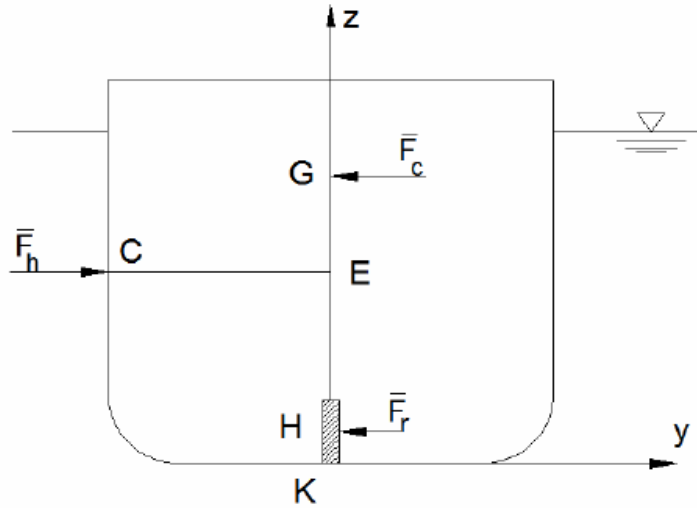
Fig. 5. Disposition of forces during a turn
Source: Basic Ship Theory, Vol. 2, 1994, p.549

At the phase of initial deflection of the rudder, the inertial terms dominate and the sway equation becomes:

$$(m - Y_{\dot{v}})\dot{v} - (Y_{\dot{r}} - mx_G)\dot{r} = Y_\delta \delta \tag{44}$$

Because the coefficients of $\dot{r}$ are rather small, the vessel will first heel to starboard (positive) for a positive rudder action. As soon as the steady turning conditions are reached (usually after $90°$ change of heading), the hydrodynamic forces equalize the centrifugal force mUr and the rudder force $Y_\delta \delta$. The sway equation now becomes:

$$-Y_v v + (mU - Y_r)r = Y_\delta \delta \tag{45}$$

The centrifugal force acts above the waterline and thus the vessel will ultimately heel to port (negative) for a positive rudder action.

3.3. Zig-Zag Manoeuvre

The zig-zag manoeuvre is carried out to investigate more closely the initial response of the ship to rudder action. However, the results of this test depend not only on the effectiveness of the rudder, but also on the stability characteristics of a given ship.

The typical manoeuvre is a 10/10 zig-zag test, where the first value indicates the set rudder angle and the second the set heading angle. Alternatively, a 20/20 or 10/20 zig-zag tests can be performed. In a 10/10 manoeuvre, the ship is first brought to a steady course. On a steady approach, the rudder is deflected to the angle $\delta = 10°$ (first execute) and hold in this position until the change of heading has reached 10°. Once this is done, the rudder is then immediately deflected to the opposite side with the same angle (second execute) and held whilst the ship achieves a 10° heading angle in the other direction. At this very moment the rudder is reversed again and the procedure can be repeated (third execute, etc.).

It can be observed [Fig. 6] that after the counter rudder has been applied (second execute), the ship keeps on turning in the original direction with decreasing turning speed until the yaw motion changes direction. This phenomena is called the overshooting and the certain values of the yaw overshoot angle are one of the main IMO requirements concerning the zig-zag test. It just needs to be added that the higher the speed of the vessel the bigger overshoot angle will she achieve, demonstrating that the zig-zag manoeuvre results are speed-dependent.

The zig-zag manoeuvre provides several important characteristics of the yaw response. These characteristics are as follows: the initial turning time (time to reach a given heading), the yaw first and second overshoot (amount the vessel exceeds imposed rudder angle when the rudder has been brought the other way) and the period of the cycle. The first value is a direct measure of the ability of a vessel to rapidly change course. It improves with increased rudder effectiveness and with decreased controls-fixed stability (Arentzen and Mandel, 1960). The latter values are numerical measures of counter-manoeuvring ability and indicate the amount of the anticipation required by a helmsman, mainly when navigating in restricted waters. It is interesting to know that the magnitude of the yaw-angle overshoot was found to decrease with increased stability but to increase with increased rudder effectiveness. Additionally, such results as the time necessary to obtain the first maximum value of the heading angle as well as the advance (time between the first

execute of the rudder angle and the first zero value of the heading angle after the second execute) would be of a significant interest for a ship designer as well as the operating crew onboard the ship.
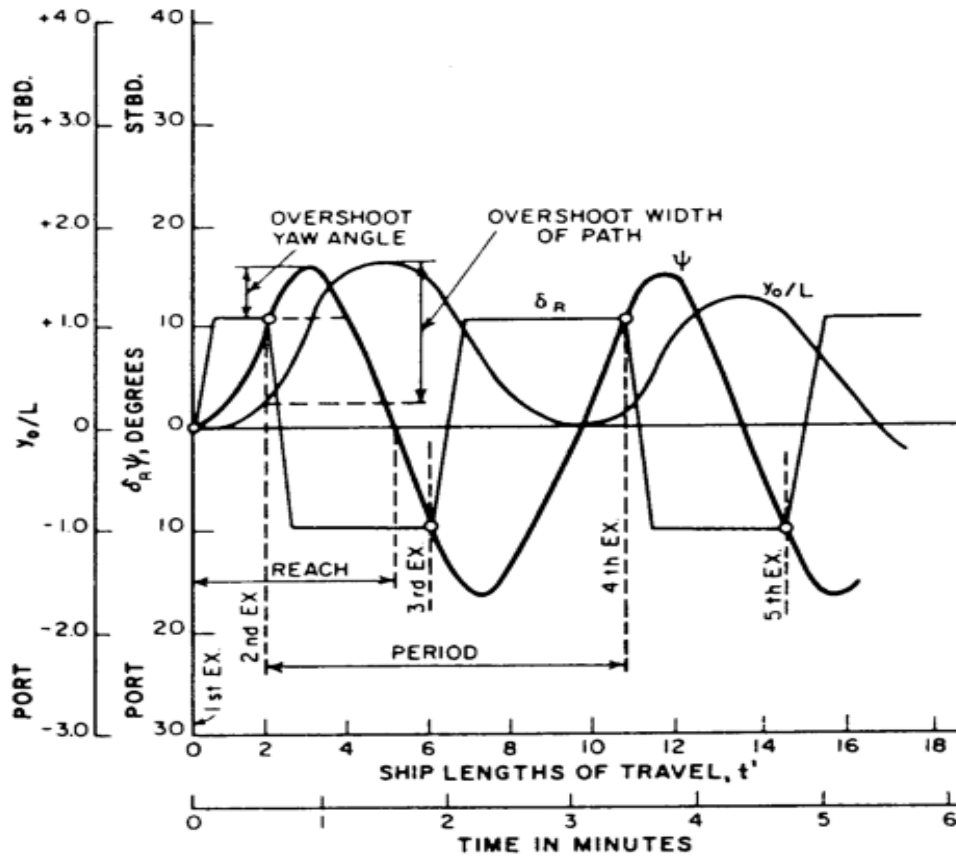
Fig. 6. 10/10 Zig-zag test
Source: Principles of Naval Architecture, Vol. III, 1989, p. 206

For a10/10 manoeuvre IMO requires the first overshoot angle, $\alpha 10_1$, to be:

- $< 10°$ if $L/V \leq 10$ sec.,
- $< [5 + 0.5 \cdot (L/V)]°$ if $L/V < 30$ sec.,
- $< 20°$ if $L/V \geq 30$ sec.

and second overshoot angle, $\alpha 10_2$, to be less than $\alpha 10_1 + 15°$.

For a 20/20 test IMO imposed only one criteria, requiring the first overshoot angle, $\alpha 20_1$, to be less or equal to 25°.

3.4. Spiral Manoeuvre

The spiral test is performed to estimate the controls-fixed straight line stability of the ship and reveals whether the ship has the memory effect. However, one can distinguish between direct spiral manoeuvre (Dieudonne, 1953) and reverse (indirect) spiral manoeuvre (Bech, 1968).

The direct spiral test begins with the ship being on an initial straight course. Once these conditions are achieved, the rudder is given a certain angle of deflection until the ship reaches a steady turning rate. Subsequently, the rudder angle is decreased in steps of a constant small value (typically 2° for -10°÷10° heading angles and 5° for 10°÷25° heading angles) and again held until a steady condition is reached. The procedure is then repeated until the rudder has covered the whole range to the maximum rudder angle on the other side ($\delta_{max} = -\delta_{max}$) with the rate of turn being noted for each angle.

In the reverse spiral test the vessel is steered at a constant rate of turn and the mean rudder angle required to produce this yaw rate is measured. This action is then repeated for a range of yaw rates until a complete relationship of yaw rates versus rudder angles is built.

The numerical measures obtained from a spiral test are the steady yawing rates in function of a rudder angle. A plot of these values reflects the stability characteristics of a ship. In case of a directionally stable ship the curve will be a single function [Fig. 7, left]. For an unstable ship, there may exist three possible heading angles for one given rudder angle, as shown in the right part of Fig. 7. The dotted line represents an unstable state that can be revealed only by the indirect method. In the direct method, indicated by dotted arrows, the rate of turn moves from one vertical sections of the curve to the other if the rudder angle is changed, creating a curve knows as a hysteresis loop. Obviously, the larger the loop, the more unstable the investigated vessel. However, it has been observed that many ships obtain a small hysteresis loop (within the range [-3°; 3°]) having a very small range of directional instability. As the course-keeping stability increases with the increased lateral immersed area of the aft part of the ship (increase of the N_v hydrodynamic derivative), the most common solutions for this problem could be either increasing the rudder area or introducing a skeg in the stern part. However, both cases are often limited by inherent geometrical or physical constraints.
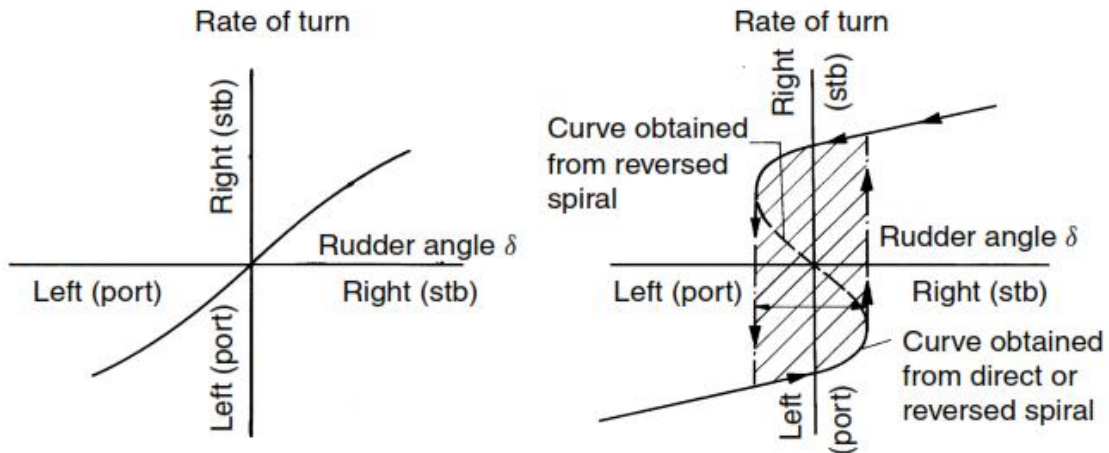
Fig. 7. Results of Spiral Test for a yaw-stable and yaw-unstable vessel
Source: Practical Ship Hydrodynamics, 2000, p.171

4. HYDRODYNAMICS OF A PASSIVE CONTROL SURFACE

4.1. General Concept of a Rudder

Control surfaces are designed as tools to produce a force that helps to control the motion of the vehicle. These surfaces may be either fixed or movable, but as long the naval architecture is concerned, most of them would be a movable ship rudder.

Standard rudder is a hydrofoil normally placed at the stern of the vessel behind the propeller(s), in order to produce a transverse force and steering moment about the ship's center of gravity by deflecting the water flow to a direction of a foil plane [2].

The height of the rudder is limited by both draft and shape of the stern part of the ship. It needs, however, to be increased as much as possible in order to obtain the biggest aspect ratio [*see 5.2.3*]. On the other hand, the bottom plate of the rudder should be kept above the bottom of the keel for protection. Additionally, the rudder should be fully immersed in order to avoid negative effects of free surface and ventilation of the upper part of the rudder, since these phenomena are known to decrease the hydrodynamic efficiency.

The selection of the rudder depends on many factors with most important being the type and size of the vessel, shape of the stern profile, size of rudder required, placing (or not) a propeller upstream of the rudder, etc. The most common rudder concepts, classified on the basis of the stock location, are as follows [7]:

- non-balanced rudders with the rudder stock located in the vicinity of the leading edge [Fig. 8a];
- semi-balanced rudders with the rudder stock between $0.5t$ and $0.25c$ from the leading edge [Fig. 8b], with t being the thickness and c the chord of the profile;
- balanced rudders with the rudder stock location between $0.25c$ and $0.33c$ from the leading edge [Fig. 8c and 8d].

Depending on the attachment way to the vessel's hull, one can classify the rudders as:

- simplex rudders, supported with bearings both at the upper and bottom part of the rudder [Fig. 8a and 8c];
- semi-balanced rudders, where a fixed rudder horn extends over the upper plate of the rudder [Fig. 8b];
- spade rudder, with both bearings at the upper part, inside the hull [Fig. 8d].
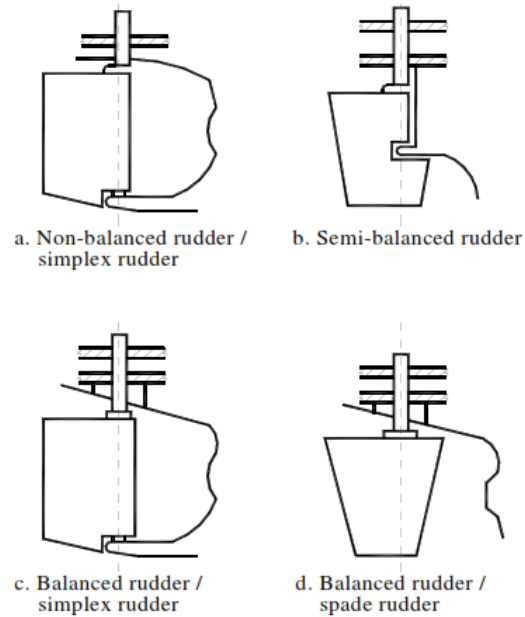
Fig. 8. Main concepts of the rudder
Source: Manevrabilitatea Navei, 2008, p. 107

The main reasons why are the rudders usually placed at the ship's stern (behind the propeller) can be summarized as follows:

- when maneuvering, the rudder moment that makes the ship to turn is created by the transverse force acting on the rudder and an opposite transverse force applied on the hull acting near the bow. The moment increases as the distance between the rudder force and the hull force increases;
- rudders situated outside the propeller's slipstream lose their efficiency at very low speeds (e.g. during berthing manoeuvre). Similarly, these types or rudders are far less effective also at usual forward speed;
- bow-placed rudders are usually ineffective in the forward motion since the oblique water flow created by the turned rudder is redirected longitudinally by the hull. Therefore, the transverse forces acting on a bow rudder and on a forward moving hull cancel each other.

Summing up, the rudder effectiveness while manoeuvring depends mainly on the maximum transverse force acting on the rudder. This effectiveness can be improved by optimization of the rudder arrangement in the propeller slipstream, increasing of the rudder area, shortening the rudder steering time, etc.

4.2. Hydrodynamic Performance of a Rudder

Fig. 9 represents the rudder forces and moments generated by the dynamic pressure distribution on the deflected rudder surface with an incident angle, α. The resistance components in flow speed direction, v, and perpendicular to it are termed drag component, P_x, and lift component, P_y, respectively. The force components in the centerline plan of the profile and perpendicular to it are termed normal component, P_n, and tangent component, P_t, respectively.
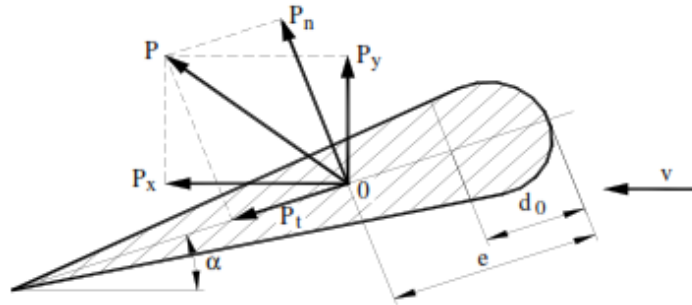
Fig. 9. Rudder forces
Source: Manevrabilitatea Navei, 2008, p. 110

The resistance components are typically described by means of a dimensionless coefficients, C_L and C_D:

$$C_L = \frac{Lift(L)}{0.5\rho A U_0^2} \tag{46}$$

$$C_D = \frac{Drag(d)}{0.5\rho A U_0^2} \tag{47}$$

with A being the planform area, U_0 the fluid free-stream velocity, ρ the fluid density and α the angle of attack or incidence.

Fig. 10 represents the coefficients C_L and C_D plotted against the angle of incidence α. It can be observed that, initially, C_L rises almost linearly with the incidence α creating a characteristic "lift slope". At some point it starts to rise more steeply until it reaches a maximum value and ultimately falls down rapidly. With this point reached, the foil is considered to be stalled. On the other hand, C_D rises almost parabolically with incidence α

until about a "stall point" after which a significant increase in the rate of rise can be observed.

The idea of stall can be explained with the help of Fig. 11. At a small angle of attack the flow around the foil is smooth (laminar) and attached to both upper and lower surfaces [Fig. 11a], with the points of separation of the flow in the vicinity of the trailing edge. As the angle of attack increases, the flow detaches from the upper surface. However, there is an increase of pressure on the upper side of the foil (pressure becomes less negative) as the flow moves towards the trailing edge. As the incidence α increases, a further increase in the adverse pressure gradient can be observed, with the separation point moved forward [Fig. 11b]. This phenomena is known as stall and leads to a loss of lift and increased in drag, as presented on Fig. 10 [6].
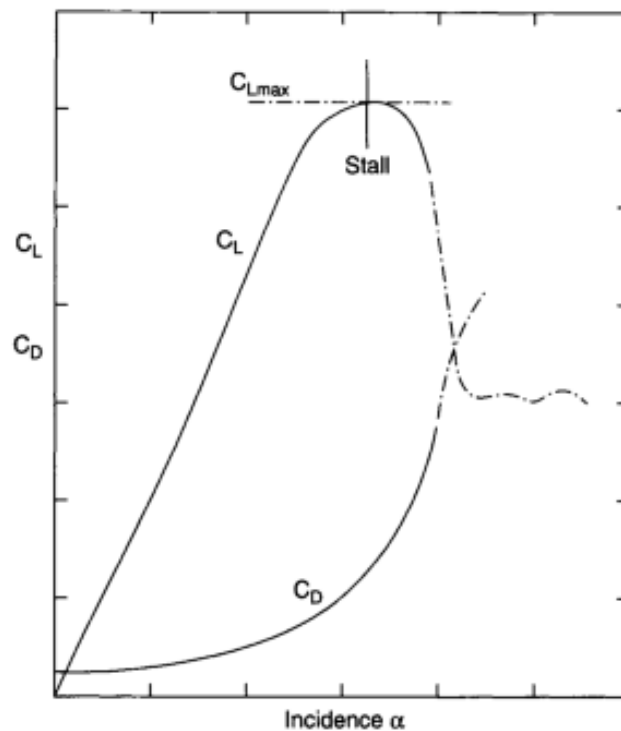
Fig. 10. Lift and drag characteristics
Source: Molland A.F., Turnock S.R., Marine Rudders and Control Surfaces, 2007, p. 40
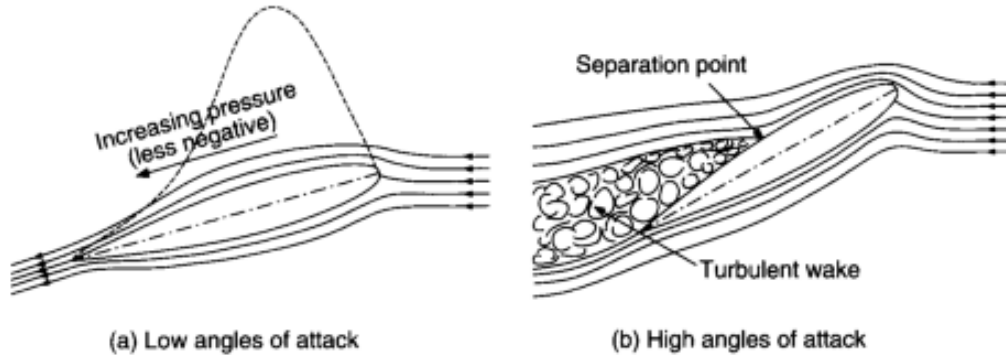
Fig. 11. Flow behavior over a foil at different angles of attack
Source: Molland A.F., Turnock S.R., Marine Rudders and Control Surfaces, 2007, p. 41

4.3. Rudder-Propeller Interaction

During a forward motion of the vessel, the flow passing through the propeller is accelerated and rotated. This action influences the forces and moments developed by the rudder, which are requisitive to determine the overall manoeuvring characteristics of a ship. On the other hand, the rudder itself both blocks and diverts the upstream flow onto and through the propeller influencing at the same time the thrust and torque developed by the propeller.

Because the rudder forces are proportional to the flow velocity squared at the rudder, the adequate determination of the speed in the propeller slipstream at the rudder position is required to correctly estimate rudder forces [2]. On the basis of the momentum theory of the propeller, the mean axial speed of the slipstream far behind the propeller is:

$$V_\infty = V_A \sqrt{1 + C_{Th}} \tag{48}$$

with C_{Th} being the thrust loading coefficient:

$$C_{Th} = \frac{8}{\pi} \cdot \frac{K_T}{J^2} = \frac{T}{\frac{\rho}{2} V_A^2 A_p} \tag{49}$$

where K_T is the thrust coefficient expressed as $K_T = T/(\rho n^2 D^4)$, J is the advance number defined as $J = V_A/(nD)$, V_A the average inflow speed to the propeller, and A_p the propeller area. The theoretical slipstream radius r_∞ far behind the propeller can be obtained using

the law of continuity, assuming that the mean axial speed at the propeller is the average between V_A and V_∞:

$$r_\infty = r_0 \sqrt{\frac{1}{2}\left(1+\frac{V_A}{V\infty}\right)}$$

(50)

where r_0 is half the propeller diameter D. However, as the rudder is normally placed not very far from the propeller plane, the slipstream radius as well as the axial velocity may be approximated by the following formulas (Söding, 1982):

$$r_x = r_0 \cdot \frac{0.14(r_\infty/r_0)^3 + r_\infty/r_0 \cdot (x/r_0)^{1.5}}{0.14(r_\infty/r_0)^3 + (x/r_0)^{1.5}}$$

(51)

and

$$V_x = V_\infty \cdot \left(\frac{r_\infty}{r}\right)^2$$

(52)

with x normally expressing the distance of the centre of gravity of the rudder area from the propeller plane.

4.4. Influence of Hull on Rudder-Propeller Interaction

The wake of the hull placed upstream of an isolated rudder-propeller combination decreases the inflow velocity to the rudder and increases the propeller load. Additionally, the hull affects the inflow angle during the turning manoeuvre, having a flow-straightening effect.

The speed reduction from ship velocity, V_S, to wake or effective velocity, V_A, can be estimated by means of a characteristic wake fraction, w_T, for a particular ship or boat type:

$$V_A = V_S(1-w_T)$$

(53)

The value of w_T can be as low as 0.05 for a fine high-speed vessel up to 0.450 a large full-form tanker [6]. At the initial design stage, the average wake fraction can be estimated

using the empirical data. For small single-screw vessels (and sailing crafts) with the block coefficient $C_B = 0.40 - 0.60$, Barnaby (1863) suggested the following formulae:

$$w_T = 0.80 C_B - 0.26 \qquad (54)$$

When a ship is moving forward with a non-zero rudder angle, an interaction between the flow around rudder and hull occurs, decreasing the lift force applied on the rudder. However, an additional transverse force acting in same direction is generated at the aftbody. When comparing with the rudder lift without hull interaction, it can be observed that the total transverse force is increased by the factor: $1 + a_H \cdot a_H$, which can be calculated with the formulae suggested by Söding (1982):

$$a_H = \frac{1}{1 + (4.9 \cdot e / T + 3 \cdot c / T)^2} \qquad (55)$$

where T is the mean draft of the ship, e the mean distance between the front edge of the rudder and the aft end of the hull and c the mean rudder chord length.

4.5. Rudder Cavitation

Rudder cavitation, likewise propeller cavitation, is caused by water evaporation at point of high flow velocity, where the pressure locally drops below the vapor pressure of the water. This may lead to such called cavitation erosion, resulting in damage and loss of the material and further formation of grooves, valleys, wavy surfaces, holes etc. which finally lead to reduced hydrodynamic performance of the control surface.

The following types of rudder cavitation can be distinguished:

- bubble cavitation of the rudder side plating [Fig. 12],
- propeller tip vortex cavitation [Fig. 13],
- propeller hub cavitation,
- rudder sole cavitation [Fig. 14],
- cavitation of the surface irregularities [Fig. 15].

It has been found that for large rudder angles the cavitation occurrence is unavoidable in ships of more than 10 knots operating speed [2]. For this reason, the rudder cavitation

of the fishing vessel, which design speed is 12 knots, should be carefully investigated [*Chapter 5.2.3*].

Fig. 12. Bubble cavitation
Source: The Hamburg Ship Model Basin
Newsletter, No. 1, 2003
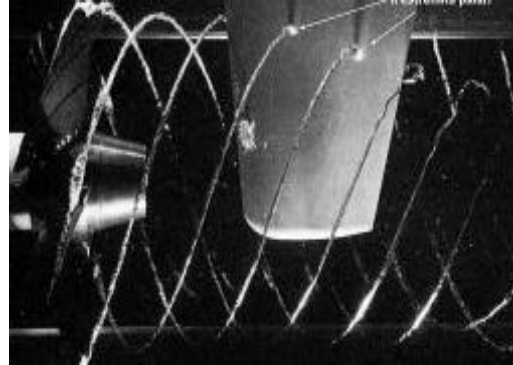
Fig. 13. Propeller tip vortex cavitation
Source: The Hamburg Ship Model Basin
Newsletter, No. 2, 2004

Fig. 14. Rudder sole cavitation
Source: Schiffbau, No. 12, 2005

Fig. 15 Cavitation of the surface irregularities
Source: Manevrabilitatea Navei, 2008

4.6. Rudder Requirements

The main requirement of the rudder is the capability of developing the sufficient sideforce to maintain the vessel on a steady course at nominal service speeds and to manoeuvre at lower speeds. Additionally, in case of course-keeping, the rudder should be able to minimize the deviations from the set course. However, a highly manoeuvrable

vessel will be less controllable, and vice versa. Therefore, a compromise between two characteristics needs to be accepted, depending largely on the service(s) to be provided by a certain vessel.

To turn the ship in a desired manner, the rudder must be capable of putting and holding the ship at a given angle of attack against the flow of water past the hull. This angle of attack produces relatively large hydrodynamic forces to act on the hull causing the vessel to turn, whereas the rudder provides only a small effect at this stage. The forces acting on a ship during a steady turn are illustrated on the picture below [Fig. 16], with F_H being the force applied on the hull and F_R representing the rudder force.

The force acting on the rudder, F_R, depends upon the cross-sectional shape of the control surface area A, the velocity V through the water and the angle of attack α:

$$F_R = const.\rho A V^2 f(\alpha) \tag{56}$$

The constant in (56) depends upon the cross-section and the rudder profile, in particular the ratio between the rudder depth and its chord length. The lift is also sensitive to the clearance between the upper surface of the rudder and the hull. The typical rudder area in a merchant ship is between 1/60 to 1/70 of the product of length and draught [10].

It just needs to be added that the radial components of the forces on the rudder and the hull, F_R and F_H, must have a resultant causing the radial acceleration.

Classification Societies provide some rules and/or recommendations concerning rudder application, blade and stock scantling, forces and moments acting on the rudder etc. Bureau Veritas Rules [Pt B, Ch 10, Sec 1] state that for the ordinary profiles, the maximum orientation of the rudder at maximum speed should be limited to 35° on each side. Deflections greater than 35° are acceptable only for navigation or manoeuvres at very low speeds.

An undesirable feature of the rudder is that it produces a heel during the turn, as mentioned in sub-chapter 3.2. Although the rudder is intended to develop the motions only in the *xy*-plane (yaw motion), some other motions are induced by cross-coupling into the *xz*-plane (pitch) and *yz*-plane (roll). While the magnitude of pitch motion is respectively

small and can be neglected, the roll motion magnitude is usually large enough to be of significance for the designer.
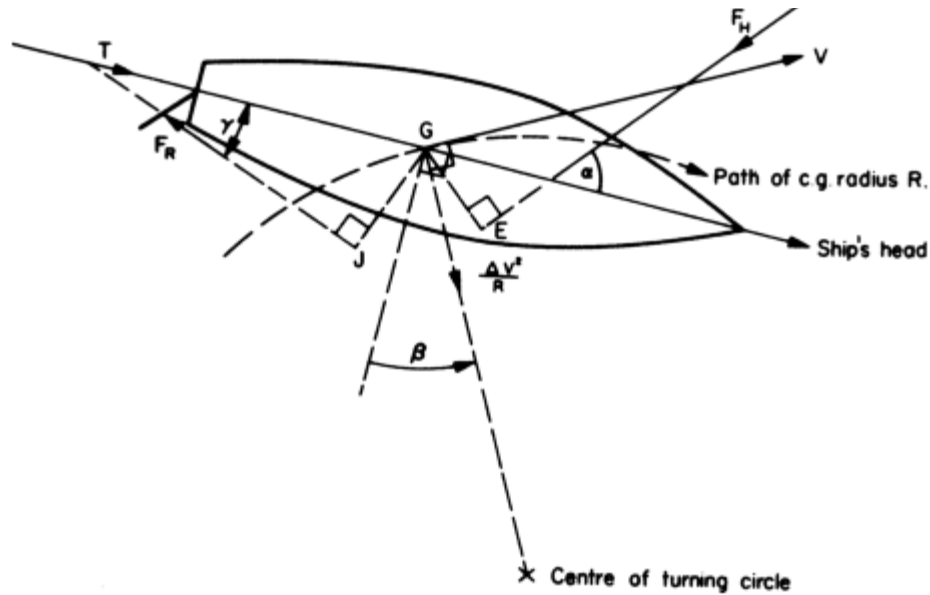
Fig. 16. Action of rudder in turning ship
Source: Rawson K.J., Tupper E.C., Basic Ship Theory, Vol. 2, 2001, p. 546

It just needs to be remembered that all the above concepts are based on a linear theory of motion. However, in full-scale ship performance, most of the problems appear to be non-linear which requires the introduction of higher degrees of derivatives to better capture the realistic deviations of forces and moments from a steady state condition.

5. GENERAL CHARACTERISTICS OF THE FISHING VESSEL

5.1. General Concept of a Fishing Vessel

A general definition of a fishing vessel describes this type of ship as "a vessel that commercially engages in the catching, taking, or harvesting of fish or an activity that can reasonably be expected to result in the catching, taking, or harvesting of fish" (46 U.S.C.A. §2101(11a)). Furthermore, commercial fishing vessels can be classified by architecture, the type of fish they catch, the fishing method they use or finally by the geographical region they operate within. However, detailed classifications are not of the interest of this thesis, hence will not be introduced in further details.

The size and autonomy of a fishing vessel is largely determined by its ability to handle, process and store fish onboard. The factors which influence the design of a fishing vessel maybe me grouped as follows (FOA, 2011):

- the species, location, abundance and dispersion of the fish resources;
- fishing gear and methods;
- geographical and climatic characteristics of the operating area;
- seaworthiness of the ship and safety of the crew;
- handling, processing and stowage of the catch;
- laws and regulations applicable to fishing vessel design, construction and equipment;
- availability of boatbuilding and fishing skills;
- choice of construction materials;
- economic viability.

According to FAO (2004), the world fishing fleet exceeds four million units, with about one-third being the decked vessels. However, the decked vessels of the length larger than 24 m (> 100 GT) amount to about 1 percent of the world fishing fleet, the average decked unit being around 10-15 m long (about 20 GT).

5.2. Fishing Vessel's Characteristics

5.2.1. Main Characteristics of the Ship and Model

The table below [Table 2] contains the main characteristics of the full-scale ship and the model under a full load condition. The vessel, called "Città di Genova" [17], has been actually operating in the Mediterranean Sea area and can be considered as a benchmark in hydrodynamic studies of fishing vessels.

Table 2. Main characteristics of the ship and model (full load condition)

Main characteristics	Full scale	Model scale (1/12)
Length overall, L_{OA} [m]	32.7	2.725
Length between perpendiculars, L [m]	25.0	2.083
Moulded breadth, B [m]	8.0	0.667
Volumetric displacement, ∇ [m^3]	296.0	0.171
Draft at fore perpendicular, T_F [m]	2.42	0.202
Draft at aft perpendicular, T_A [m]	2.74	0.228
Medium draft, T_M [m]	2.58	0.215
Longitudinal centre of gravity, x_G [m]	11.32	0.943
Vertical centre of gravity, z_G [m]	3.05	0.254
Transverse metacentre height, GM_T [m]	0.65	0.054
Block coefficient, C_B	0.574	0.574
Waterline are coefficient, C_W	0.819	0.819
Natural roll period, T_ϕ [s]	6.2	1.8
Roll radius of gyration, k_{xx} [m]	2.46	0.205
Pitch radius of gyration, k_{yy} [m]	6.78	0.565
Yaw radius of gyration, k_{zz} [m]	6.9	0.575
Area of load waterline, A_{WL} [m^2]	163.74	1.137
Propeller diameter, D [m]	1.8	0.15
Ship speed, U	12 kn	1.8 m/s

5.2.2. Hull Geometry

The body plan of the vessel "Città di Genova" [Fig. 17, 18] represents a typical hull geometry of a fishing vessel designed to operate on the Mediterranean Sea. The characteristic double hard chine and explicit rectangular bar keel can be easily noticed on the figures below.
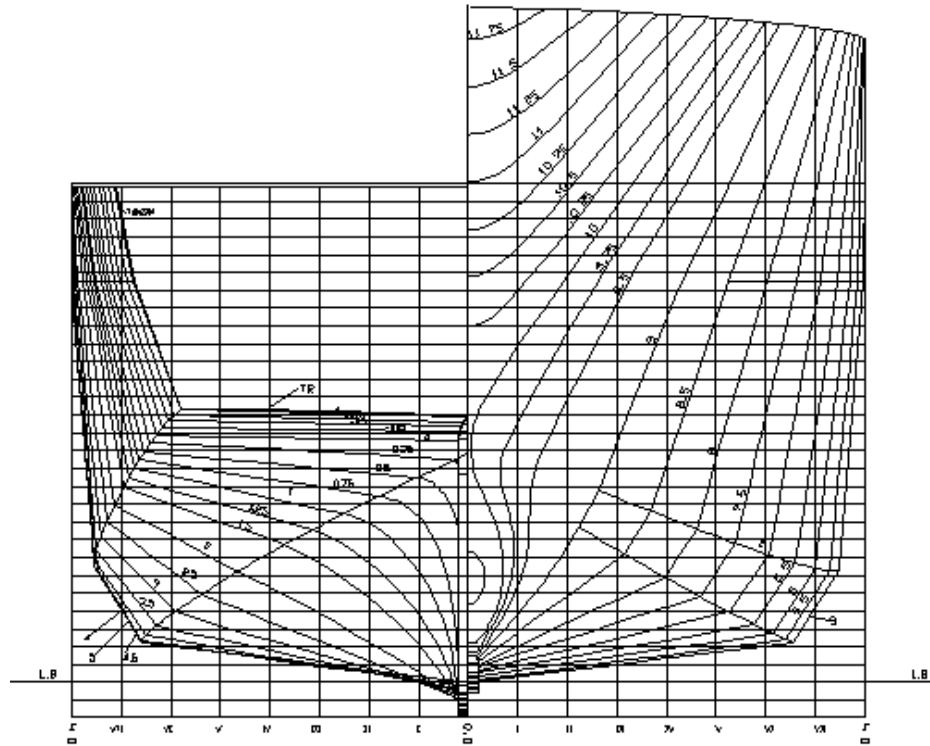
Fig. 17. 2D body plan of the fishing vessel "Città di Genova"
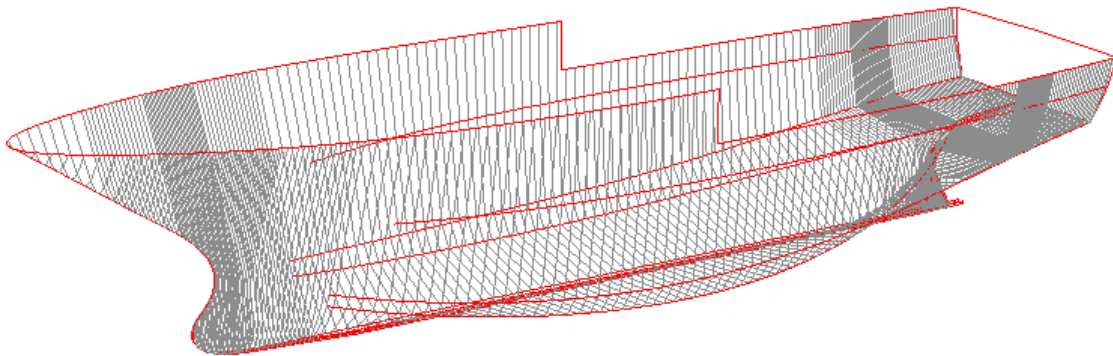
Fig. 18. 3D body plan of the fishing vessel "Città di Genova"

5.2.3. Rudder Design and Hydrodynamic Performance

Fig. 19 represents the main geometric elements of the rudder:

- mean span, $\bar{b}$;

- mean chord, $\bar{c} = (\bar{c}_r + \bar{c}_t)/2$;

- root chord, $\bar{c}_r$;

- tip chord, $\bar{c}_t$;

- taper ratio, $TR = \bar{c}_t / \bar{c}_r$;

- root thickness, $\bar{t}_r$;

- tip thickness, $\bar{t}_t$;

- mean thickness, $\bar{t} = (\bar{t}_r + \bar{t}_t)/2$;

- aspect ratio, $\lambda = \bar{b} / \bar{c}$;

- relative thickness, $\bar{t} / \bar{c}$.
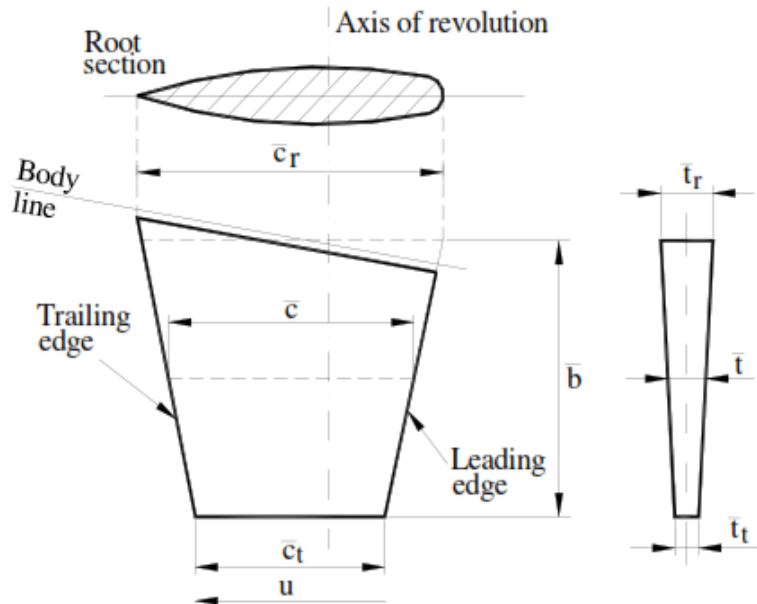
Fig. 19. Geometric elements of the rudder
Source: Manevrabilitatea Navei, 2008, p. 108

Basing on the previously-mentioned geometry, Table 3 provides the typical values of the geometric ratios for different types of ships [7]:

Table 3. Typical values of rudder geometric ratios

TYPE OF SHIP		Aspect ratio $\overline{b}/\overline{c}$	Relative thickness $\overline{t}/\overline{c}$
Ships with single screw	Passengers and cargo ships	1.8	0.18
	Coaster ships	1…1.15	0.16…0.18
	Tugs	1.8	0.185
	Fishing vessels	1.5…3.33	-

As mentioned in Chapter 4, rudders are designed in such a manner to provide high lift effect with minimum drag. However, there is no general rule to determine the area of the rudder due to the various steering and manoeuvring requirements for different ships and different operational conditions. Manoeuvrability properties itself are very complex and dependent on factors involving body lines, propellers and rudder geometry. Additionally, the rudder torque may also vary significantly, depending whether the ship is fully or partly loaded. For this reason, it is difficult to provide a general solution to determine the rudder area that would guarantee good manoeuvrability performance for all kind of ships.

However, as a result of several research activities, Det Norske Veritas succeeded to develop a formulae to estimate the minimum rudder area for the merchant vessels:

$$\frac{A}{L \times T} = 0.01 \left[1 + 50 C_B^2 \left(\frac{B}{L} \right)^2 \right] \tag{57}$$

One just has to remembered that vessels such as tugs, trawlers, supply vessels, ferries and warships generally require relative larger rudder area than seagoing merchant ships. Table 4 offers guidance for a preliminary estimation of area for a range of coastal and seagoing ships [6]. In both cases, the rudder area, A, is expressed in terms of an approximation to the underwater lateral area ($L \times T$) and is the sum of the areas if more than one rudder is fitted.

Table 4. Rudder areas for different types of ships

SHIP TYPE	$\dfrac{A}{L \times T}$
Single-screw merchant ships	0.016 - 0.018
Twin-screw merchant ships	0.016 – 0.022
Warships	0.024 – 0.028
Tugs, trawlers etc.	0.030 – 0.040

Using the DNV formulae (57), the minimum rudder area of the investigated fishing vessel, expressed in terms of underwater area, should be equal to 0.027, which is a little less than the minimum value provided in Table 4. However, as the (57) has been developed for the merchant ships, the obtained value should only serve as a starting point for further and more accurate calculations.

Basing on the minimum rudder area obtained from the DNV formulae, as well as on the typical values of geometric ratios and rudder areas [Table 3 and 4], the following rudder geometry [Fig. 20] has been design to be mounted on the investigated ship:
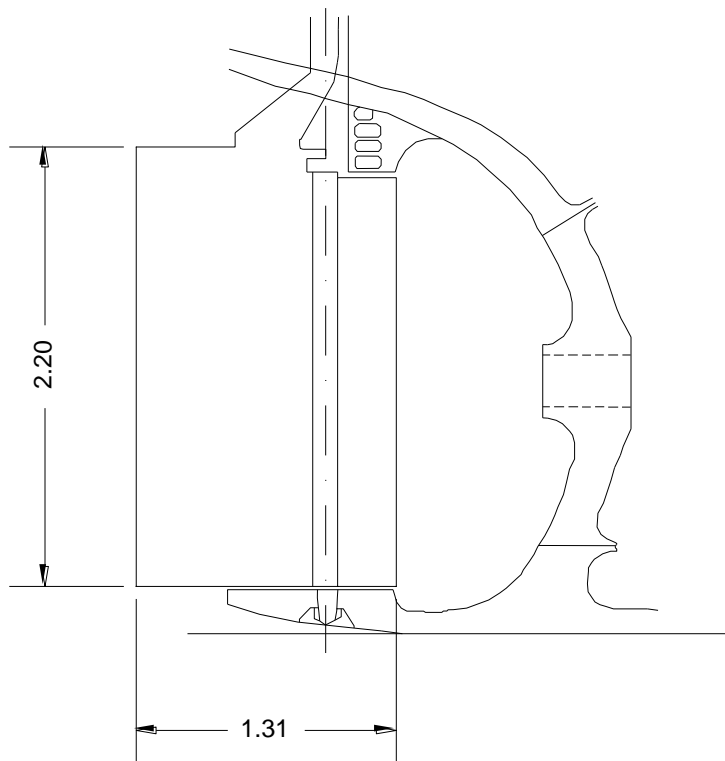
Fig. 20. Rudder geometry

Searching for a relatively small thickness and, at the same time, the capability of withstanding the important forces acting on it, NACA 0018 profile has been chosen as the optimal one for the designed rudder. To verify the proposal, the results of previously performed hydrodynamic analysis of different rudders have been investigated [11]. These results prove that the NACA 00 rudders generate the largest maximum lift coefficient and stall angle among other rudders with the same thickness. Additionally, the stock moment coefficient of the NACA 00 rudder is much smaller than other rudder profiles, which is favorable from the manoeuvring point of view. Finally, it had been found that thicker NACA 00 rudders give larger C_{Lmax} and greater α_{stall} without much increase in drag force [11]. For all the above reasons, NACA 0018 seemed to be the optimal rudder profile for the investigated fishing vessel.

The NACA 0018 hydrofoil is symmetrical (00 indicates no chamber) [Fig. 21]. The last two digits describe the maximum thickness of the foil as percent of the chord, hence the maximum thickness of the designed rudder equals: $t_{max} = 0.18\,\overline{c} = 0.24$ m.

The main rudder geometry data is presented in Table 5:

Table 5. Main geometric parameters of the rudder

span [m]	$\overline{b}$	2.20
chord [m]	$\overline{c}$	1.31
area [m^2]	A_R	2.88
max. thickness [m]	t_{max}	0.24
aspect ratio [-]	λ	1.68
relative thickness [-]	$\overline{t}\,/\,\overline{c}$	0.18
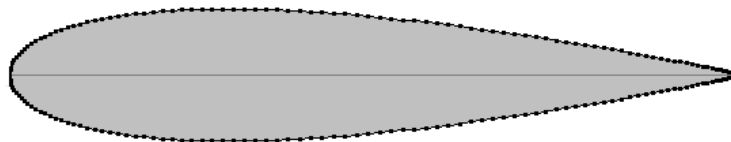
Fig. 21. NACA 0018 profile

Subsequently, with a use of the Preliminary Hydrodynamics Performance (PHP) program developed at the Naval Architecture Faculty of the "Dunarea de Jos" University of Galati (Romania), the hydrodynamic performance of designed rudder has been computed. The main objective of this computation was to estimate the hydrodynamic torque applied on the rudder in order to choose the optimal steering gear for the investigated vessel.

The software allows the user to choose one of three basic types of the rudder:

- semi-balanced rudder;
- suspended rudder with the upper edge situated at a certain distance from the hull, which is less than the max. thickness of the rudder blade;
- suspended rudder with the upper edge situated at a certain distance from the hull, which is greater than the max. thickness of the rudder blade.

Since the distance of the upper edge of the designed rudder to the ship's hull is greater than the max. thickness of the NACA 0018 profile (0.24 m) and equals 0.26 m, the third option has been chosen as the input data, with H = 2.465 m, h_i = 0.152 m and $\bar{b}$ (span) = 2.2 m [Fig. 22].
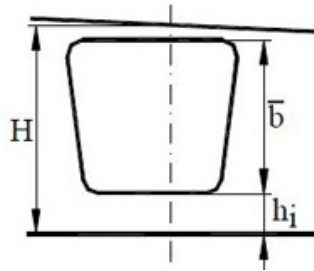
Fig. 22. Main dimensions of the designed rudder

Accordingly, the following position [Fig. 23] of the rudder-propeller system has been selected, with d = 1.17 m, r = 0.15 m and R = 0.9 m.
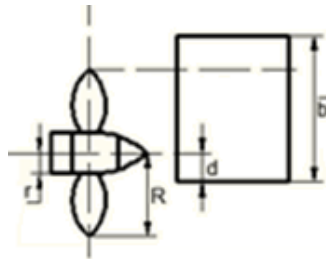
Fig. 23. Position and main dimensions of the rudder-propeller system

After running the computation process, the following output data have been provided by the PHP program [Table 6]. The optimum position of the rudder stock has been found by means of implemented Voitkounsky method (1985).

Table 6. Hydrodynamic characteristics of the designed rudder

Characteristics	Value
Optimal distance from the rudder stock to the leading edge [m]	0.240
Optimal distance from the rudder stock to the trailing edge [m]	-1.070
Maximum hydrodynamic torque [kNm]	32.247
Supplementary torque due to friction [kNm]	6.449
Total hydrodynamic torque [kNm]	38.697

Additionally, basing on the calculated total hydrodynamic torque, the following steering gear [Table 7] has been selected from the commercial catalogue [*for more details, see Appendix 1*]:

Table 7. Main characteristics of the steering gear

Brand	Type	Max. stock diam. [mm]	Max. working torque [kNm]	Max. rudder angle [deg]	Weight approx. [kg]	Max radial load [kN]	Max. axial load [kN]
Rolls Royce	SR 562-FCP	160	40	2 x 61.0	400	175	104

Having the initial rudder design completed, the bubble cavitation on the rudder side plating has been finally investigated by means of Brix method (1983) introduced in the PHP program. The calculation has been performed for three different inflow angles, α, estimated on the basis of the rotation of the propeller slipstream (eq. 58) [3], with the results presented in Table 8. Equation 58 is derived from the momentum theorem with an empirical correction term for the local wake (Nishiyama, 1975):

$$\alpha(°) = \arctan\left(4.3 \cdot \frac{K_Q}{J^2} \cdot \sqrt{\frac{1-\bar{w}}{1-w_{local}}} \Big/ \frac{V_{max}}{V_A} \right) \tag{58}$$

with $\bar{w}$ being the mean wake number, w_{local} the wake number at the respective position, V_{max} the maximum speed of the ship, V_A the advance speed of the propeller, K_Q the torque coefficient and J the advance coefficient.

Table 8. Results of the rudder cavitation calculation

Flow angle, α [deg]	Static pressure [kPa]	Dynamic pressure [kPa]	Total pressure [kPa]
13	112.320	-54.014	58.306
22	112.320	-74.642	37.678
26	112.320	-86.624	25.696

If the resulting minimum pressure on the suction side is negative or slightly positive, the side plating of the rudder is prone to cavitation. For a right turning propeller, the cavitation will occur on starboard side in the upper part of the rudder and on the port side in the lower part of the rudder (relative to the propeller axis) [3]. However, as for all the flow angles, α, the resulting pressure is positive, no blade side cavitation should be expected on the designed rudder.

6. HYDROSTATIC CHARACTERISTICS OF THE LOADING CONDITION

6.1. Introduction to the Hydrostatics of a Ship

On the prediction of ship manoeuvring performance at the initial design stage, it is considered that a loading condition is one of the important parameters caused for the manoeuvring characteristics. Additionally, the hydrostatic properties of a vessel are extremely important within its project before it can be moved on into hydrodynamic performance simulation.

Usually the input to the hydrostatic calculation is an offset file of transverse stations, provided in a computer file. On the other hand, the common procedure to display the hydrostatic calculation results is to present them either in a tabular form or graphically as a set of hydrostatic curves. These curves normally represent the hydrostatic information relevant to zero-trim condition with the following information plotted against varying drafts:

- longitudinal and vertical centre of buoyancy (LCB and VCB, respectively),
- longitudinal centre of flotation (LCF),
- transverse metacentre above the keel (KM_T),
- displacement of the vessel (∇),
- tonnef per centimeter immersion (TPC),
- moment to change trim one centimeter (MTC).

The first three characteristics depend only upon the hull geometry and are affected neither by the density of the water nor by the weight of the ship. The following three features depend greatly on the weight density of the water, with the MTC being additionally related to the vertical position of the ship's centre of gravity.

In the hydrostatic curves, the draft is usually placed on the vertical axis and dependent quantities are plotted on the horizontal one. However, as these quantities are given in different units and widely varying magnitudes, the usual practice is to scale them by power of 10 (or other factor) to fit graphically on the plot.

The hydrostatic table would usually contain some additional properties, such as longitudinal metacentric height (KML), wetted surface area (WSA) or waterplane area (WPA), as well as some geometrical coefficients.

6.2. Hydrostatic Characteristics of the Fishing Vessel

6.2.1. Input Ship Data

The hydrostatic characteristics of the investigated fishing vessel are calculated by means of TRIBON Initial Design software, which is a naval architecture CAD/CAM family of programs widely used in shipbuilding and offshore industry. The Calc Module of TRIBON provides the main tool by which the hydrostatics, stability and other routine naval architecture calculations can be performed, allowing the designer to assess the hullform characteristics as well as the effects of internal arrangements and loading.

To obtain the hydrostatic results, the designer is first obliged to introduce some general ship data which, together with the input hull geometry model, provides the basic data for many subsequent activities. Hydrostatic particulars can then be calculated for the main hull (including appendages, if defined) for either moulded or extreme drafts, for a range of draft, and for a single combined trim and heel condition. In the phase of initial design of the fishing vessel, the range of moulded drafts from $0 - 3$ meters with the increment of 0.25 m have been introduced. Additionally, the design draft (2.58 m) have been implemented as additional input draft. The pivot point along the *x*-axis has been chosen to be placed in the amidships, e.i. at the distance of 12.5 m from the aft perpendicular. The calculation is performed for the calm water conditions (no waves) for a non-trimmed vessel. The ship is equipped with a conventional type of rudder of 2.88 m^2 planform area with the shaft line situated at the aft perpendicular. All the input data for the hydrostatic calculation have been gathered in the table below [Table 9].

Table 9. Fishing vessel input data for the hydrostatics calculation

Length overall [m]	32.7
Length between perpend. [m]	25
Breadth moulded [m]	8
Depth moulded [m]	6.8
Design draft [m]	2.58
Range of drafts [m]	0 - 3
Rudder area [m^2]	2.88
Water density [t/m^3]	1.025
Water temperature [°C]	15

6.2.2. Output of the Hydrostatics Computation

The results of the hydrostatics computation are presented to the designer in both graphical and tabular form. The graphics include the Hydrostatic Curves diagram [Fig. 24] and the Sectional Area Curves (a.k.a Bonjean Curves) [Fig. 25], whereas the tables consist of detailed hydrostatic characteristics and additional properties of the fishing vessel [Table 10] as well as values of sectional areas at various waterlines [Table 11].
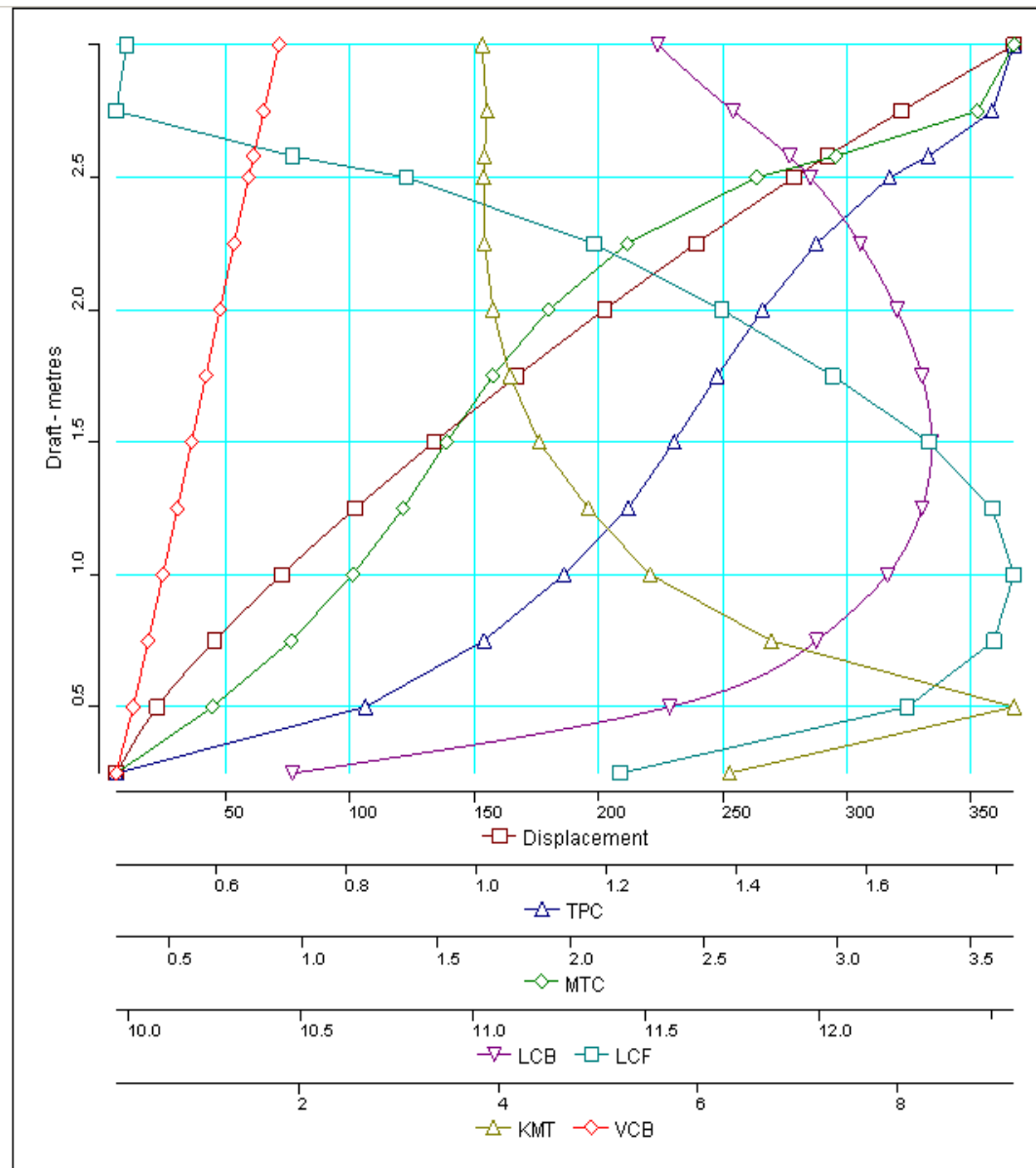
Fig. 24. Hydrostatic Curves of the fishing vessel
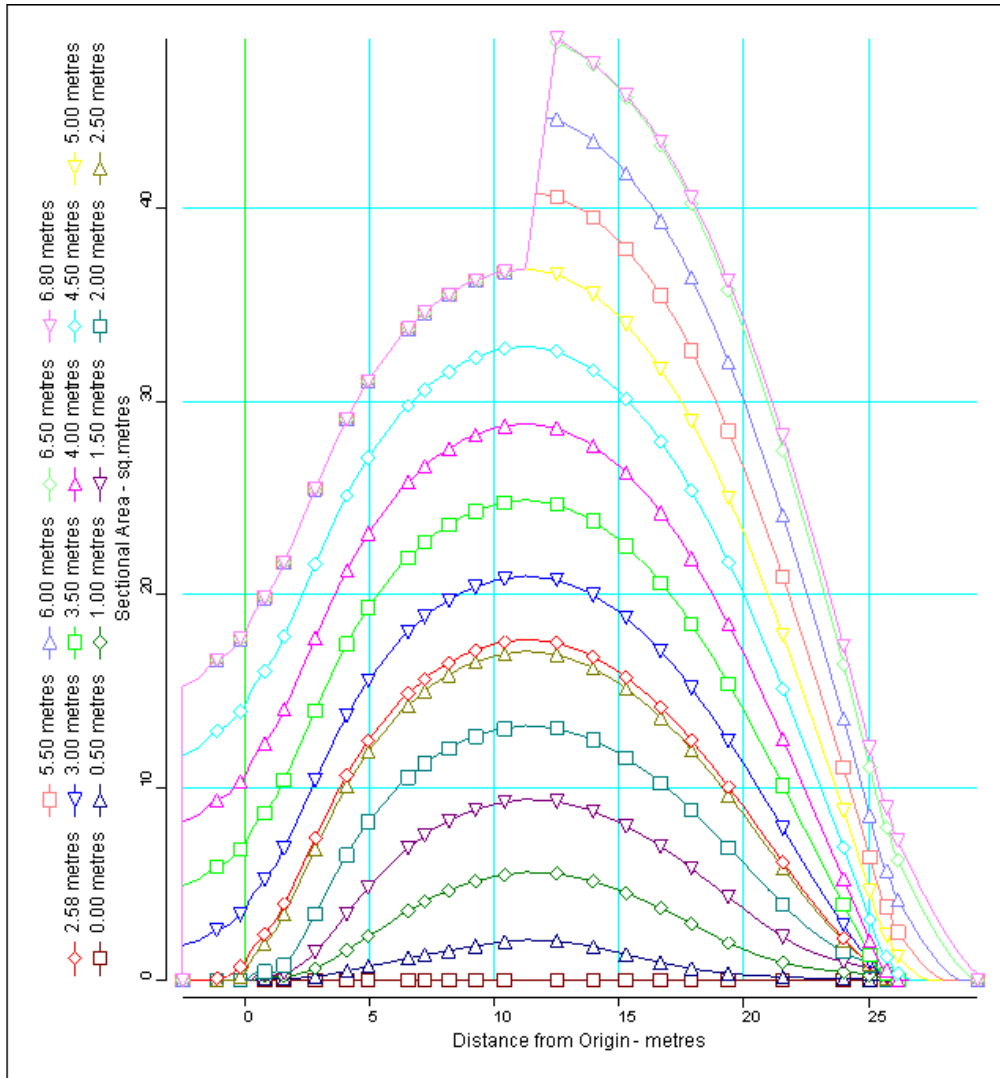
Fig. 25. Bonjean Curves of the fishing vessel

With the results given in Tables 10 and 11, the basic hullform coefficients can be calculated for the vessel at the design draft:

- the block coefficient, C_B, determining the fullness of the submerged hull, is obtained as follows:

$$C_B = \frac{\nabla}{\rho \cdot L \cdot B \cdot T} = \frac{292.22}{1.025 \cdot 25 \cdot 8 \cdot 2.58} = 0.553 \qquad (59)$$

- the waterplane area coefficient, C_W, expressing the fullness of the waterplane at a design draft, can be obtained with the following formulae:

$$C_W = \frac{WPA}{L \cdot B} = \frac{165.32}{25 \cdot 8} = 0.827 \tag{60}$$

- the midship section coefficient, C_M, describing the fullness of the underbody, is given by:

$$C_M = \frac{A_M}{B \cdot T} = \frac{17.503}{8 \cdot 2.58} = 0.848 \tag{61}$$

- finally, the prismatic coefficient, C_P, being used to evaluate the distribution of the volume of the underbody, can be written as the ratio between C_B and C_M:

$$C_P = \frac{C_B}{C_M} = \frac{0.553}{0.848} = 0.652 \tag{62}$$

Table 10. Hydrostatic characteristics of the fishing vessel at a certain draft

Draft (m)	Displt (t)	LCB (m)	VCB (m)	WPA (m^2)	LCF (m)	KML (m)	KMT (m)	WSA (m^2)	TPC (t/cm)	MTC (t-m/cm)
0.25	6.07	10.478	0.158	43.58	11.425	124.585	6.316	46.76	0.45	0.30
0.50	22.48	11.568	0.326	80.89	12.257	73.949	9.178	87.94	0.83	0.66
0.75	45.69	11.994	0.480	98.70	12.507	52.803	6.738	111.49	1.01	0.96
1.00	72.58	12.199	0.627	110.70	12.565	41.525	5.522	130.30	1.13	1.19
1.25	102.25	12.299	0.772	120.31	12.502	34.397	4.901	147.69	1.23	1.38
1.50	133.99	12.327	0.915	127.16	12.320	29.604	4.406	164.36	1.30	1.54
1.75	167.40	12.299	1.057	133.65	12.041	26.598	4.113	181.53	1.37	1.71
2.00	202.52	12.226	1.199	140.48	11.719	24.901	3.942	199.42	1.44	1.92
2.25	239.52	12.120	1.342	148.52	11.349	24.450	3.859	218.58	1.52	2.21
2.50	278.91	11.975	1.488	159.51	10.806	25.663	3.848	241.83	1.64	2.70
2.58	292.22	11.915	1.536	165.32	10.477	27.150	3.858	252.83	1.69	2.99
2.75	322.00	11.753	1.641	174.89	9.967	28.993	3.881	272.06	1.79	3.52
3.00	367.25	11.534	1.793	178.14	9.997	26.709	3.835	289.16	1.83	3.66

It can be observed that the above coefficients, C_B and C_W, differ slightly from the main characteristics of the experimental model. The main reason for this is that at the design stage, the numerical computation has been performed for a non-trimmed vessel. Additionally, the above coefficients have been obtained on the basis of the hydrostatic

calculation of TRIBON, where the numerical model of the ship can be slightly different from the experimental one.

Table 11. Sectional areas of the fishing vessel

WL Heights Station	0.00	0.50	1.00	1.50	2.00	2.50	2.58	3.00	3.50	4.00	4.50	5.00
-0.500	0.000	0.000	0.000	0.000	0.000	0.000	0.081	2.543	5.827	9.283	12.865	16.527
-0.375	0.000	0.000	0.000	0.000	0.000	0.000	0.129	2.694	5.993	9.457	13.055	16.736
-0.250	0.000	0.000	0.000	0.000	0.000	0.003	0.240	2.902	6.216	9.687	13.299	16.999
-0.125	0.000	0.000	0.000	0.000	0.000	0.086	0.562	3.263	6.618	10.123	13.763	17.484
0.000	0.000	0.000	0.000	0.000	0.000	0.383	0.893	3.633	7.027	10.565	14.233	17.975
0.250	0.000	0.089	0.212	0.327	0.430	1.604	2.125	4.918	8.379	11.988	15.721	19.512
0.500	0.000	0.078	0.183	0.268	0.448	2.606	3.137	5.988	9.502	13.140	16.891	20.715
0.750	0.000	0.079	0.238	0.511	1.253	4.197	4.742	7.647	11.209	14.896	18.682	22.536
1.000	0.000	0.150	0.459	1.071	2.647	5.937	6.490	9.442	13.058	16.787	20.616	24.507
1.500	0.000	0.395	1.284	2.900	5.762	9.295	9.868	12.911	16.615	20.408	24.286	28.228
2.000	0.000	0.738	2.344	4.907	8.317	11.957	12.545	15.664	19.444	23.297	27.218	31.191
2.500	0.000	1.081	3.398	6.562	10.207	13.929	14.530	17.710	21.552	25.453	29.405	33.386
3.000	0.005	1.392	4.305	7.800	11.540	15.329	15.939	19.167	23.056	26.994	30.978	34.984
3.500	0.000	1.676	4.952	8.632	12.424	16.260	16.877	20.138	24.060	28.023	32.017	36.020
4.000	0.002	1.935	5.382	9.135	12.960	16.821	17.443	20.721	24.660	28.638	32.640	36.634
5.000	0.001	2.026	5.527	9.268	13.059	16.887	17.503	20.757	24.670	28.624	32.610	36.606
6.000	0.000	1.431	4.687	8.191	11.766	15.401	15.988	19.096	22.852	26.669	30.534	34.423
6.500	0.000	1.048	3.996	7.289	10.674	14.134	14.695	17.671	21.284	24.972	28.723	32.520
7.000	0.000	0.717	3.233	6.224	9.351	12.565	13.088	15.874	19.277	22.775	26.357	30.009
7.500	0.000	0.451	2.359	4.962	7.746	10.647	11.121	13.663	16.796	20.044	23.403	26.864
8.000	0.000	0.285	1.612	3.724	6.093	8.599	9.013	11.246	14.033	16.961	20.030	23.240
8.500	0.000	0.194	1.030	2.520	4.364	6.385	6.724	8.574	10.933	13.460	16.163	19.053
9.000	0.000	0.119	0.668	1.591	2.801	4.230	4.477	5.858	7.688	9.726	11.986	14.483
9.250	0.000	0.100	0.557	1.281	2.176	3.265	3.459	4.569	6.098	7.860	9.870	12.141
9.500	0.000	0.071	0.458	1.031	1.652	2.374	2.510	3.327	4.530	5.993	7.730	9.753
9.750	0.000	0.053	0.384	0.836	1.233	1.590	1.663	2.153	2.994	4.127	5.570	7.325
10.000	0.000	0.017	0.288	0.634	0.830	0.909	0.924	1.046	1.449	2.209	3.332	4.803
10.125	0.000	0.000	0.199	0.469	0.547	0.552	0.553	0.557	0.694	1.248	2.188	3.502
10.250	0.000	0.000	0.051	0.141	0.153	0.170	0.173	0.186	0.195	0.483	1.240	2.393
10.375	0.000	0.000	0.000	0.000	0.000	0.000	0.000	0.000	0.008	0.228	0.794	1.791
10.500	0.000	0.000	0.000	0.000	0.000	0.000	0.000	0.000	0.000	0.000	0.301	1.129

7. MANOEUVRABILITY PERFORMANCE PREDICTION IN THE INITIAL DESIGN PHASE

7.1. TRIBON Powering Calculation

7.1.1. Resistance of the Fishing Vessel

The Powering Module of TRIBON incorporates a number of well-proven empirical methods to estimate the resistance of a given hullform and its appendages, which will be subsequently used to predict the manoeuvring performance of the vessel.

The hydrodynamic calculation is done on the basis of the loading condition described in the previous chapter. However, additional information need to be introduced in order to obtain the most reliable results. One of them would be the appendage resistance factor $(1+k_2)$ which allows to take into account the hydrodynamic performance of various types of appendages. Basing on the values provided by Holtrop & Mennen [13], the resistance factor for the rudder behind the skeg of the fishing vessel has been given a value of 1.750.

TRIBON provides various empirical methods to estimate the ship's resistance. However, some of them would only give accurate results for a certain types of vessels. Among them the two following methods, anticipated to give the most precise results, have been chosen to assess the resistance of the fishing vessel:

- Holtrop & Mennen method, with accuracy claimed to be satisfactory for 95% of the cases as long as the following hull parameters are preserved:

for trawlers, coasters, tugs: $Fn \leq 0.38$ $0.55 \leq C_P \leq 0.65$ $3.9 \leq L/B \leq 6.3$ $2.1 \leq B/T \leq 3.0$

- Van Oortmerssen method, generally developed to estimate the resistance of small ships such as trawlers or tugs. The limitations of this method are as follows:

$Fn \leq 0.50$ $0.50 \leq C_P \leq 0.73$ $3.0 \leq L/B \leq 6.2$ $1.9 \leq B/T \leq 4.0$ $8.0 \leq L_{WL} \leq 80.0$

To validate the choice of the resistance calculation method, the following hull parameters of the investigated vessel have been found:

$Fn = 0.39$ $C_P = 0.652$ $L/B = 3.1$ $B/T = 3.1$ $L_{WL} = 26.7\ m$

It can be noticed that all the above parameters fit well within the range of Van Oortmersen method, whereas at the same time all of them slightly exceed or fall below the scope concerning the Holtrop & Mennen method.

However, as both of the above-mentioned methods have been initially developed to provide the resistance of a fishing vessel, both of them have been used in the computation process. The results have then been verified by comparing them with the ones obtained during the experiments performed in a towing tank and extrapolated into a full scale vessel [Table 12, Fig. 26].

Table 12. Empirical and experimental results of the fishing vessel resistance

Speed [kn]	Ship resistance [kN] *Holtrop & Mennen*	Ship resistance [kN] *Van Oortmerssen*	Ship resistance [kN] *Experimental*
6	5.13	4.57	6.7
7	7.02	6.42	9.4
8	9.55	9.02	13.1
9	13.56	17.18	19.5
10	19.01	24.03	27.5
11	25.34	33.89	38.4
12	36.75	64.21	59.2
13	57.53	104.45	N/A
14	79.58	138.03	N/A

It can be observed [Fig. 26] that the resistance results obtained by means of the Holtrop & Mennen method differ quite significantly comparing with two other methods. At the same time, some similarities between the curves indicating the resistance results obtained with Van Oortmerssen and experimental method can be noticed, since both curves represent quite similar trend. Additionally, the numerical values of these methods are fairly comparable, whereas the ones given by Holtrop & Mennen method vary considerably, especially for the velocities over 10 knots [Table 12]. For these reasons, the Van Oortmerssen empirical method seems to be much more accurate for this type of vessel.
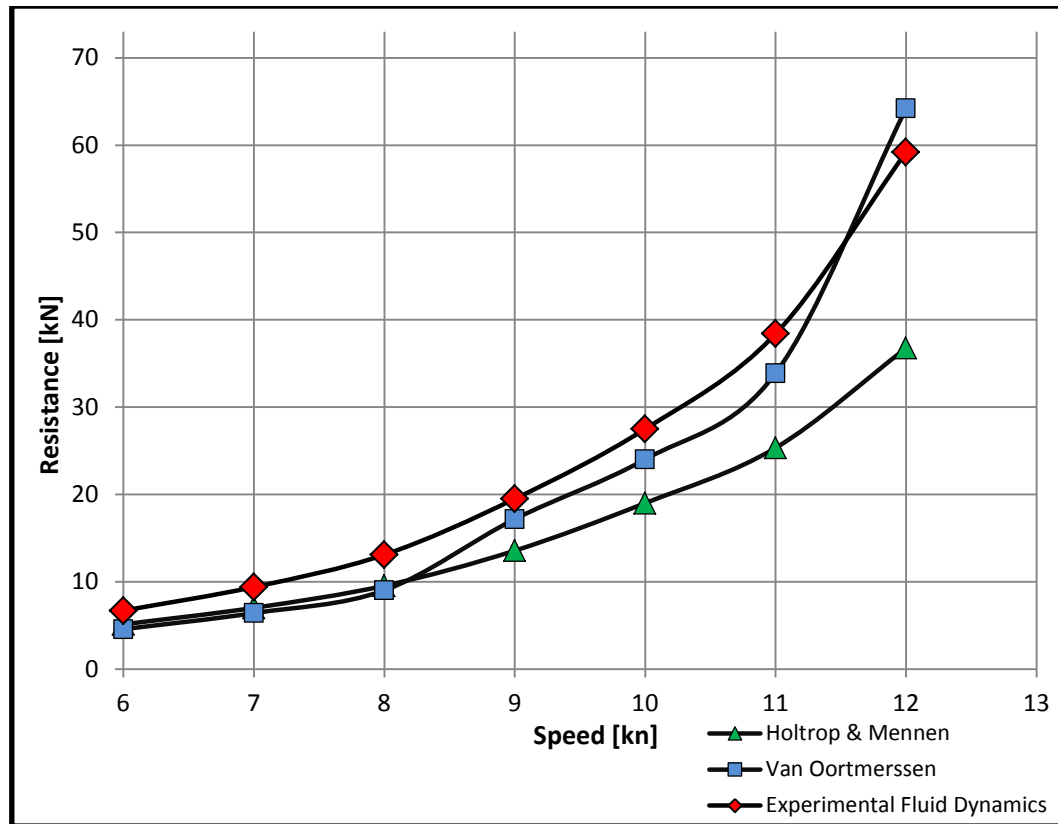
Fig. 26. Resistance comparison: experimental and empirical methods

7.1.2. *Propulsion of the Fishing Vessel*

Apart from the resistance calculation, the Powering Module of TRIBON facilitates the reliable estimation of the powering characteristics for a given hullform. The propeller characteristics are determined using standard series data of Wageningen B-Series and Gawn-Burril Series. The propulsion factors (wake fraction, ω, thrust deduction fraction, t and relative rotative efficiency, η_R) can be obtained by different empirical methods including Holtrop & Mennen as well as Van Oortmerssen method. Furthermore, on the basis of the input data and methods chosen, the basic propeller optimization is performed.

The input data for both calculation methods is presented in Table 13. The Wageningen B-series has been chosen as a reference data, as it is known to be suitable for classical vessels, whereas the Gawn-Burril series propellers are more appropriate for the higher loading conditions of warships.

Table 13. Propeller design input data

Design speed [kn]	12
Propeller diameter [m]	1.8
Number of blades	4
Pitch	fixed
Shaft height [m]	1.2
Min. effective BAR	0.7
Cavitation safety factor	1
Transmission efficiency	0.941
Propeller series	Wageningen B-series
Optimisation mode	by given speed and diameter

The propeller optimization process checks the proposed design against cavitation. For this reason, the shaft height (measured from the keel to the centre of the propeller shaft) needs to be introduced, from which the cavitation number is calculated. By interpolating the cavitation line with the value of the cavitation number, a minimum allowable value of blade area ratio is obtained. The program then ensures that the actual blade area ratio is greater than the minimum allowable value multiplied by the user-specified cavitation safety factor.

Using the resistance estimation and propulsion factors derived, the propeller characteristic is interpolated at each speed using the appropriate value of K_T/J^2. This provides the appropriate advance coefficient and open water efficiency at each speed from which the propeller RPM and delivered power are obtained from the following calculation:

$$P_E = R_T \cdot V \cdot (1 + SVC / 100) \tag{63}$$

$$\eta_H = (1 - t) / (1 - \omega) \tag{64}$$

$$\eta_O = (J \cdot K_T) / (2 K_{QO}) \tag{65}$$

$$\eta_R = K_{QO} / K_{QB} \tag{66}$$

$$\eta_D = \eta_O \cdot \eta_H \cdot \eta_R \tag{67}$$

$$N = 60 \cdot V \cdot (1 - \omega) / (J \cdot D) \tag{68}$$

$$P_D = P_E / \eta_D \tag{69}$$

$$P_S = P_D / \eta_T \qquad (70)$$

where V is the ship speed, R_T the total ship scale appended resistance, SVC the service margin, P_E the effective power, t the thrust deduction fraction, ω the wake fraction, J the advance coefficient, K_T the thrust coefficient, K_{QO} the open water torque coefficient, K_{QB} the behind torque coefficient, η_H the hull efficiency, η_O the open water efficiency, η_R the relative rotative efficiency, η_D the quasi propulsive efficiency (QPC), η_T the transmission efficiency, N the rotations per minute, P_D the delivered power and P_S the shaft power.

After running the calculation process, the following characteristics of the optimum propeller, presented in the Tables 14 and 15, have been proposed:

Table 14. Optimum propeller (H&M method)

Diameter	1.800	metres
Pitch ratio	0.937	
Effective BAR	0.700	(0.596 min)
Local Cavitation no	0.632	
Thrust load. coeff.	0.176	(0.207 max)
Kt/J^2	0.685	
Adv. coeff. J	0.558	
Thrust coeff. Kt	0.213	
Torque coeff. Kq	0.0338	
Open water eff.	0.558	

Table 15. Optimum propeller (VO method)

Diameter	1.800	metres
Pitch ratio	0.941	
Effective BAR	0.881	(0.880 min)
Local Cavitation no	0.448	
Thrust load. coeff.	0.167	(0.167 max)
Kt/J^2	1.057	
Adv. coeff. J	0.486	
Thrust coeff. Kt	0.250	
Torque coeff. Kq	0.0394	
Open water eff.	0.491	

Accordingly, the following powering results of the investigated fishing vessel have been obtained [Table 16 and 17] together with the graphical output of effective and shaft powers [Fig. 27 and 28].

Table 16. Speed-Power results – Holtrop & Mennen method

Speed kts	Pe (kW)	THDF	WFT	ETAR	ETA0	QPC	Ps (kW)	RPM
6.000	15	0.236	0.259	0.994	0.624	0.639	26	116.28
7.000	25	0.236	0.258	0.994	0.624	0.638	42	135.90
8.000	39	0.236	0.257	0.994	0.620	0.634	65	157.00
9.000	62	0.236	0.256	0.994	0.608	0.622	107	182.28
10.000	97	0.236	0.256	0.994	0.594	0.607	171	210.01
11.000	143	0.236	0.255	0.994	0.583	0.595	255	237.50
12.000	226	0.236	0.255	0.994	0.558	0.569	423	275.33
13.000	384	0.236	0.255	0.994	0.518	0.528	774	327.49
14.000	572	0.236	0.254	0.994	0.493	0.502	1213	374.79

Table 17. Speed-Power results – Van Oortmerssen method

Speed kts	Pe (kW)	THDF	WFT	ETAR	ETA0	QPC	Ps (kW)	RPM
6.000	14	0.251	0.212	1.102	0.623	0.653	22	117.64
7.000	23	0.240	0.214	1.090	0.622	0.655	37	137.63
8.000	37	0.230	0.216	1.076	0.618	0.652	60	159.46
9.000	79	0.222	0.217	1.061	0.583	0.615	137	198.36
10.000	123	0.215	0.219	1.045	0.570	0.599	219	227.40
11.000	191	0.210	0.221	1.029	0.552	0.576	353	260.78
12.000	396	0.206	0.223	1.011	0.490	0.506	831	329.57
13.000	698	0.203	0.224	0.993	0.444	0.453	1639	399.73
14.000	993	0.202	0.225	0.974	0.425	0.426	2476	451.27

It can be easily observed on the below figures, that both effective and shaft powers calculated on the basis of Van Oortmerssen method are much higher (almost double) for the design speed comparing to the results obtained with the Holtrop & Mennen method.

To verify the obtained results and to choose the most reliable method for the manoeuvring performance calculation, the comparison between the empirical and experimental results has been subsequently performed [Table 18, Fig. 29 and 30].
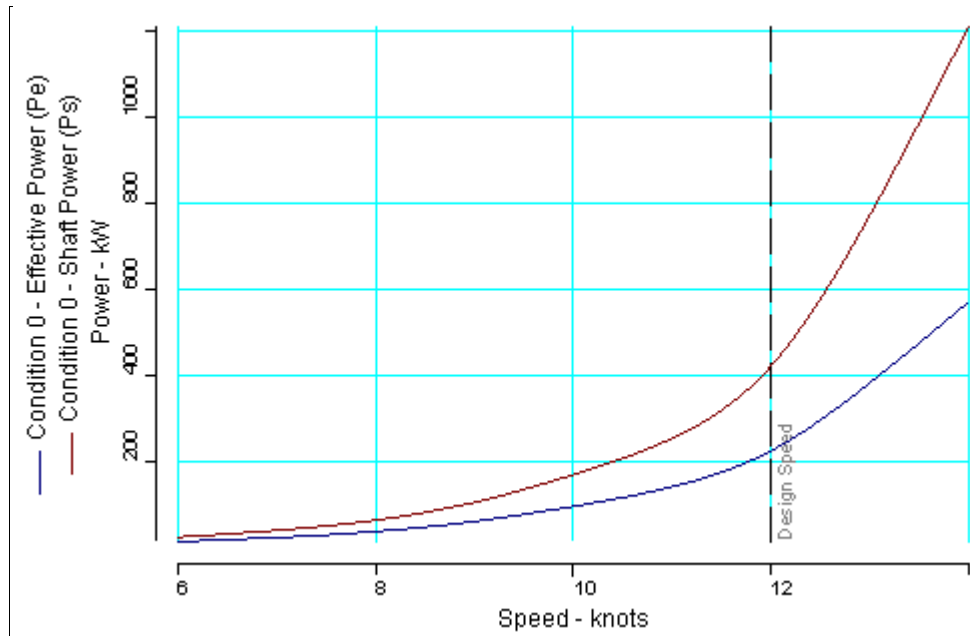
Fig. 27. Effective and shaft power vs. ship's speed – Holtrop & Mennen method
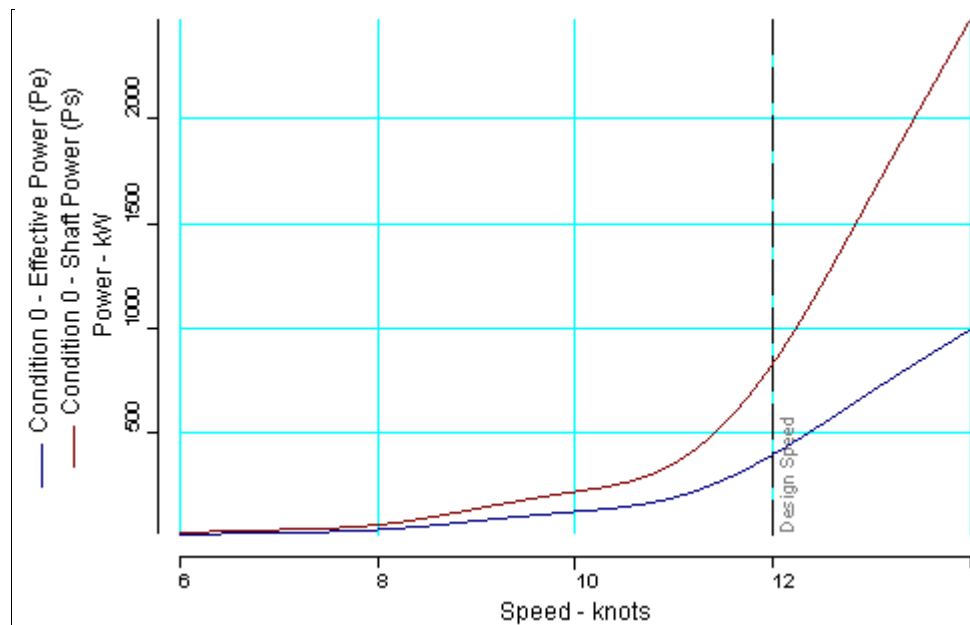
Fig. 28. Effective and shaft power vs. ship's speed –Van Oortmerssen method

Table 18. Empirical and experimental results comparison of effective power and rpm

Speed [kn]	Effective power [kW]			Propeller revolutions [rpm]		
	H&M method	*VO method*	*EFD*	*H&M method*	*VO method*	*EFD*
6	15.0	14.0	20.7	116.3	117.6	129.2
7	25.0	23.0	33.7	135.9	137.6	150.2
8	39.0	37.0	53.7	157.0	159.5	172.5
9	62.0	79.0	90.0	182.3	198.4	204.5
10	97.0	123.0	141.4	210.0	227.4	236.8
11	143.9	191.0	217.1	237.5	260.8	274.0
12	226.0	396.0	365.0	275.3	329.6	328.9
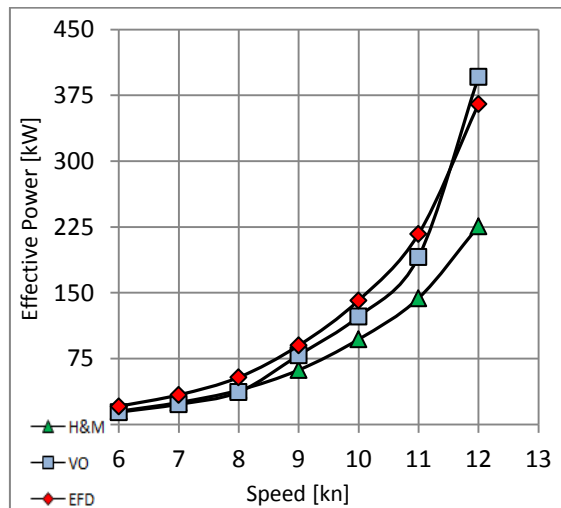
Fig. 29. Effective power comparison
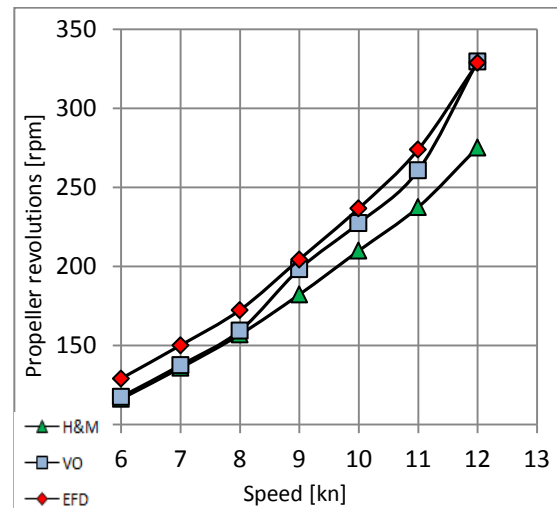
Fig. 30. Propeller revolutions comparison

It can be noted from the figures above that, similarly to resistance estimation, the Van Oortmerssen calculation method gives the results much more comparable to the experimental ones than the Holtrop & Mennen method. For this reason the following manoeuvring performance prediction of the fishing vessel will be estimated basing on the results obtained by the Van Oortmerssen method.

7.2. TRIBON Manoeuvring Performance Estimation

7.2.1. Manoeuvring Module of TRIBON

The Manoeuvring Module of TRIBON has been developed to predict the ship manoeuvring characteristics in the early design stages. The methods employed are of semi-empirical formulation type. The program calculates the hydrodynamic derivatives of the manoeuvring equation, ship resistance, propeller thrust and rudder forces and moments. The differential equations of ship motion in the horizontal plane are solved numerically in the time-domain to simulate the ship manoeuvring motion for certain rudder movements.

All the following manoeuvring simulations have been performed in a deep water conditions at the design speed. The input data concerning the vessel is the one obtained in Hydrostatics and Powering Module.

7.2.2. Turning Circle Manoeuvre

The Turning Circle manoeuvre has been simulated with the maximum rudder deflection (35 deg.) to portside. The output data, given in a graphical as well as tabular form, is presented below [Fig. 31, Table 19]. To allow easier comparison with other available data, the output results are given in a non-dimensional form.

Table 19. Summary of the turning circle test

Advance/L	at 90 deg	4.24
Transfer/L	at 90 deg	-1.84
Tactical diameter/L	at 180 deg	-4.01
Steady turning diameter/L	-	-3.03
Steady drift angle [deg]	-	-14.14
Speed/Approach speed	at 360 deg	0.60
Time [sec]	at 360 deg	70.00
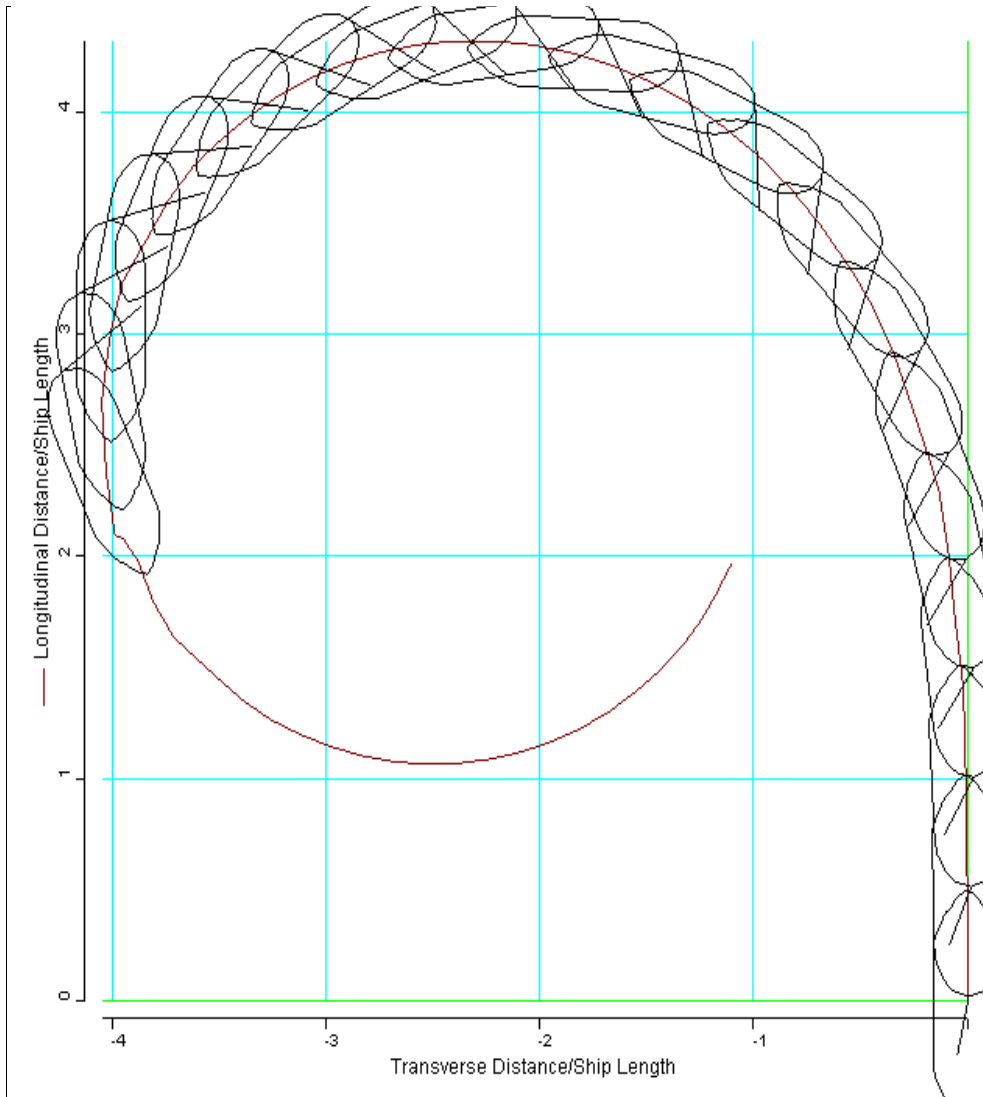
Fig. 31. Turning trajectory of the fishing vessel in deep water

It can be observed that the obtained results are lower than the maximum values imposed by IMO regulations, so the vessel has "passed" the turning circle test. The graphical instability met at around 190 degrees is probably caused by some of the vessel's characteristics that do not comply with the requirements imposed by the program on the vessels to be investigated [see *7.2.2. Limits of Applicability*].

7.2.3. Zig-Zag Manoeuvre

The Zig-Zag manoeuvre has been run for the 10 degrees rudder angle as well as 10 degrees heading check angle. Thie initial 'zig' has been performed in portside with the output data presented below [Fig. 32, Table 20].

The IMO requirements concerning in this manoeuvre the maximum value of first and second overshoot angle are fulfilled.

Table 20. Summary of the zig-zag test

Characteristics	Numerical result	IMO max. value
1st overshoot angle [deg]	10.31	10.00
2nd overshoot angle [deg]	14.21	25.00
Period [sec]	48.00	-
Initial turning time [sec]	8.00	-
1st time to check yaw [sec]	6.00	-
Time to 1st max. heading angle [sec]	14.00	-
Reach time (0 deg. heading angle) [sec]	26.00	-
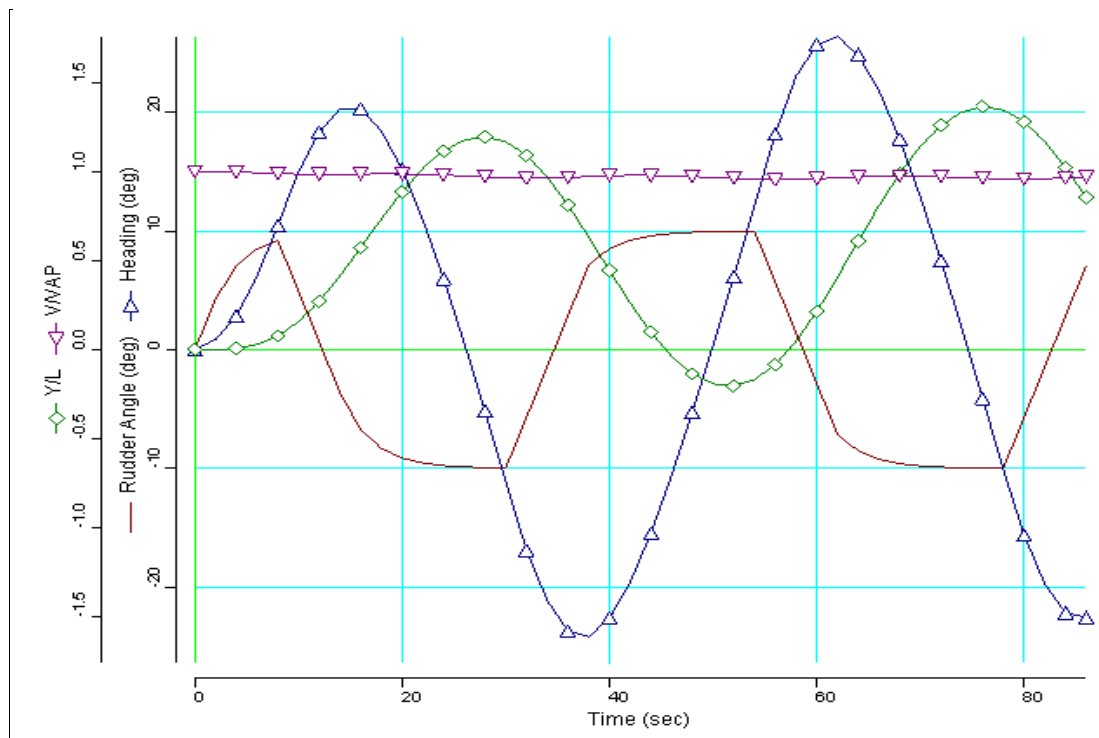
Fig. 32. Zig-zag characteristics of the fishing vessel in deep water

7.2.4. Reverse Spiral Manoeuvre

The reverse spiral manoeuvre has been performed to determine the directional stability of the fishing vessel. Calculation has been carried out for port and starboard sides for the rudder angles from 15 to 35 degrees with intervals of 5 degrees. The results, proving the dynamic stability of the ship, are presented in a tabular [Table 21] as well as graphical form [Fig. 33] below.

Table 21. Reverse spiral test values

Starboard Rudder Deflection				Portside Rudder Deflection			
Rudder angle [deg]	Yaw rate [deg/sec]	Yaw rate [non.dim.]	Ship speed / Approach speed	Rudder angle [deg]	Yaw rate [deg/sec]	Yaw rate [non.dim.]	Ship speed / Approach speed
0.00	-0.02	-0.00	1.00	0.00	0.00	0.00	1.00
0.50	0.65	0.06	0.83	-1.54	-0.60	-0.05	0.82
4.07	1.05	0.09	0.79	0.02	-1.44	-0.13	0.77
6.26	1.46	0.12	0.84	-6.36	-1.61	-0.14	0.85
8.37	2.19	0.18	0.84	-8.97	-2.17	-0.18	0.86
12.19	2.79	0.23	0.85	-11.78	-2.79	-0.23	0.85
15.00	3.93	0.31	0.89	-15.00	-4.00	-0.32	0.89
20.00	4.59	0.39	0.83	-20.00	-4.73	-0.40	0.83
25.00	5.05	0.47	0.76	-25.00	-5.17	-0.48	0.75
30.00	5.44	0.56	0.69	-30.00	-5.35	-0.56	0.68
35.00	5.57	0.64	0.62	-35.00	-5.66	-0.67	0.60
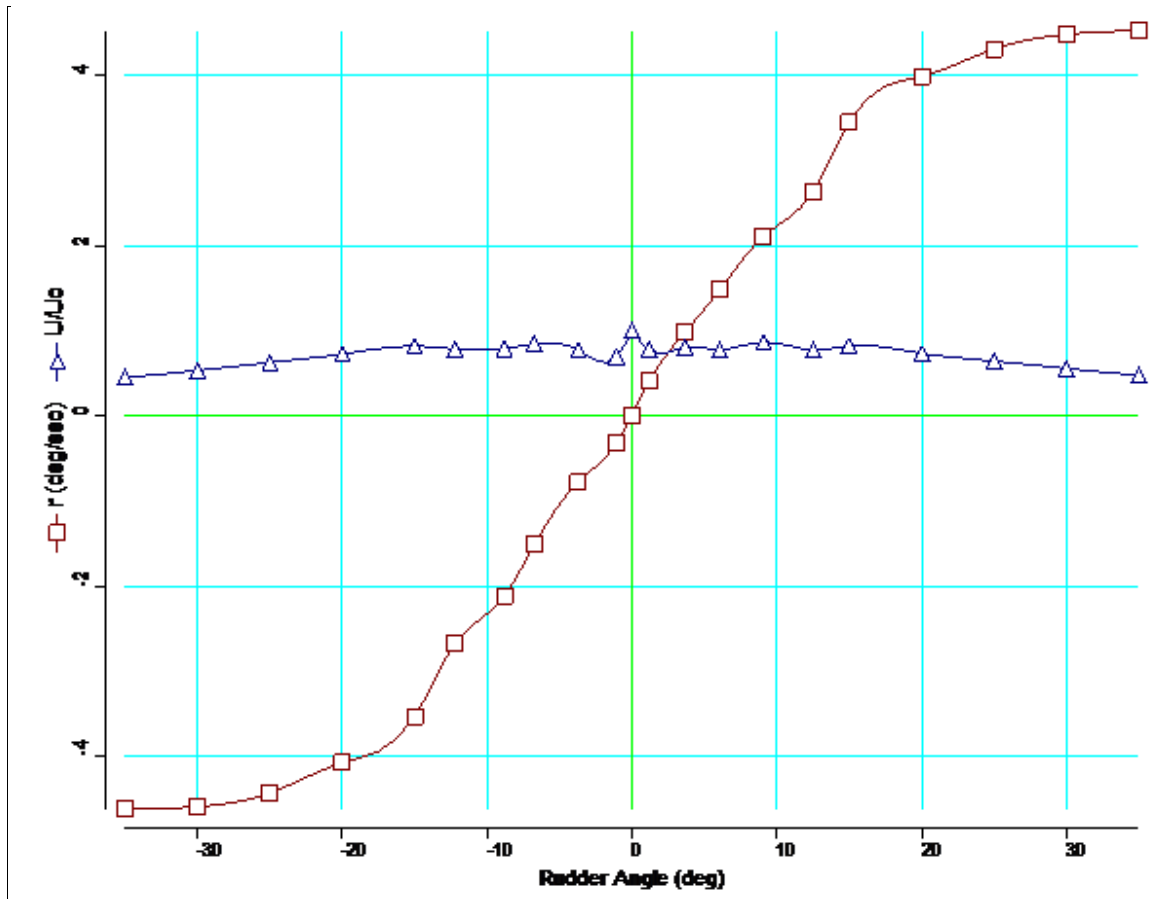
Fig. 33. Reverse spiral manoeuvre of the fishing vessel in deep water

Additionally, the following output data [Table 22] has been obtained for all the above mentioned manoeuvres:

Table 22. Propulsion point at manoeuvring speed

Wake fraction	0.220
Thrust deduction fraction	0.212
Propleller RPM	304.53
Total ship resistance [kN]	49.48

7.2.5. *Limits of Applicability*

In the author's opinion, the main limitation of the Manoeuvring Module is the estimation of ship resistance [Table 22], which is done with the use of BSRA[2] Methodical Series. The user is not given a choice to perform the calculation with other methods, even though the resistance computation in the Powering Module was done by means of different method. The same problem occurs when estimating the wake fraction and thrust deduction in a straight ahead motion in deep water. Additionally, the BSRA Methodical Series uses the analysis of Methodical Series Experiments on Single-Screw Ocean-Going Merchant-Ship Forms with the block coefficient $0.55 < C_B < 0.85$, the conditions not every investigated ship can fulfill. The other observed disadvantage is that in the Manoeuvring Module, only the conventional rudders are considered, whereas the other modules allow the user to choose between the conventional, Becker or Schilling rudder type.

Apart from the above-mentioned disadvantages, the Manoeuvring Module of TRIBON has the below-presented limits introduced for simulating the merchant ship manoeuvring performance [Table 23]. It just needs to be added that the manoeuvring calculations in TRIBON are based on mathematical models derived from regression analysis of data sets of manoeuvring characteristics. However, as these data sets were used for the analysis of merchant and naval vessels only, the fishing vessel has to be considered in this case as a merchant vessel.

It can be observed that two characteristics of the fishing vessel (*L/B* and *L/T* ratios) do not comply with the requirements imposed by the program on the merchant vessels. This might be one of the reasons for unstable result of the turning circle performed by TRIBON Manoeuvring Module.

---

[2] BSRA: British Shipbuilding Research Association

Table 23. Merchant ship limits

SHIP	Min. value:	Max. value:	Fishing vessel	OK?
Block coefficient (C_B)	0.480	0.850	0.553	YES
Length/Beam (L/B)	4.0	8.0	3.1	NO
Length/Draft (L/T)	13.66	40.11	9.69	NO
Beam/Draft (B/T)	2.15	6.247	3.1	YES
LCG from midships/Length	-0.050	0.057	-0.023	YES
Draft	0.67*Prop. diam.	-	2.58	YES
RUDDER	**Min. value:**	**Max. value:**	**Fishing vessel**	**OK?**
N-r of rudders	1	4	1	YES
Rudder Area/Length*Draft (A_R/LT)	-	0.075	0.045	YES
Rudder height	0.75*Prop. diam.	Mean draft - Trim	2.2	YES
Aspect Ratio	0.75	2.80	1.68	YES
Rudder rate [deg/s]	1.0	7.0	2.14	YES
PROPELLER	**Min. value:**	**Max. value:**	**Fishing vessel**	**OK?**
N-r of propellers	1	3	1	YES
N-r of blades	3	5	4	YES

7.3. Manoeuvring Prediction Program MPP1

To verify the TRIBON Initial Design predictions of the manoeuvring characteristics at the preliminary design stage, additional computations have been performed by means of Manoeuvring Prediction Program MPP1 developed in the Department of Naval Architecture and Marine Engineering of University of Michigan, USA.

MPP1 is aimed to be used at the parameter stage of design, before a detailed hull concept is developed and offsets available. MPP1 uses methods given by Clarke et al to assess the course stability, turnability and controllability by a helmsman as well as the regression results of Lyster and Knights to estimate the turning circle characteristics of a displacement vessel.

The input data to the MPP1 program, taken from the hydrostatics characteristics of the vessel, is given in the Table 24:

Table 24. MPP1 input data

vessel characteristics:	
length of the waterline (LWL)	26.728 m
max. beam (B)	8.0 m
forward draft (T_F)	2.58 m
aft draft (T_A)	2.58 m
block coefficient on LWL (C_B):	0.565
longitudinal center of gravity (LCG) in % LWL from amidships, +ve foreward	-2.8 %
yaw radius of gyration K_{33} (as a fraction of LWL)	0.25 *(default value)*
difference of bow profile from a plumb bow (as a fraction of LWL*T)	0.01
steering characteristics:	
total rudder area (A_R) as a fraction of LWL*T	0.04
steering gear time constant (T_E)	2.5 sec *(default value)*
center of effort of rudder (X_R) in % LWL from amidships, +ve aft	49% *(default value)*
number of propellers	1
single screw stern type	closed
operating conditions:	
water depth to ship draft ratio (H/T)	1000 *(default value)*
initial or reference vessel speed (V_K)	12 kn
water properties:	
type and temperature of water	salt, 15°C

It should be noted that the MPP1 program, opposite to TRIBON, computes the results on the basis of length of the waterline (LWL) instead of length between perpendiculars (LPP). Resulting from this, all the non-dimensional values obtained from MPP1 are presented by dividing the dimensional ones by LWL. These results, compared with the ones provided by TRIBON as well as IMO requirements are presented in Table 25:

Table 25. MPP1 and TRIBON results comparison

	MPP1	TRIBON	% Difference TRIBON/MPP1	IMO max.	MPP1 / TRIBON vs. IMO
non-dimen. Advance	3.04	4.24	28.3 %	4.5	YES / YES
non-dimen. Transfer	1.60	1.84	13.0 %	-	-
non-dimen. Steady Turning Diam.	2.36	3.03	22.1 %	-	-
non-dimen. Tactical	3.35	4.01	16.5 %	5.0	YES / YES
Steady Speed in Turn/App. Speed	0.40	0.60	33.3 %	-	-
Directional Stability (C > 0)	NO	YES	-	-	-

7.4. Observations and Discussion

The main goal of using TRIBON Initial Design and MPP1 program was to investigate whether the input data of main dimensions of the vessel only (initial design stage) can lead to a reliable first hydrodynamic results. However, it have been found that the existing codes are still unreliable providing results of a significant differences, especially for the unusual types of hull [Table 25].

In author's personal opinion, some more research should be performed concerning the initial design manoeuvring programs. Additionally, special attention should be put to estimation of the hydrodynamic characteristics of the uncommon hull shapes, like the investigated fishing vessel, with double hard and rather small length, which makes them operate at relatively high values of Froude number.

8. TIME-DOMAIN SIMULATION CODE FOR STANDARD SHIP MANOEUVRES

8.1. Introduction of the Problem

In order to apply theoretical calculations in different design stages, the numerical code, validated by the experimental tests, has been developed as a result of cooperation of two research and academic institutions: Naval Architecture Faculty of the "Dunarea de Jos" University of Galati, Romania and Department of Naval Architecture, Ocean and Environmental Engineering of the University of Trieste, Italy.

As far as the investigated fishing vessel is concerned, the Planar Motion Mechanism experiments had been performed in order to evaluate the hydrodynamic derivates, which have been subsequently implemented in the simulation model.

As there are only a few full nonlinear simulation models of merchant vessels e.g. VLCC tanker, ro-ro passenger, container, ferry, etc. known in literature (Bertram, 2000; Nielsen et al., 2001; Lee and Fujimo, 2003), this model, if reliable, can be used as a benchmark for further investigation on the fishing vessels hydrodynamic performances.

The simulations results, as well as their verification with the experimental data, are presented in the current chapter.

8.2. Hydrodynamic Derivatives Estimation

Ship steering and manoeuvring can be described by a system of simultaneous equations of motion in the horizontal plane (eq. 13). The terms in these equations which represent the hydrodynamic forces and moments acting on the vehicle are often expanded in Taylor series about some convenient reference condition (eq. 15, 16). For a surface ship this reference condition is usually chosen to be the equilibrium condition of forward motion at constant speed U_0. The partial derivatives of these forces and moments are known as hydrodynamic coefficients or hydrodynamic derivatives [15].

There are 36 first order hydrodynamic coefficients which could be evaluated to describe the dynamics of the ship. However, as most of the ships are symmetric about the x-z plane, many of these coefficients tend to be equal to zero.

Different methods have been developed to estimate these derivatives. Clarke (1998) has undertaken an extensive research of all 36 linear hydrodynamic coefficients and succeeded to develop empirical formulas basing on regression analysis of experimental data. Using Clarke's method (eq. 39), the hydrodynamic derivatives of the investigated fishing vessel has been found [Table 26] and compared with the measured ones [Table 27] obtained by means of a standard Planar Motion Mechanism model tests in still water (Obreja, 2001).

Even though the method is regarded as quite simple and based on the principal dimensions of the ship and rudder attached (LPP, B, T_M, C_B), it has been found to provide satisfactory results of hydrodynamic derivatives estimation. The numerical results fall in the same range as experimental ones with only one numerical derivative having opposite sign as its experimental equivalent. For this reason it can be concluded that estimation of the various hydrodynamic derivatives by analytical means is possible and, accordingly, reliable prediction of ship steering and manoeuvring can be made in the early stages of ship design.

Table 26. Fishing vessel's hydrodynamic derivatives by Clarke method

Derivative of sway force with respect to sway acceleration	Y_v'	-0.0255134
Derivative of sway force with respect to angular acceleration	Y_r'	-0.0061119
Derivative of yaw moment with respect to sway acceleration	N_v'	-0.0075238
Derivative of yaw moment with respect to angular acceleration	N_r'	-0.0002673
Derivative of sway force with respect to sway velocity	Y_v	-0.0572792
Derivative of sway force with respect to angular velocity	Y_r	0.0014743
Derivative of yaw moment with respect to sway velocity	N_v	-0.0250164
Derivative of yaw moment with respect to angular velocity	N_r	-0.0064150
Derivative of sway force with respect to rudder angle	Y_δ	0.0138336
Derivative of yaw moment with respect to rudder angle	N_δ	-0.0069168

Table 27. Numerical and experimental derivatives comparison

Derivative	Measured value $\times 10^5$	Computed value $\times 10^5$
Y_v'	-2551.34	-991.90
Y_r'	-611.19	-1259.97
N_v'	-752.38	867.83
N_r'	-26.73	-211.09
Y_v	-5727.92	-4539.40
Y_r	147.43	4158.40
N_v	-2501.64	-1793.60
N_r	-641.50	-743.77
Y_δ	1383.36	624.70
N_δ	-691.68	-278.00

8.3. Stability Criteria

Basing on the computed hydrodynamic derivatives and additional data concerning vessel's main parameters: LPP, LCG, vessel's weight and yaw radius of gyration, the stability criteria has been evaluated on the basis of the Abkowitz model (eq. 18). In this case, the vessel has been found to be directionally unstable with the stability parameter, *C*, having negative value: $C = -0.645 \times 10^{-3}$. Similar results of unstable ship have been obtained using the preliminary design code, MPP1 *[see 7.3]*.

However, with the hydrodynamic derivatives measured during the PMM model test and introduced into the simulation code, the vessel has been found to be directionally stable with the stability parameter equal to: $C = 0.176 \times 10^{-3}$. Additionally, this results is in a good agreement with the positive dynamic stability parameter found by means of TRIBON Initial Design program *[see 7.2.4]*.

8.4. Time-domain Simulation

The manoeuvres at high rudder deflection angles require the consideration of nonlinear hydrodynamic and inertial components. This can only be done by the use of nonlinear hydrodynamic models, which include higher order terms of Taylor's series expansion of the hydrodynamic external forces and moments.

The main difficulty in creating a reliable theoretical manoeuvring model comes from the lack of knowledge of these forces and moments applied on the hull. The known thing is that their magnitude is directly related to the properties of the body and fluid, ship motion and rudder deflection [17].

In the investigated code, the general form of the nonlinear model, represented by the set of differential equations (eq. 26), has been used, including the certain functions (f_1, f_2, f_3) containing hydrodynamic derivatives (eq. 27, 28, 29). Additionally, the hypothesis of symmetrical body was considered, which reduces the number of derivatives different from zero. The higher order terms of the acceleration as well as the coupled speed-acceleration terms have been neglected (Abkowitz, 1964; Chislett and Strom-Tejsen, 1965).

The trajectory developed by the fishing vessel during the simulation of a turning circle test is shown on Fig. 34, whereas Table 28 compares the numerical characteristics of the manoeuvre with the experimental ones as well as with the values obtained with initial design manoeuvring programs and IMO limits.

Similarly, the graphical and numerical results of the time-domain simulations, additionally compared with the experimental results, are presented for the 10°/10° zig-zag manoeuvre [Fig. 35, Table 29] and the direct spiral test [Fig. 36, Table 30].

Table 28. Characteristics of the turning circle test ($\delta = -35°$)

CHARACTERISTICS	SIMUL. CODE	TRIBON	MPP1	IMO MAX.
Advance/L [m]	3.44	4.24	3.04	4.5
Transfer/L [m]	1.39	1.84	1.60	-
Tactical diameter/L [m]	3.04	4.01	3.35	5.0
Steady diameter/L [m]	3.02	3.03	2.36	-
Steady drift angle [deg]	8.10	14.14	-	-
Speed/Approach speed	0.59	0.60	0.40	-
Stability criterion, C	0.000176	+ ve	- ve	-
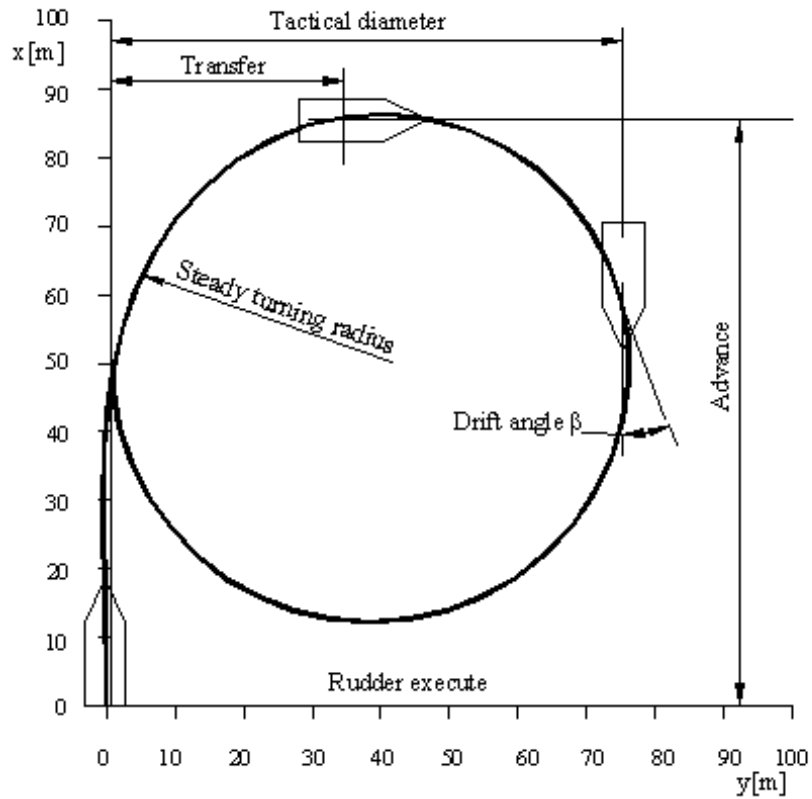
Fig. 34. Turning circle simulation result
*Source: Identification of hydrodynamic coefficients for manoeuvring simulation
model of a fishing vessel, Ocean Engineering 37, 2010*
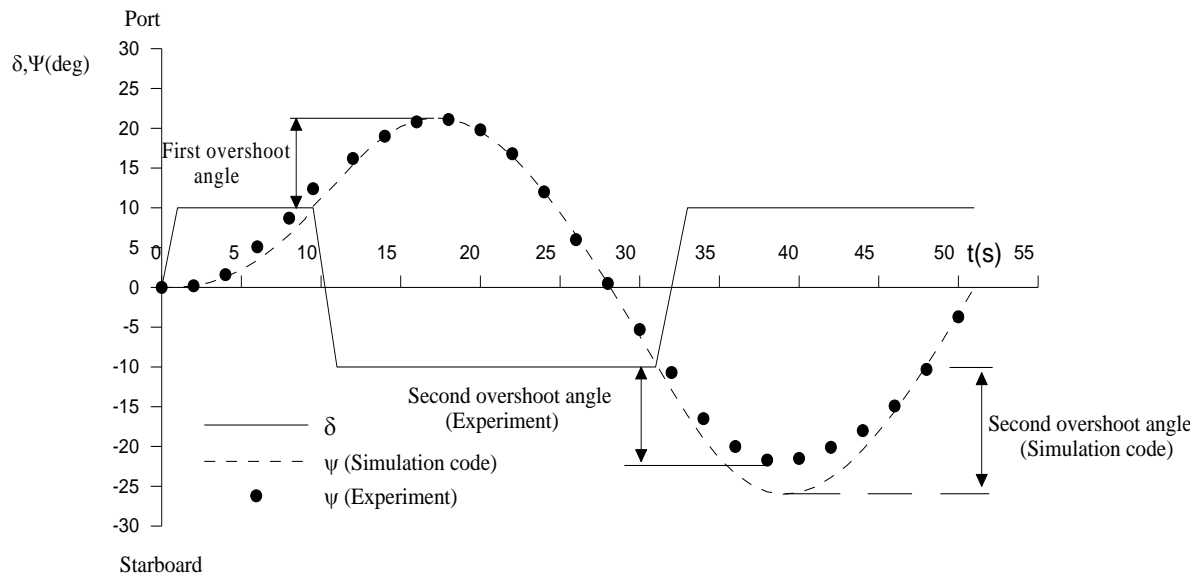
Fig. 35. Zig-zag manoeuvre simulation and experimental results
*Source: Identification of hydrodynamic coefficients for manoeuvring simulation
model of a fishing vessel, Ocean Engineering 37, 2010*

Table 29. Simulated and measured zig-zag manoeuvre (10°/10°) results

CHARACTERISTICS	SIMULATION CODE	MODEL TEST	TRIBON	IMO MAX.
1st overshoot angle [deg]	11.3	11.3	10.3	10.0
2nd overshoot angle [deg]	16.0	11.9	14.2	25.0
Initial turning time [sec]	9.8	-	8.0	-
Time to 1st max. heading [sec]	17.0	-	14.0	-
Reach time [sec]	28.0	-	26.0	-
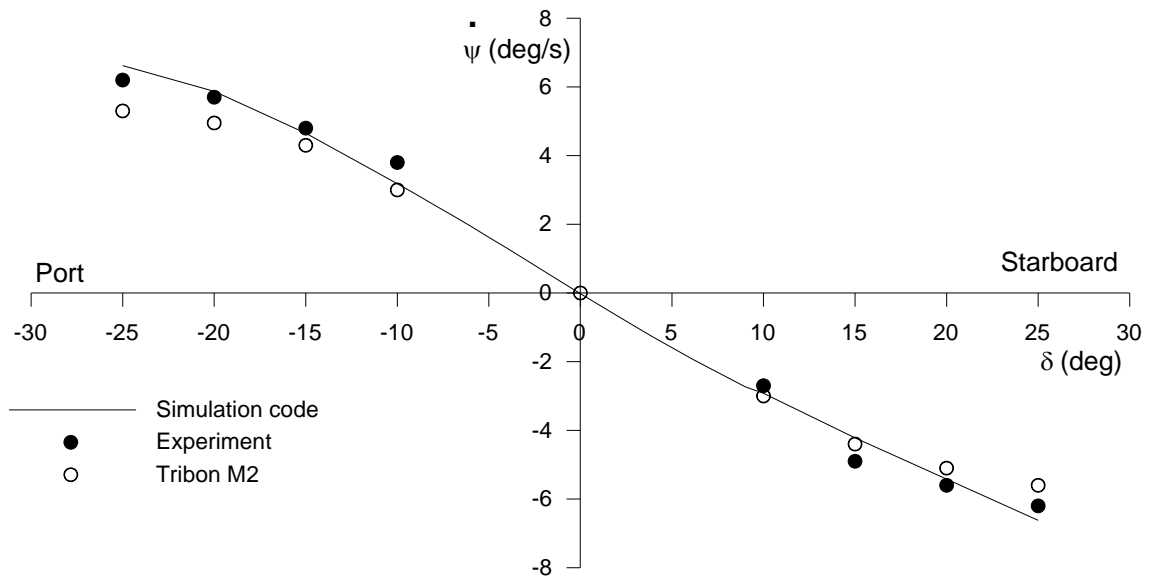
Fig. 36. Direct spiral test simulation and experimental result
Source: Identification of hydrodynamic coefficients for manoeuvring simulation model of a fishing vessel, Ocean Engineering 37, 2010

Table 30. Controls-fixed straight line stability comparison

CHARACTERISTIC	SIMULATION CODE	MODEL TEST	TRIBON	MPP1
Vessel condition	stable	stable	stable	unstable

8.5. Verification of Hydrodynamic Derivatives Influence on the Standard Manoeuvres Parameters

The previously described time-domain simulation code of the standard manoeuvres (*see 8.4*) uses the non-linear mathematical model (eq. 26) based on 23 hydrodynamic derivatives obtained experimentally by means of PMM tests (Obreja, 2001). Having found a good agreement between numerical and experimental results of the standard manoeuvres, the verification of the importance of each hydrodynamic derivative on the final manoeuvring parameters have been investigated.

It has been observed that the influence of the hydrodynamic derivatives on the manoeuvring performance of the vessel is not constant and differ significantly between different manoeuvres. Having all the 23 derivatives investigated, they have been finally divided into two groups, basing on their influence on obtaining correct simulation results. Table 31 presents the derivatives proving a significant importance for most of the results obtained by means of the applied mathematical model, whereas Table 32 tabulates the derivatives with minor or no influence on the investigated manoeuvring parameters.

Table 31. Hydrodynamic derivatives with major influence of the manoeuvring performance

Hydrodynamic derivative	Turning circle test			Zig-zag test	Spiral test	Stability criterion C
	Tactical diameter	*Advance*	*Transfer*	*Overshoot angles*	*Rate of heading*	
$Y_{\dot{v}}$	Yes	Yes	Yes	Yes	No	No
$Y_{\dot{r}}$	Yes	Yes	Yes	Yes	No	No
Y_v	Yes	Yes	Yes	Yes	Yes	Yes
Y_r	Yes	No	Yes	Yes	Yes	Yes
Y_δ	Yes	Yes	Yes	Yes	Yes	No
$N_{\dot{r}}$	Yes	Yes	Yes	Yes	No	No
N_v	Yes	Yes	Yes	Yes	Yes	Yes
N_r	Yes	Yes	Yes	Yes	Yes	Yes
N_δ	Yes	Yes	Yes	No	Yes	No
N_{vvr}	Yes	Yes	Yes	No	Yes	No
$N_{vv\delta}$	Yes	Yes	Yes	No	Yes	No
$N_{\delta\delta v}$	Yes	Yes	Yes	No	No	No

T able 32. Hydrodynamic derivatives with minor influence of the manoeuvring performance

Hydrodynamic derivative	Turning circle test			Zig-zag test	Spiral test	Stability criterion C
	Tactical diameter	*Advance*	*Transfer*	*Overshoot angles*	*Rate of heading*	
X_{vv}	No	No	No	No	No	No
$X_{\delta\delta}$	No	No	No	No	Yes	No
$X_{v\delta}$	No	No	No	No	Yes	No
Y_{vvv}	No	No	No	No	No	No
$Y_{\delta\delta\delta}$	No	No	No	No	No	No
Y_{vvr}	Yes	No	No	No	Yes	No
$Y_{vv\delta}$	Yes	No	Yes	No	No	No
$Y_{\delta\delta v}$	No	No	No	No	No	No
$N_{\dot{v}}$	No	No	No	Yes	No	No
N_{vvv}	No	No	No	No	No	No
$N_{\delta\delta\delta}$	No	No	No	No	No	No

8.6. Observations and Discussion

As mentioned before, the mathematical model used in the code includes terms up to the third order only. The higher order hydrodynamic derivates have been neglected not only due to limited accuracy of the measurement techniques (Chislett and Strom-Tejsen, 1965), but also in order to create a simple design tool for estimating the horizontal motions of fishing vessels. However, in spite of neglecting the higher order terms, a satisfactory correlation between numerical and experimental results has been found.

The positive value of the dynamic stability parameter, *C*, calculated on the basis of hydrodynamic derivatives, presents a very good agreement with the results of the experimental spiral test.

Good correlation between the value of the ship's drift angle and the loss of speed (greater drift angle = greater speed losses) can be found in the turning circle simulation results [*Appendix 2*].

Plotted numerical and experimental results of the spiral test and zig-zag manoeuvre [Fig. 35 and 36] present similar hydrodynamic behavior of the ship in the same certain

conditions. However, in both cases (simulation code and experimental investigation), the recommendations of IMO are not fulfilled for the first overshoot angle.

The 23 hydrodynamic derivatives applied in the non-linear mathematical model show miscellaneous influence on the standard manoeuvres simulation results. Twelve of them prove a significant importance on the manoeuvring parameters, whereas other eleven derivatives show minor or no influence on the final results. The more detailed conclusions on the hydrodynamic derivatives importance can be defined as follows (Obreja, 2010):

- the linear derivatives Y_v, N_v and N_r have a major influence on all results given by the proposed mathematical model;

- the linear derivatives $Y_r, Y_\delta, Y_{\dot{v}}, Y_{\dot{r}}, N_{\dot{r}}, N_\delta$ as well as the nonlinear ones N_{vvr} and $N_{vv\delta}$ have a significant influence on the results. Hence, only Y_r is influencing the stability criterion, but does not have any influence on advance parameter; $Y_{\dot{v}}, Y_{\dot{r}}$ and $N_{\dot{r}}$ are not practically influencing the spiral tests results and N_δ, N_{vvr} and $N_{vv\delta}$ are not affecting the values of the overshoot angle;

- the nonlinear derivatives $Y_{vvr}, Y_{vv\delta}$ and $N_{\delta\delta v}$ have a significant influence on the results of the gyration test, mainly on the tactical diameter;

- the nonlinear derivatives $X_{\delta\delta}$ and $X_{v\delta}$ have a clear influence on the rate of heading of spiral tests while the linear derivative $N_{\dot{v}}$ is affecting only the value of the overshoot angle;

- the nonlinear derivatives $X_{vv}, Y_{vvv}, Y_{\delta\delta\delta}, Y_{\delta\delta v}, N_{vvv}$ and $N_{\delta\delta\delta}$ do not have any significant influence on the investigated parameters.

However, the mathematical model cannot be simplified by neglecting simultaneously the above mentioned derivatives due to their influence on the gyration and spiral tests results. In such a case 3% lower values of the tactical diameter and 6% higher values of the rate of heading have been obtained for the fishing vessel.

9. CFD Techniques in Manoeuvring Prediction

9.1. Introduction to Numerical Techniques

9.1.1. RANS –based Methods used in Simulations

The previously used mathematical model of Abkowitz considers the flow around the ship to be inviscid and incompressible. To take account of the viscosity and to simulate a detailed flow around the ship, several numerical codes have been developed so far. Most of them integrate the steady or unsteady partial differential equations of fluid motion, thus allowing the direct computation of the hydrodynamic forces.

Two basic equation systems suffice to describe all real flow physics for ship flows: the Navier-Stokes equations and the continuity equation, whereas the simplified ideal flow theory (describing the velocity field as the gradient of velocity potential and, thus, reducing the number of unknowns) employs the simplified Laplace's and Euler's equations.

For practical reasons, the fundamental equations of fluid motion need to be Reynolds-averaged and these equations for continuity and momentum are solved for the primitive variables to describe the steady flow around a three-dimensional ship hull.

9.1.2. Mathematical Model

The following continuity equation states that the mass in conserved:

$$\frac{1}{\rho}\frac{\partial \rho}{\partial t} + \frac{\partial U_i}{\partial x_i} = 0 \tag{71}$$

However, as only the incompressible flow in the present investigation is considered, the (71) can be written as:

$$\frac{\partial u_i}{\partial x_i} = 0 \tag{72}$$

The Navier-Stokes equations of motion can be presented in the following form:

$$\rho\frac{\partial U_i}{\partial t} + \rho\frac{\partial (U_j U_i)}{\partial x_j} = \rho R_i + \frac{\partial \sigma_{ij}}{\partial x_j} \tag{73}$$

where σ_{ij} is the total stress and for a Newtonian fluid can be written as:

$$\sigma_{ij} = -P\delta_{ij} + 2\mu\left(S_{ij} - \frac{1}{3}S_{kk}\delta_{ij}\right)$$

(74)

with S_{ij} being the strain-rate defined as:

$$S_{ij} = \frac{1}{2}\left(\frac{\partial U_i}{\partial x_j} + \frac{\partial U_j}{\partial x_i}\right)$$

(75)

S_{kk} in (74) equals zero for an incompressible flow:

$$S_{kk} = \frac{1}{2}\left(\frac{\partial U_k}{\partial x_k} + \frac{\partial U_k}{\partial x_k}\right) = \frac{\partial U_k}{\partial x_k} = 0$$

(76)

The RANS equations can be derived from (73) by splitting the instant velocity components, U_i, and the instant pressure, P, in time-mean velocity, u_i, and pressure, p, and time-fluctuating velocity, $u_i^{''}$, $U_i = \overline{U}_i + u_i^{''} \equiv u_i + u_i^{''}$ and fluctuating pressure, $p^{''}$, $P = \overline{P} + p^{''} \equiv p + p^{''}$. Following some simple mathematic manipulations, the time-averaged continuity equation and Navier-Stokes equation for an incompressible flow can be written as follows:

$$\frac{\partial u_i}{\partial x_i} = 0$$

(77)

$$\frac{\partial u_i}{\partial t} + \frac{\partial (u_j u_i + \overline{u_j^{''} u_i^{''}})}{\partial x_j} = \overline{R}_i - \frac{1}{\rho}\frac{\partial p}{\partial x_i} + \frac{\partial}{\partial x_j}\left(\upsilon\left(\frac{\partial u_i}{\partial x_j} + \frac{\partial u_j}{\partial x_i}\right)\right)$$

(78)

9.1.3. Turbulence Modeling

The RANS equations require external turbulence models to couple the Reynolds stresses to the time-averaged velocities. All turbulence models used for ship flows are semi-empirical. They use some theories about the physics of turbulence and supply the missing information by empirical constants. Traditionally, the Boussinesq approach has been used in practice which assumes isotropic turbulence, i.e. the turbulence properties are independent of the spatial direction [2]. This assumption simplifies the turbulence phenomena into a linear eddy viscosity model that can be written as:

$$\rho \overline{u_i'' u_j''} = \mu_T \left(\frac{\partial u_i}{\partial x_j} + \frac{\partial u_j}{\partial x_i} \right) + \frac{2}{3} \rho k \delta_{ij} \tag{79}$$

However, due to the linear simplification, the Boussinesq model sometimes fails to give satisfactory results, which can be improved by adding the nonlinear terms. The Explicit Algebraic Stress Model (EASM) is such a model that includes nonlinear terms. In this model, the Reynolds stress components are explicitly determined from the tensor functions of the velocity gradients, turbulent kinetic energy, and turbulent length scale [18]. These models have the advantage explicit solution of the Reynolds stresses at each computational iteration with the Reynolds stress tensor given by:

$$\rho \overline{u_i'' u_j''} = \frac{2}{3} \rho k \delta_{ij} - \mu_T \left(S_{ij} + a_2 a_4 \left(S_{ik} W_{kj} - W_{ik} S_{kj} \right) \right) - a_3 a_4 \left(S_{ik} S_{kj} - \frac{1}{3} S_{mn} S_{mn} \delta_{ij} \right) \tag{80}$$

whereas the turbulent viscosity can be defined as:

$$\nu_T = \max \left(-k\alpha_1, \frac{0.0005k}{\beta^* \omega} \right) \tag{81}$$

where α_1, β^*, a_2, a_3, a_4 are the numerical coefficients of the model, while W_{ij} is the rotation-rate.

For all the above reasons, the EASM turbulence model will be the one used in the following CFD simulations aimed to predict the hydrodynamic forces and moments.

In the RANS solver the convective fluxes are evaluated using the approximate Riemann solver of Roe. For the evaluation of the diffusive fluxes, central differences around the cell face centers are employed. Flux-correction with a min-mod limiter is used to increase the accuracy to second order in regions of smooth flow. The discrete equations are solved iteratively by using the ADI method. The tri-diagonal system contains the first-order Roe convective terms and the second order diffusive terms, while the second-order flux corrections are used as an explicit defect correction. The free surface is obtained as a potential-flow solution and it is kept fixed for the solution of the RANS equations.

9.2. Resistance Computation Using Potential Flow Theory

Even though the RANS codes are mostly used to simulate the ship flows, the simple resistance estimation can be easily performed using the potential flow theory. The potential flow theory assumes the flow to be irrotational, inviscid and incompressible, which simplifies the simulation process, reduces the computation time (by reducing the number of unknowns) and makes the potential flow codes still the most commonly used CFD tools in naval architecture [2].

The ship resistance is computed for seven speeds ranging from 6 to 12 knots at first, in an attempt of validating the numerical solution. Fig. 37 illustrates a comparison of the speed-resistance curves drawn for the experimental and numerical data. An overall satisfactory agreement between measured and the computed data can observed. This confirms the capability of the SHIPFLOW-XPAN numerical code (employing a fully non-linear Rankine-source based method) to estimate the ship resistance with high accuracy.
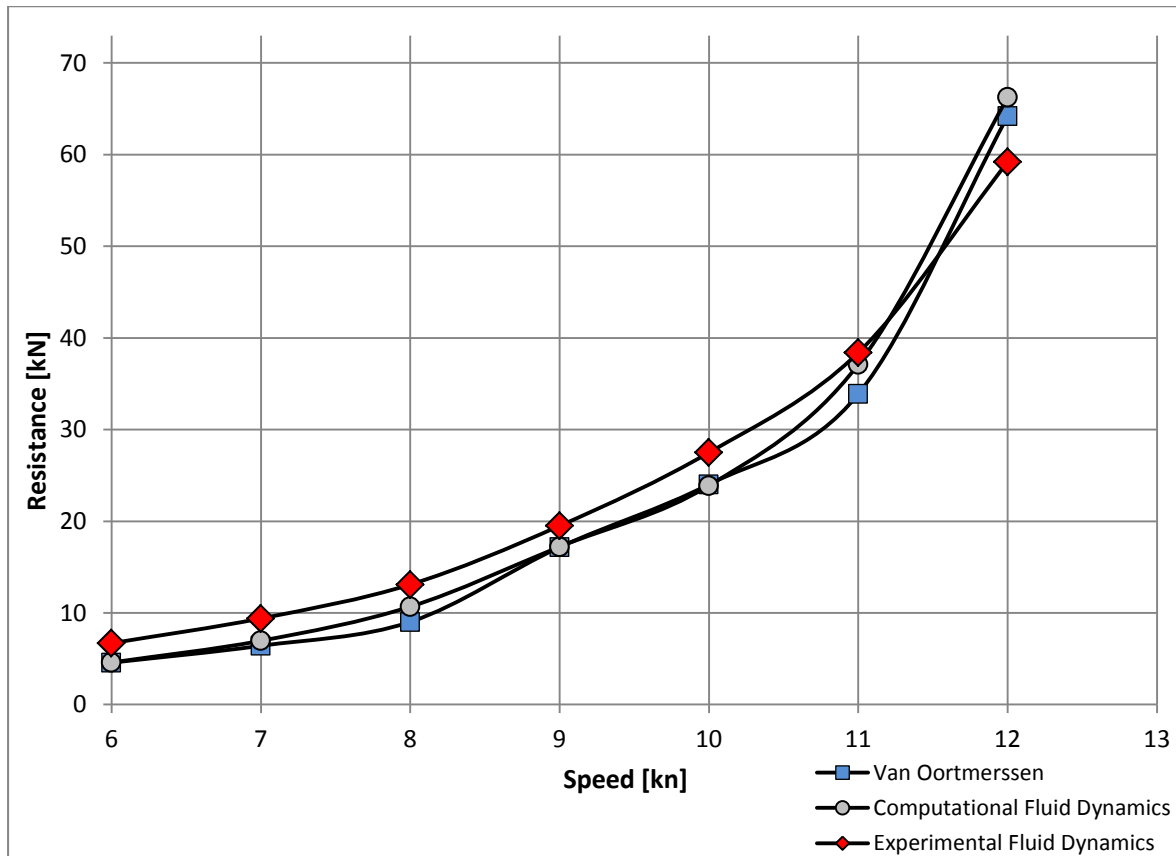
Fig. 37. Resistance comparison: experimental, empirical and numerical methods

9.3. RANS Solution for the Hydrodynamic Forces Prediction in Oblique Flow

9.3.1. *Introduction to Numerical Study of Manoeuvring Performance*

As mentioned before, the IMO regulations concerning the manoeuvrability of ships increased the demand for CFD methods in the field. However, predicting the flow behavior around the hull and appendages is much more complicated than predicting the steady flow in resistance problems. Additionally, the number of computational cells is much higher than for resistance computations, since both port and starboard sides must be discretized.

As most commercial RANS solvers, also SHIPFLOW CFD code (SHIPFLOW-XCHAP) is based on the finite volume method (FVM). FVM not only discretizes the whole fluid domain, but also ensures the conservativeness by integrating the equations for mass and momentum conservation over the individual cell before variables are approximated by values at the cell centers [2].

The numerical study is focused on the hydrodynamic prediction of steady performance and investigation of the flow features around a manoeuvring fishing vessel operating at the design speed of 12 knots. Several cases are examined for both bare hull geometry as well as the hull equipped with rudder, both placed in symmetrical ($\beta = 0°$) and non-symmetrical ($\beta \neq 0°$) inflow field. Additionally, when analyzing the appended geometry, the different rudder deflection angles ($\delta = 0°$, 10°, 20°, 30°) are applied, thanks to which the ship behavior in the turning motion can be numerically investigated. All the above combinations result in a total number of 21 cases.

9.3.2. *Preprocessing*

The preprocessing phase of the simulation involves the offset file preparation that would describe the geometry of the investigated vessel and implementing it in the correct coordinate system. SHIPFLOW uses a non-dimensionalized coordinates for the internal computations, deploying the ship length, L_{PP}, for non-dimensionalization. However, the offset points can either be input directly in full scale coordinates together with a reference length (L_{PP}) or in a non-dimensionalized form.

The set of points that describe the intersection between the hull and a constant *x*-plane creates a station. Stations, on the other hand, create groups that describe the shape of a part of the hull (bulb, main hull, bulbstern, rudder, etc).

The geometry of the fishing vessel described by the offset file is presented on the figures below [Fig 38, 39, 40]. To simplify the simulation, a small stern bulb that houses the propeller shaft has been removed from the bare hull to allow more precise cells distribution.
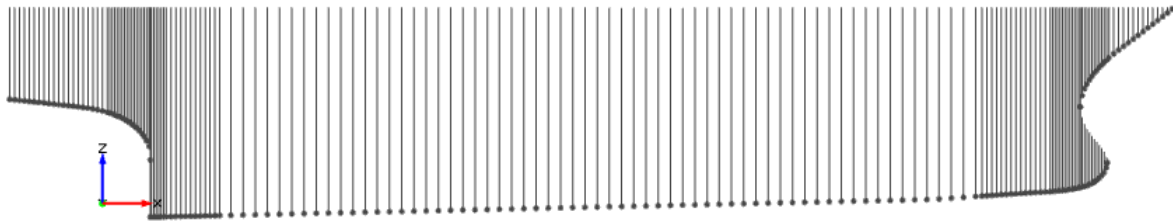
Fig. 38. Side view
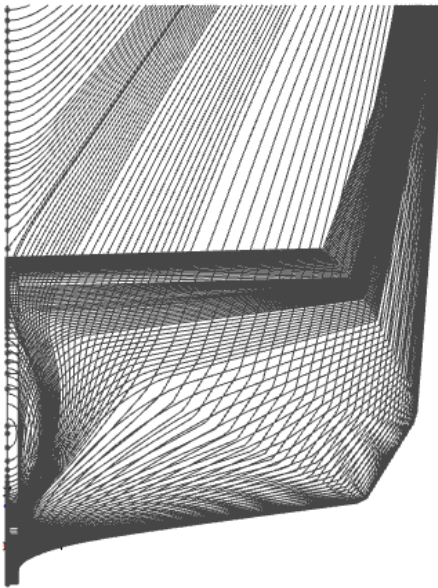
Fig. 39. Lines plan
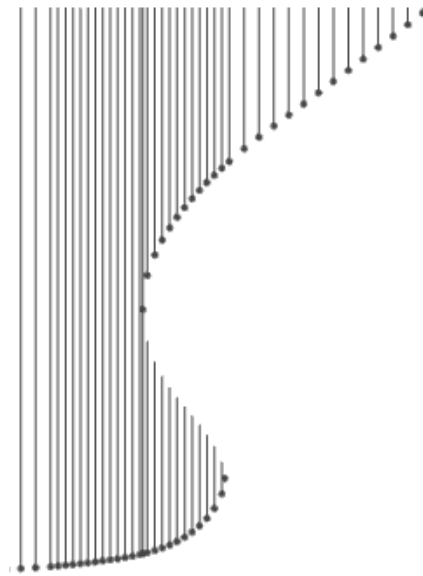
Fig. 40. Starboard view of the bulbous bow

9.3.3. Boundary Conditions

Boundary conditions are a required component of the mathematical model that governs the motion of the flow within the domain. They are formulated in terms of pressure and velocity distribution on the boundary faces of the computational domain [Fig. 41].

Table 33 tabulates the applied boundary conditions on the fishing vessel's simulation domain, with u_i being the time-averaged velocity component in Cartesian directions, p the time-averaged pressure and ξ_B the parameter direction crossing the boundary.

At the upstream part of the domain, each horizontal component of velocity has the same constant value, equal with the velocity of the ship, and the pressure is extrapolated with zero gradient. At the hull's surface, the "no slip" condition is imposed, considering the water's relative velocity on the hull to be zero ($u_i = 0$) as well as assuming zero pressure gradient. The downstream boundary presumes that the velocity gradient is equal to zero as well as no pressure is applied anymore ($p = 0$). Additionally, on the surface of the domain, all the variables are extrapolated with zero gradients ("slip" condition).

As far as the turbulence characteristics is concerned, the zero extrapolation condition is employed on all the boundaries of the domain.

Additionally, due to the hydrodynamic investigation of the fishing vessel with the different drift angles imposed, the supplementary boundary condition of "no symmetry" about the centerline of the ship needs to be introduced [Fig. 41].

Table 33. Boundary conditions

	No slip	*Slip*	*Inflow*	*Outflow*
u	$u_i = 0$	$u_i n_i = 0$ $\dfrac{\partial u_i}{\partial \xi_B} = 0$	$u_i = const.$	$\dfrac{\partial u_i}{\partial \xi_B} = 0$
p	$\dfrac{\partial p}{\partial \xi_B} = 0$	$\dfrac{\partial p}{\partial \xi_B} = 0$	$\dfrac{\partial p}{\partial \xi_B} = 0$	$p = 0$
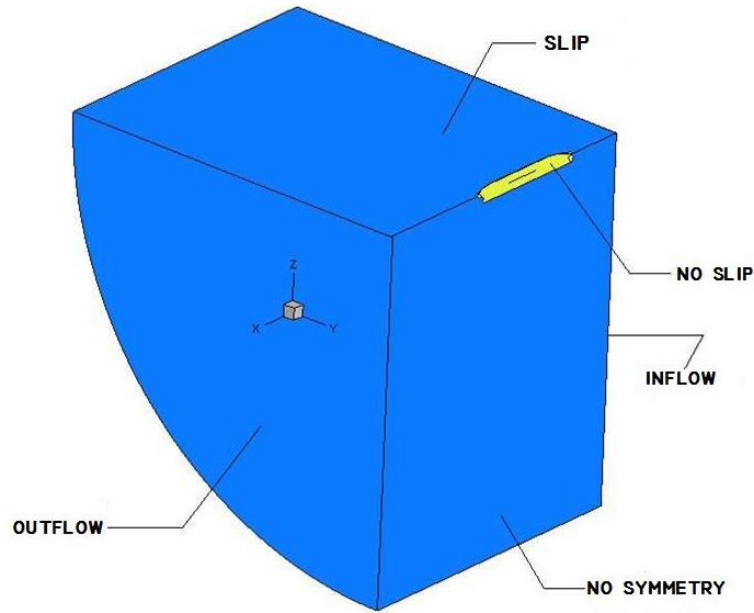
Fig. 41. Boundary conditions

9.3.4. Grid Generation

A good grid is an important prerequisite in getting an accurate numerical solution for any complex flow problem. For the numerical investigation, a global structured grid of 2.02 million cells has been generated to cover the entire computational domain. The cells are clustered around regions where the geometry is changing significantly and where the important flow details must be captured (around the bulbous bow and the stern/rudder area). A Chimera-based overlapping grid approach is employed for the appended-hull case simulation [Fig. 42], in which a total number of about 2.4 million of cells was necessary.
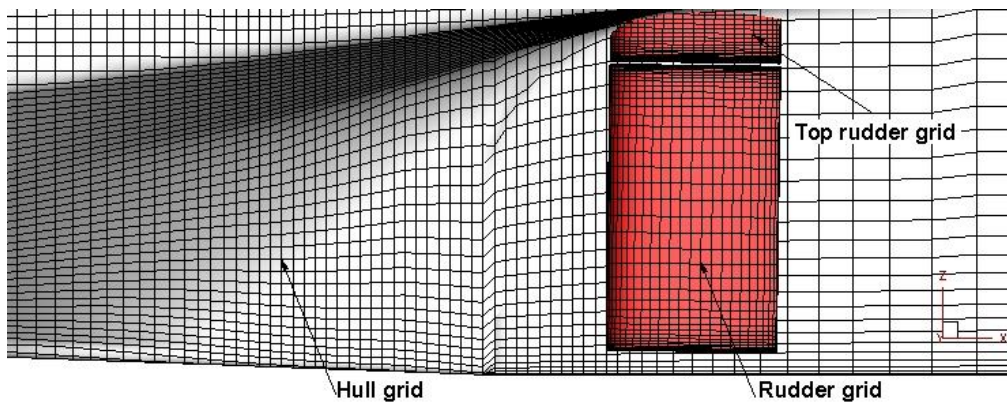
Fig. 42. Overlapping grid for appended-hull simulations

9.3.5.   Simulations at Different Drift Angles

Three different drift angles ($\beta = 0°$, $3°$, $6°$) have been considered to determine the hydrodynamic forces acting on the bare hull. The computational domain has been discretized into 2.02 million cells. To reduce the computational time, the existence of the free surface has been neglected.

Having dissembled the effect of free surface made it impossible to compute the component of the total forces due to wave-making. For this reason, only the viscous components of the hydrodynamic forces acting on the hull are investigated. Their variation in function of drift angle is depicted on Fig. 43.

One may observe that the longitudinal component of the hydrodynamic forces (F_{x_visc}) present a very small variation throughout different simulation conditions, which proves it to be independent from the vessel's drift angle. On the other hand, the lateral component of the viscous forces (F_{y_visc}) has been found to vary in function of the drift angle applied, increasing significantly with the increased drift.
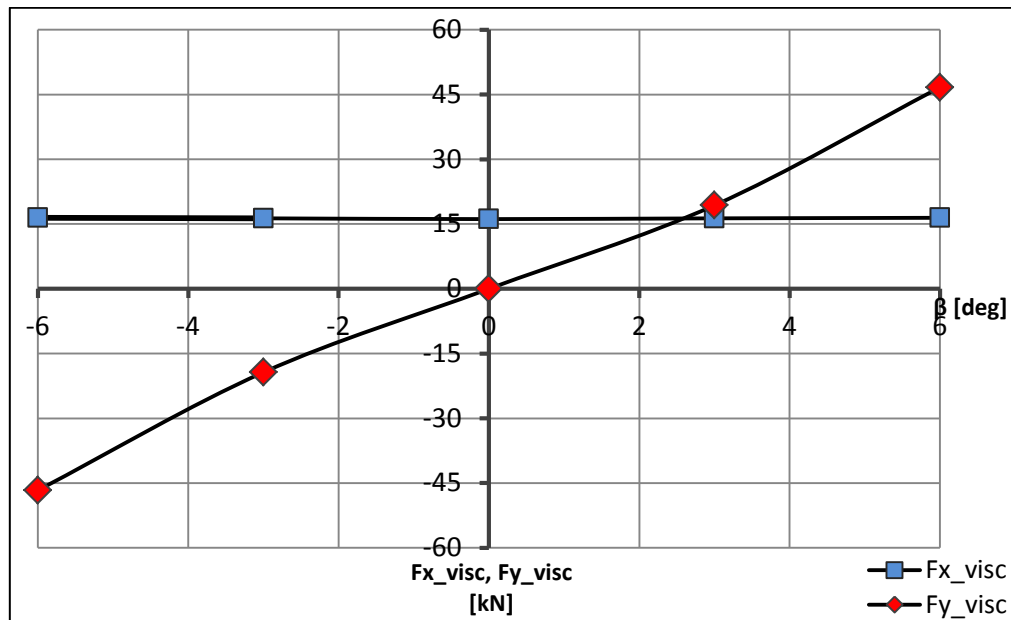
Fig. 43. Viscous components of hydrodynamic forces acting on the hull in different drift conditions

The x-velocity components in the propeller plane for different drift angles are presented on the Fig. 44 – 46, allowing the flow (a)symmetry analysis as well as the influence of the drift angle on the velocity field.
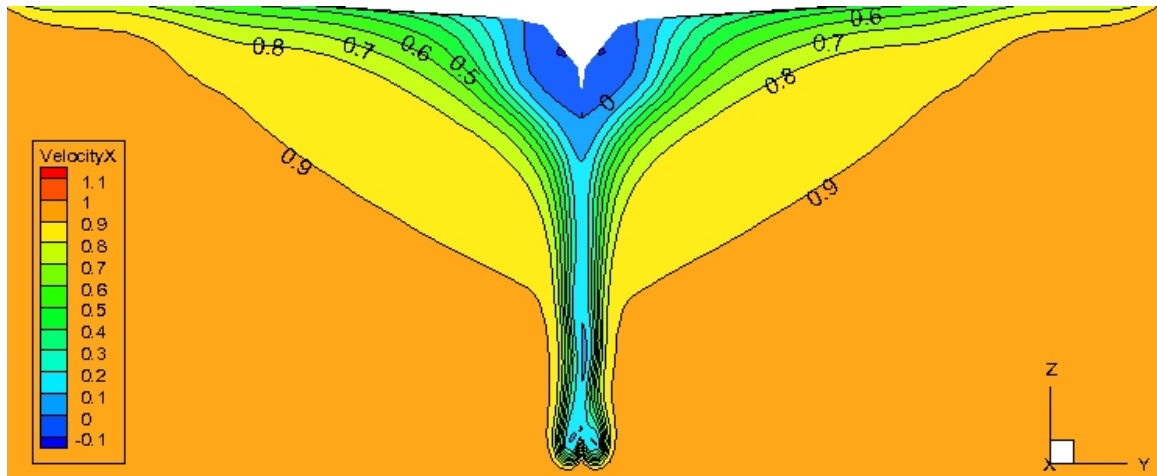
Fig. 44. *X*-velocity component around the hull at 0° drift angle condition
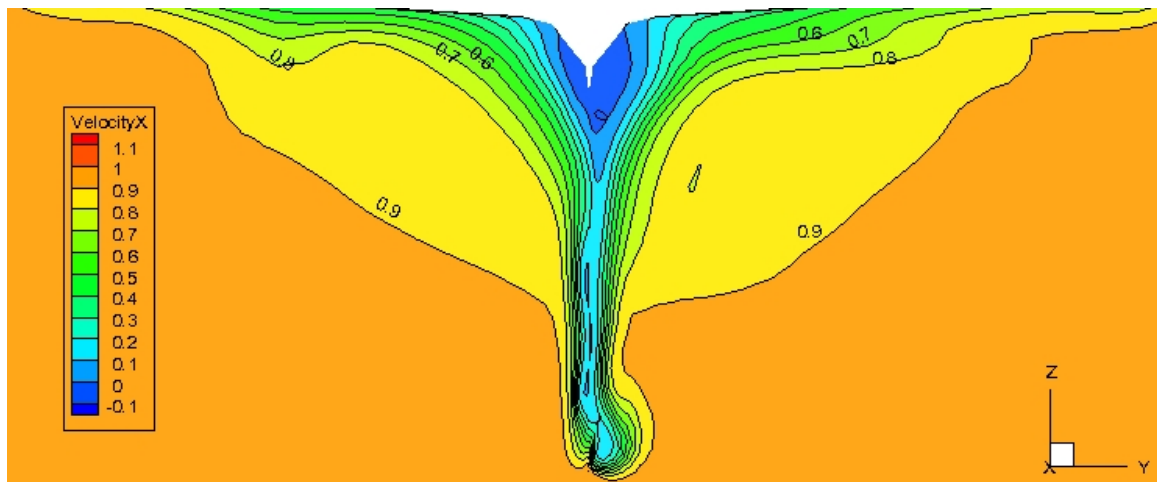
Fig. 45. *X*-velocity component around the hull at 3° drift angle condition
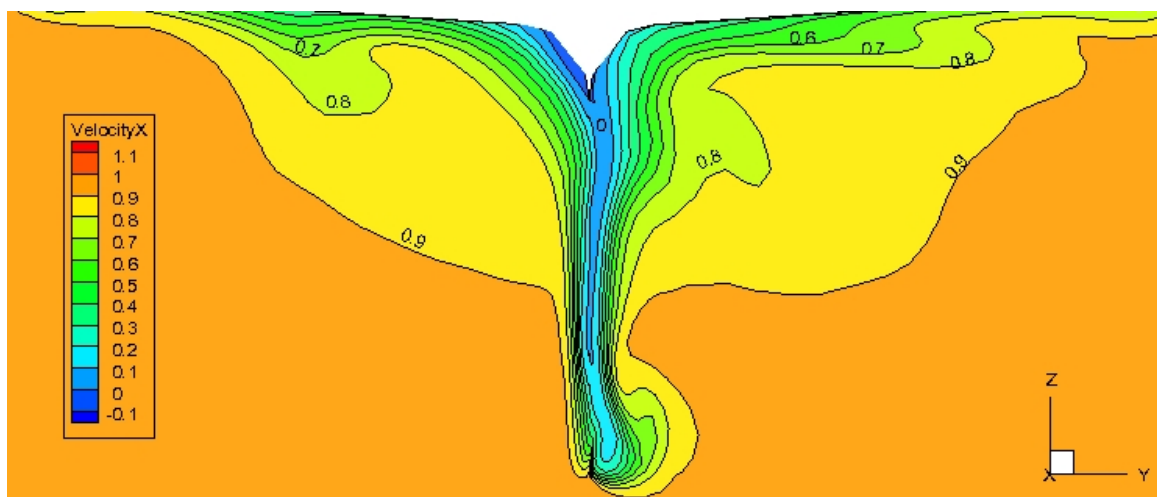
Fig. 46. *X*-velocity component around the hull at 6° drift angle condition

9.3.6. Simulations at Different Drift and Rudder Angles

To obtain a more realistic results, the rudder has been added to the bare hull geometry. Due to the rudder consideration, the number of cells composing the grid increased to 2.4 million.

The following cases [Table 34] have been numerically simulated in order to investigate the flow features around the appended geometry as well as to determine the forces acting on the hull and the rudder itself.

**Table 34. Simulation cases with drift
and rudder angles applied**

RUDDER ANGLE (δ)	DRIFT ANGLE (β)
0 deg.	0 deg.
	3 deg.
	6 deg.
10 deg.	0 deg.
	-3 deg.
	3 deg.
	-6 deg.
	6 deg.
20 deg.	0 deg.
	-3 deg.
	3 deg.
	-6 deg.
	6 deg.
30 deg.	0 deg.
	-3 deg.
	3 deg.
	-6 deg.
	6 deg.

Fig. 47 and 48 present the evolution of the viscous components of hydrodynamic forces acting on the hull. The ship is assumed to travel forward at a constant design speed and to be exposed to flow of water incoming at gradually increasing angles (from -6 deg. to 6 deg.).

Fig. 47. Viscous components of hydrodynamic forces acting on the hull in longitudinal direction
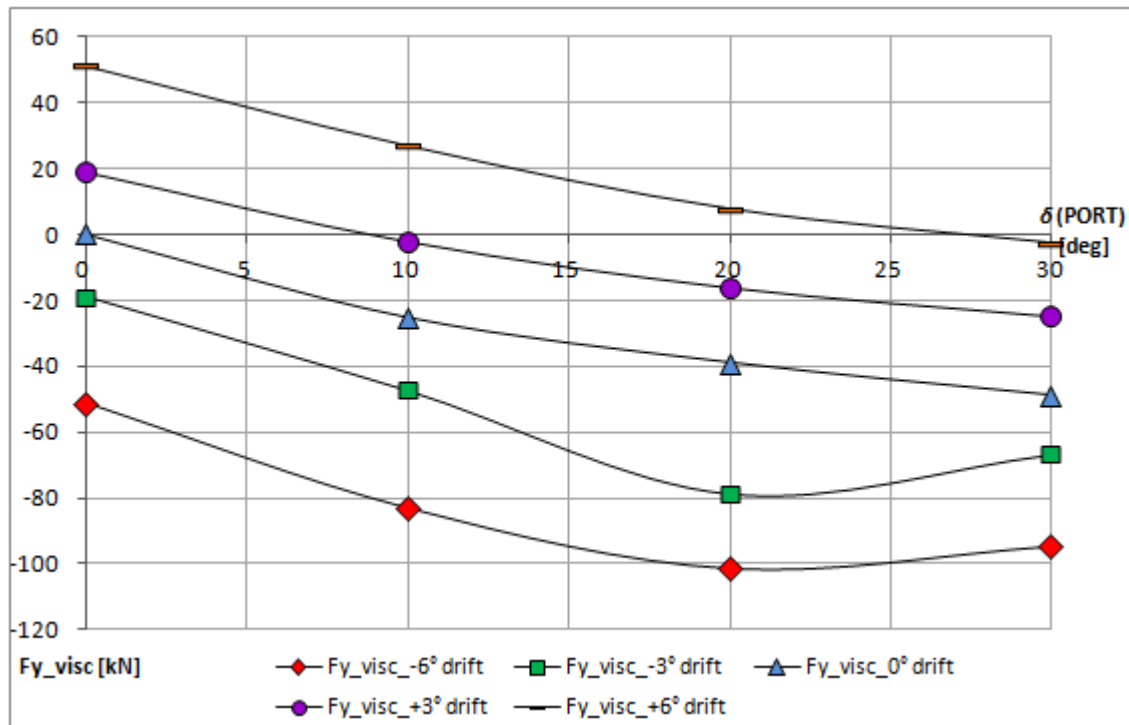
Fig. 48. Viscous components of hydrodynamic forces acting on the hull in lateral direction

The variation of hydrodynamic pressure acting on the rudder in different combinations of drift and deflection angle conditions is shown on the pictures below [Fig. 49 – 60]. The distribution is presented for the leading edge as well as the pressure side of the rudder's geometry.

Additionally, a small "top" rudder can be observed on the graphics. This part has been introduced for the reason of simplification the grid generation of the stern part of the vessel's geometry.
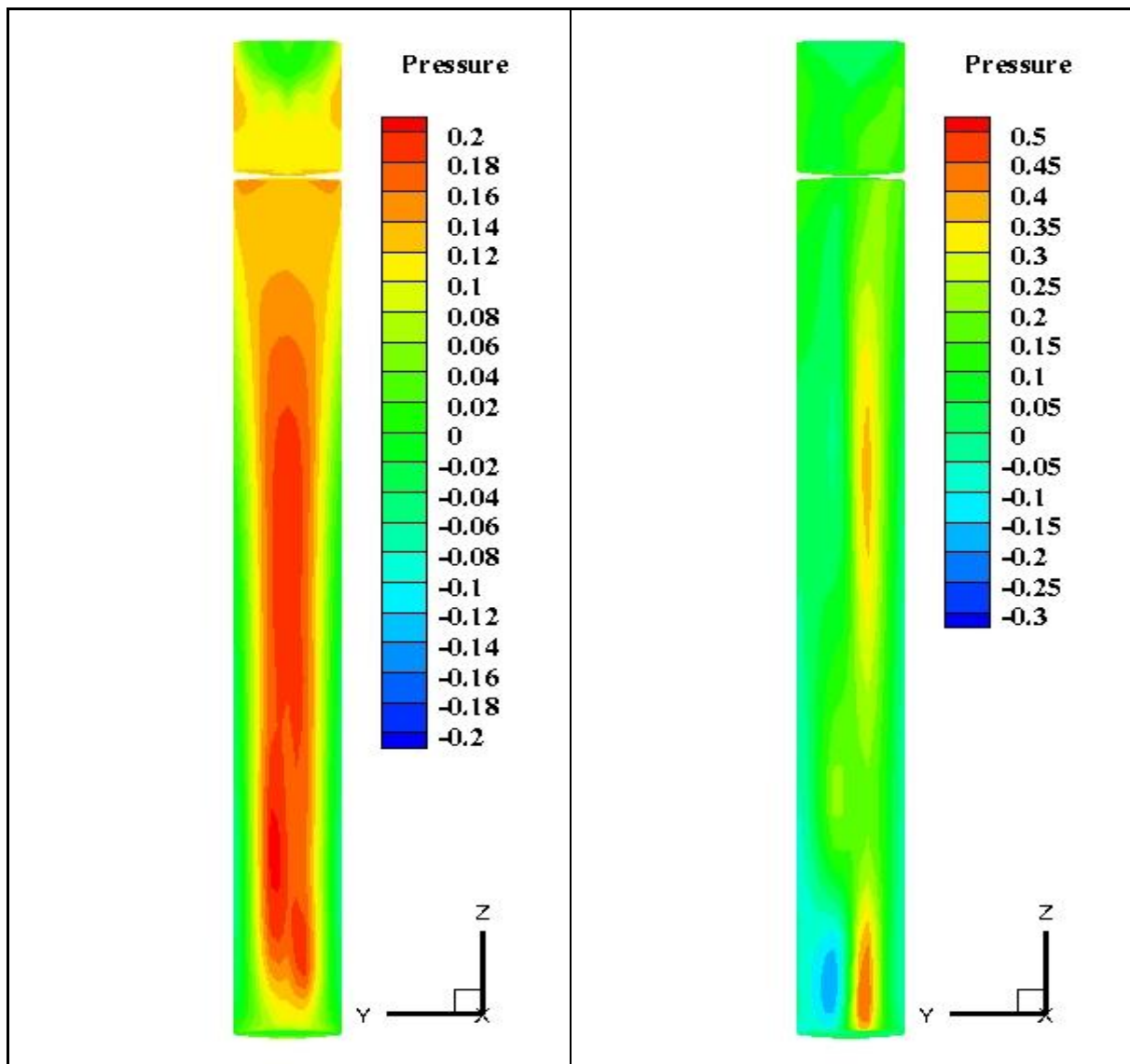
Fig. 49. 0° rudder deflection, 0°drift angle   **Fig. 50. 0° rudder deflection, 3°drift angle**
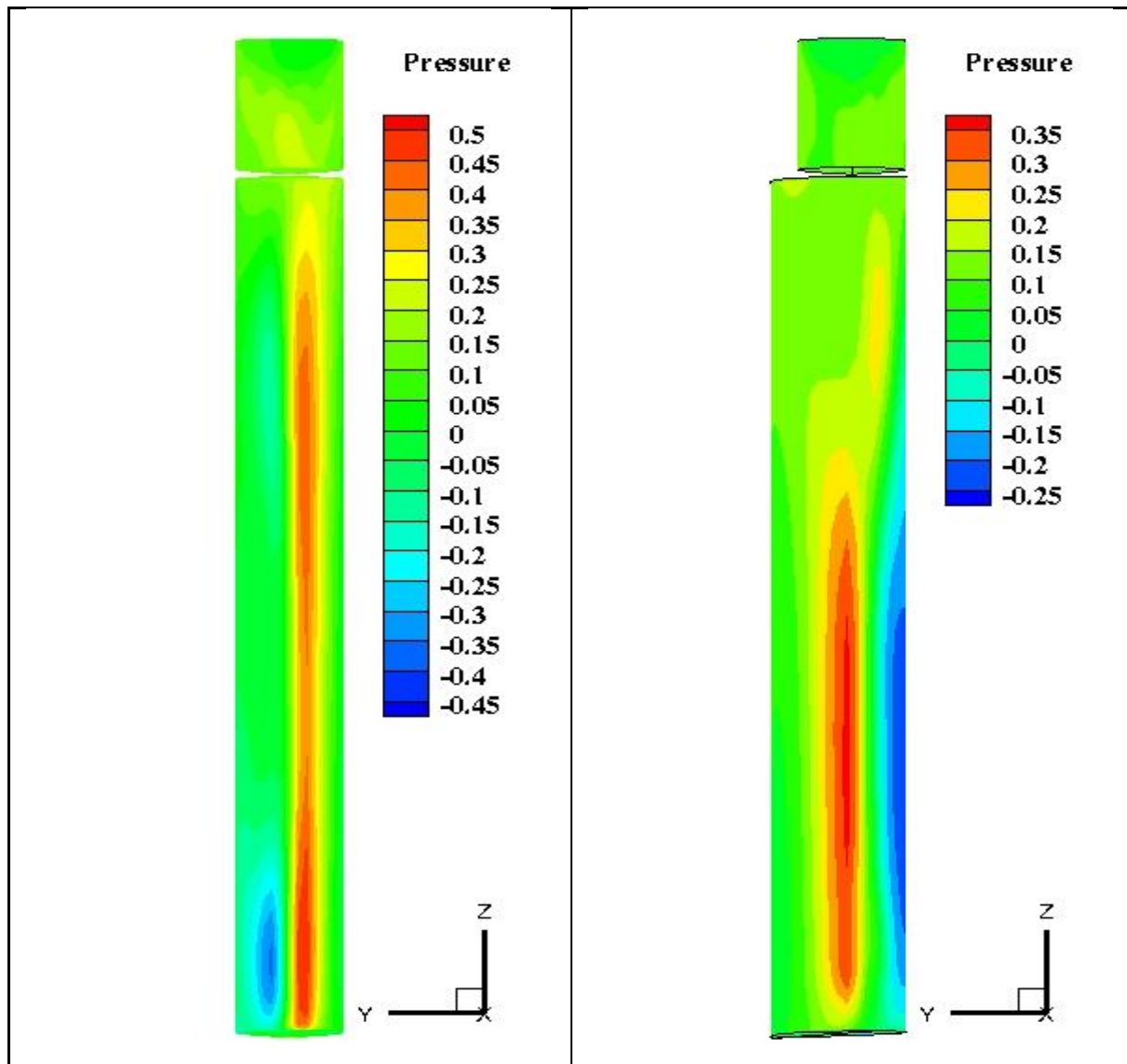
Fig. 51. 0° rudder deflection, 6°drift angle

Fig. 52. 10° rudder deflection, 0°drift angle
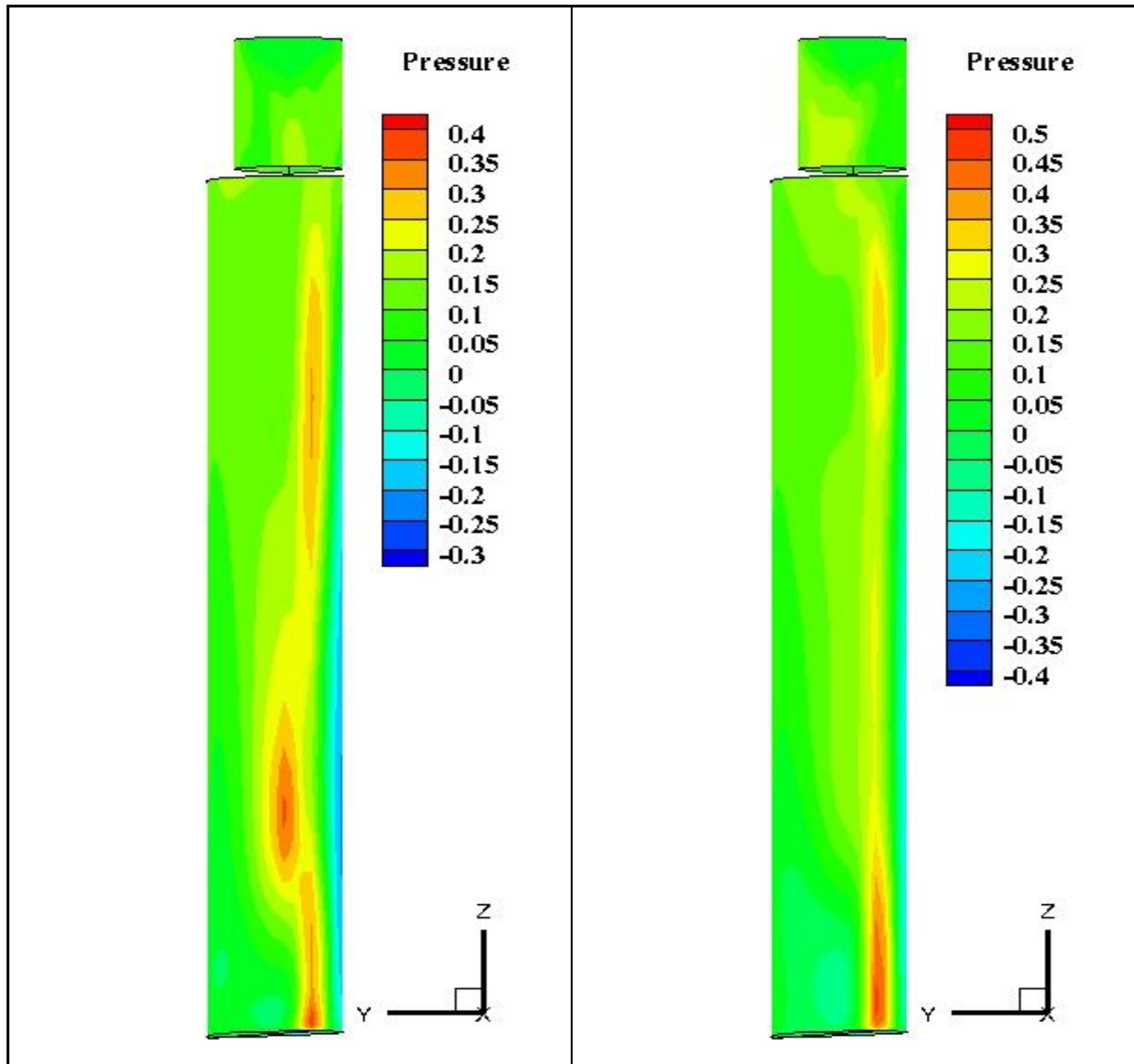
Fig. 53. 10° rudder deflection, 3°drift angle

Fig. 54. 10° rudder deflection, 6°drift angle
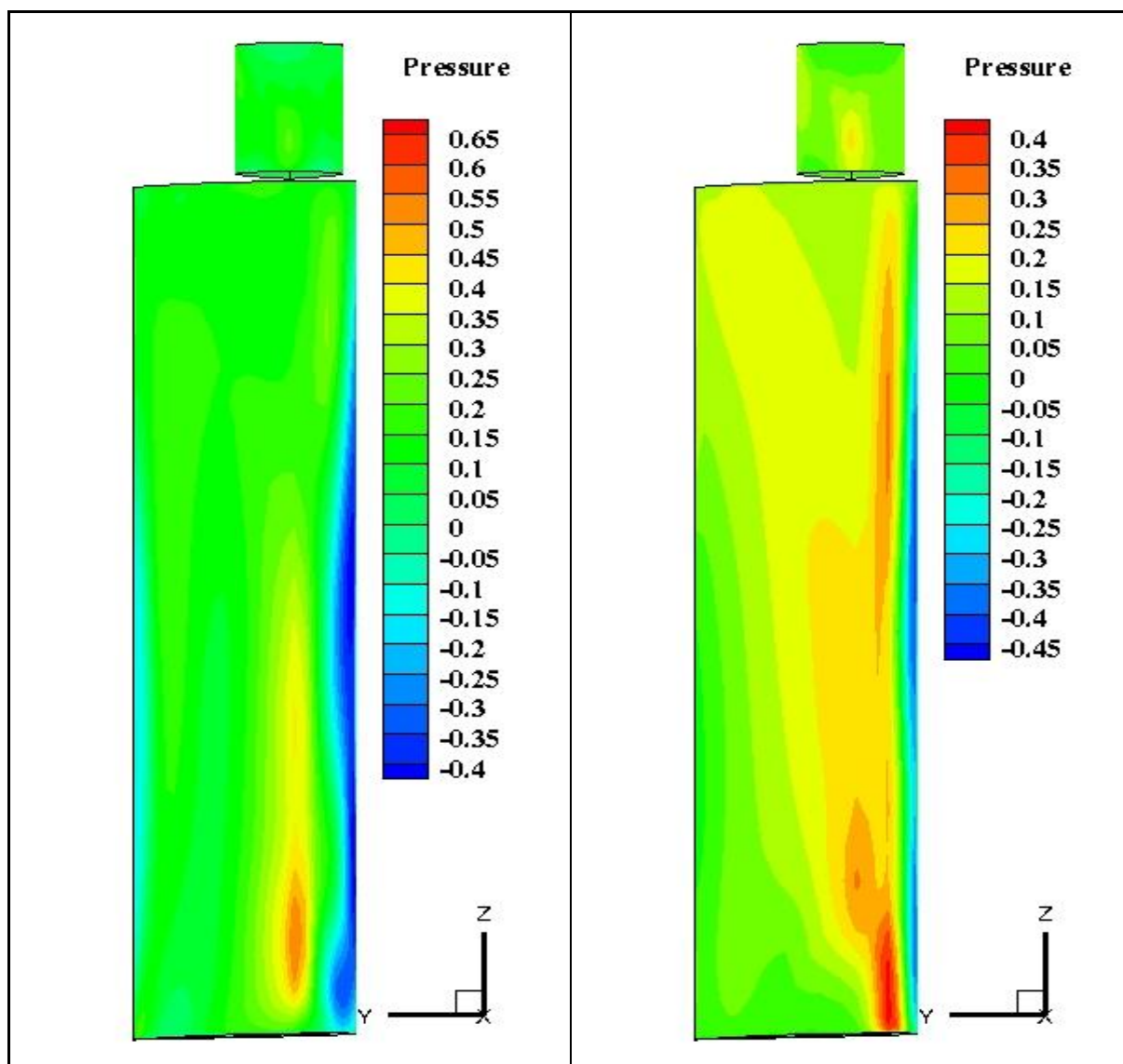
Fig. 55. 20° rudder deflection, 0°drift angle

Fig. 56. 20° rudder deflection, 3°drift angle
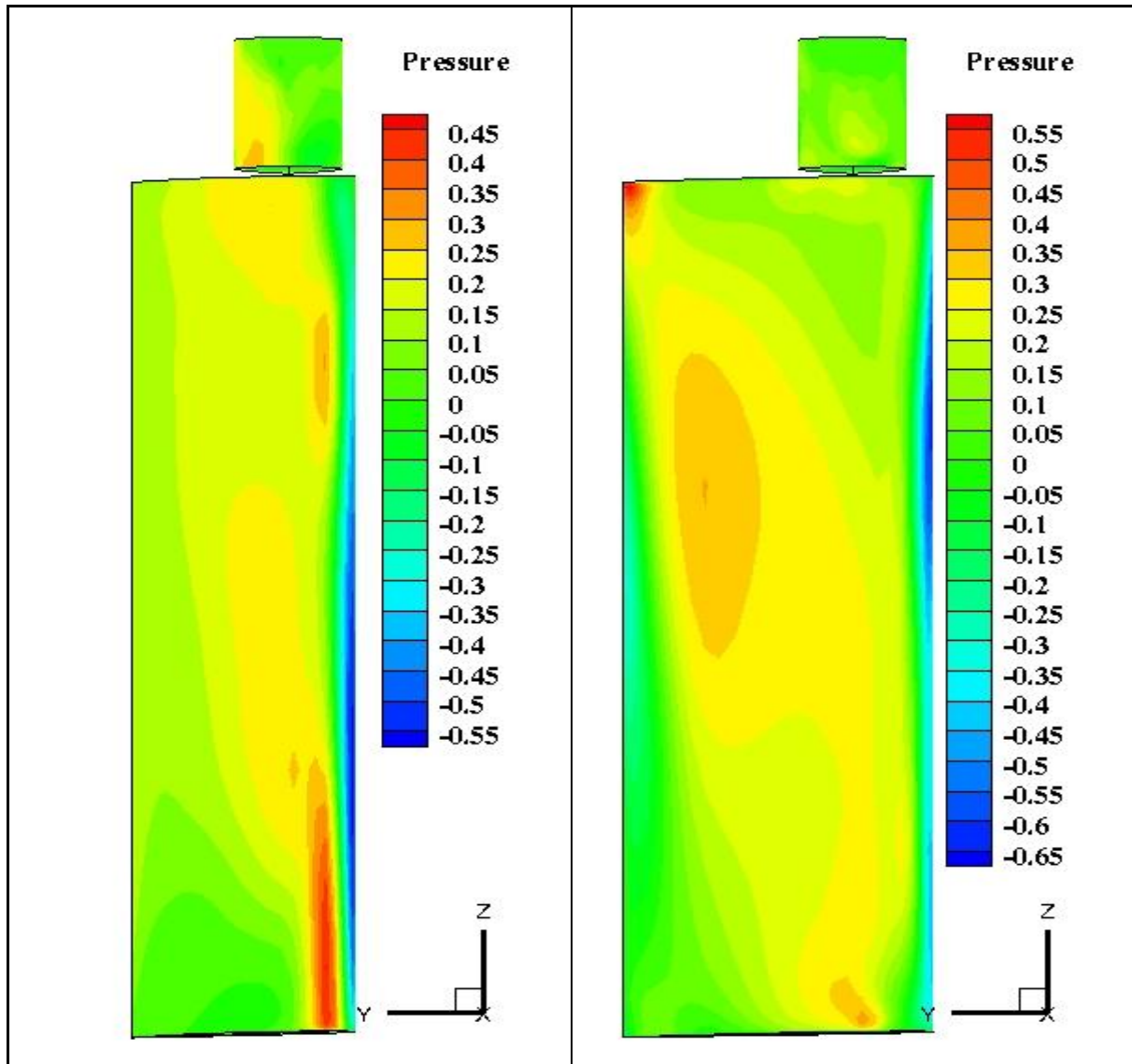
Fig. 57. 20° rudder deflection, 6°drift angle   **Fig. 58. 30° rudder deflection, 0°drift angle**
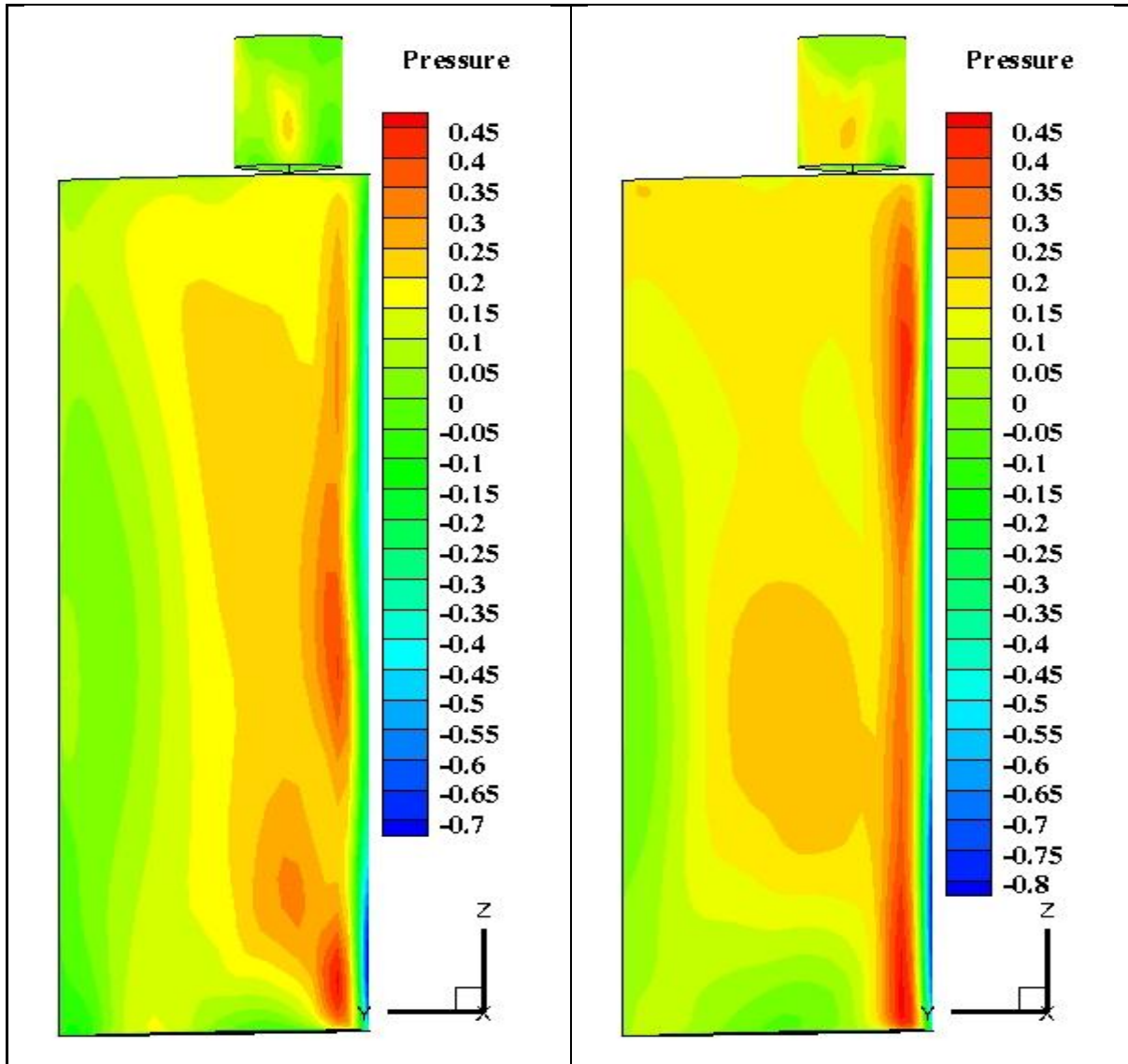
Fig. 59. 30° rudder deflection, 3°drift angle   **Fig. 60. 30° rudder deflection, 6°drift angle**

By integrating the above-presented pressure the hydrodynamic forces acting on the rudder can be computed.

The viscous components of the total hydrodynamic forces, depicted separately for longitudinally- and laterally-acting directions, are presented below [Fig. 61 and 62, respectively].
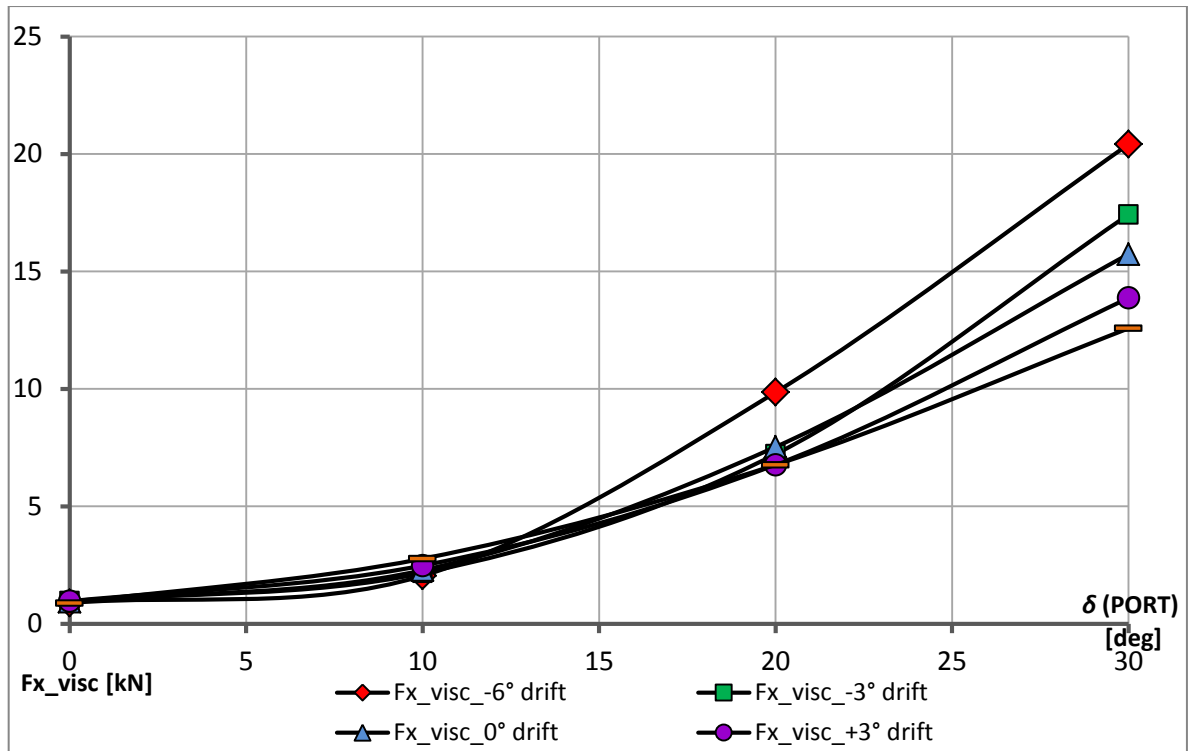
**Fig. 61. Viscous components of hydrodynamic forces acting on the rudder
in longitudinal direction**
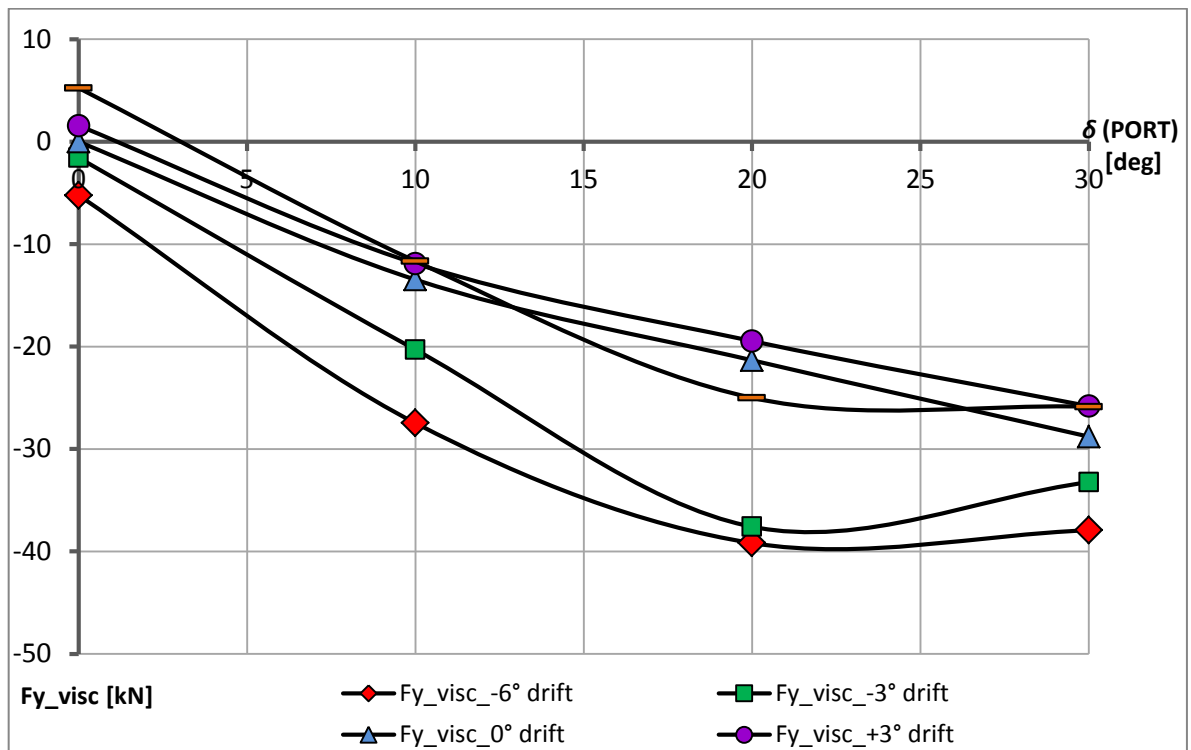
**Fig. 62. Viscous components of hydrodynamic forces acting on the rudder
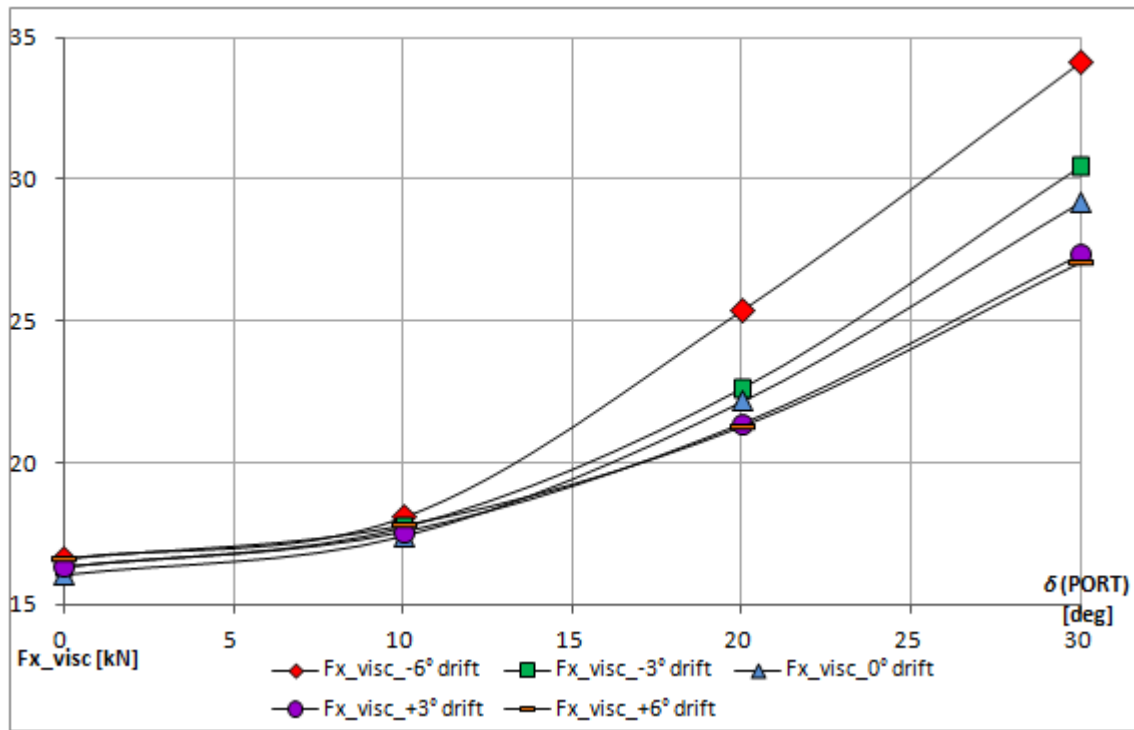in lateral direction**

9.4. Concluding Remarks

Using CFD methods for simulating a 3D viscous flow, it was possible to determine the pressure and velocity field spectra distributed around the bare and appended hull as well as on the rudder itself.

Several flow cases have been analyzed with the ship travelling either on a straight route or with a drift angle applied, varying every 3° from -6° to +6° each board side. To ensure a reliable manoeuvring conditions, the rudder geometry has been introduced into the vessel's offset file, placed either in the centre-line ($\delta = 0°$), or deflected with an angle, δ, varying every 10° from 0° to 30°.

Analyzing the curves depicted on Fig. 47 and Fig. 48 one may easily note that for a rather small drift and rudder deflection angles ($\beta \leq 6°$ and $\delta \leq 10°$) the longitudinal component of the hydrodynamic forces demonstrates a relatively small growing tendency, regardless of the side of both angles applied. On the other hand, the forces applied in the lateral direction show an important growth in their numerical values compared to the straight-course navigation condition. The biggest lateral force is found to be acting at the max. rudder deflection angle applied to the same side of the ship as the drift angle ($\delta = 20 \div 30$ deg., $\beta = -6$ deg.) (*see Fig. 1 for the convention used*).

The hydrodynamic moment on the rudder has been computed for the case of 30 deg. rudder deflection angle at 0 deg. drift condition. The result has been subsequently compared with the value obtained with the PHP program for a comparable condition (*see 5.2.3., Table 6*). A very good agreement between the two values has been found [Table 35], proving the reliability of the computational methods applied.

**Table 35. Hydrodynamic moment acting on the rudder
at max. deflection and no drift angle**

Hydrodynamic moment applied on the rudder [kNm]	
PHP program *($\beta = 35°$, $\delta = 0°$)*	CFD simulation ($\beta = 30°$, $\delta = 0°$)
38.7	38.1

10. FINAL CONCLUSION

The risk of accidents and the possible resulting incidents involving losses of lives, property and pollution of environment can be minimized by ensuring the optimum control of a ship's movement. To do so, the manoeuvring performance of the vessel should first be thoroughly investigated and IMO requirements should be met concerning the parameters of the standard manoeuvring tests.

As described in this thesis, prediction of ship manoeuvrability at the design stages can be carried out by using:

- data bases of manoeuvring qualities,
- results of experimental model tests,
- numerical simulations of manoeuvring motions.

In general, use of data bases cannot be extrapolated to new design concepts and unusual hullforms, such as the one of the investigated fishing vessel. On the other hand, the cost and uncertainty of experimental measurements (especially in the initial design stages) provide strong motivation to utilize numerical investigations, which can be done either by applied mathematical model on the ship's motion in the horizontal plane or by the Computational Fluid Dynamics methods.

Two mathematical models have been presented in this thesis.

The first one, implemented in TRIBON Initial Design software, is based on the differential equations of motions. The program calculates not only the hydrodynamic derivatives of the manoeuvring equation, but also the ship resistance, propeller thrust and torque, and rudder forces and moments. The differential equations of ship motion in the horizontal plane are solved numerically in the time-domain in order to simulate the ship manoeuvring motion for certain rudder movements.

The more complex non-linear mathematical model, based on the non-dimensional hydrodynamic derivates obtained during the experimental campaign, has been applied in a university-developed time-domain simulation code of the standard manoeuvres.

It has been observed, that the initial design softwares (TRIBON, MPP1) can only provide a reliable first estimation of the hydrodynamic performance of the investigated vessel. The significant differences between results obtained with these codes prove them to be relatively inaccurate, especially for the unusual types of hull.

For the prediction of ship manoeuvrabilty with higher accuracy, it could be reasonable to use mathematical models based on the greater number of hydrodynamic derivatives. The results of the 23-based time-domain simulation code has only confirmed this hypothesis. The obtained standard manoeuvres parameters present a satisfactory correlation between numerical and experimental results, which not only proves the simulation code to be reliable and accurate enough to be applied in a detailed design stage of a vessel, but also confirms the manoeuvring prediction dependence not only on the appropriate mathematical model, but also on the preciseness of hydrodynamic data coming from each individual ship. Additionally, since the manoeuvring characteristics of a fishing vessel cannot be found in the open literature, the results obtained by means of the described simulation code can be used as a reference in further investigation of the hydrodynamic performance of this type of ship.

The hydrodynamic forces and moments acting on the bare and appended hull, as well as on the rudder itself, have been obtained throughout an extended numerical analysis consisting of 21 simulation cases. The cases include navigation on a straight route and in oblique flow with various drift and rudder deflection angles applied. The results could serve as a base for further computation of the hydrodynamic derivatives, which might be subsequently used to estimate the standard manoeuvres parameters by means of complex derivatives-based mathematical models as well as numerical techniques.

In general, it has been observed that realistic simulation models and numerical tools, which satisfactorily estimate ship manoeuvres, are commonly accessible for naval architects. However, the research community should continue its efforts to improve the accuracy of the predictive process and to extend this capability to more complicate manoeuvres and, especially, more unusual ship types and control systems [3]. In author's opinion, a closer cooperation between the research centres and Towing Tank Institutes on the development and application of ship manoeuvring computer simulations would be highly recommended.

Further research should also be performed in developing the appropriate methods or algorithms allowing to convert the results from one water depth to other (especially deep to shallow water) with adequate accuracy.

REFERENCES

Books:

1. Barnaby, N., *On the Steering of Ships*, Transactions of the Royal Institution of Naval Architects*,* Vol. 4, 1863.

2. Bertram, V., *Practical Ship Hydrodynamics*, Butterworth-Heinemann, Oxford, U.K., 2000.

3. Brix, J., *Manoeuvring Technical Manual*, Seehafen Verlag, Hamburg, 1993.

4. Lewis E.V., *Principles of Naval Architecture, Second Revision, Vol. III*, SNAME, Jersey City, NJ, USA, 1989.

5. Mandel, P. "*Ship Maneuvering and Control*" in *Principles of Naval Architecture*, J.P. Comstock, Ed., SNAME, USA, 1977.

6. Molland A.F., Turnock S.R., *Marine Rudders and Control Surfaces*, Elsevier, Oxford, U.K., 2007.

7. Obreja D., Crudu L., Pacuraru S., *Manevrabilitatea Navei*, Galati University Press, 2008

8. Rawson K.J., Tupper E.C., *Basic Ship Theory, Vol. 2*, Butterworth-Heinemann, Oxford, U.K. 2001.

9. Triantafyllou, M.S., Hover, F.S., *Maneuvering and Control of Marine Vehicles*, Department of Ocean Engineering, Massachusetts Institute of Technology Cambridge, Massachusetts, USA, 2002.

10. Tupper, E., *Introduction to Naval Architecture*, Butterworth-Heinemann, Oxford, U.K. 1996.

Articles and Reports:

11. Chau S.-W. et al, *Investigation of hydrodynamic performance of high-speed craft rudders via turbulent flow computations, Part I: Non–cavitating characteristics*, Journal of Marine Science and Technology, Vol. 13, No. 1, 2005.

12. Hasegawa H., Amin O. Md., *Assessment of Ship Manoeuvrability in Shallow Waters*, The International Conference on Marine Technology, Dhaka, Bangladesh, 2010.

13. Holtrop, J., Menner, G.G.J., *An approximate power prediction method*, International Shipbuilding Progress, 1982.

14. *ITTC Report on Manoeuvrability Prediction*, Workshop on Mathematical Models for Operations Involving Ship-Ship Interaction, August 2005, Tokyo, Japan.

15. Jones D.A., Clarke D.B., Brayshaw I.B., Barillon J.L., Anderson B., *The Calculation of Hydrodynamic Coefficients for Underwater Vehicles*, DSTO Platforms Sciences Laboratory, Australia, 2002.

16. Lungu, A., Pacuraru F., *Numerical Study of the Hull-Propeller-Rudder Interaction,* International Conference on Numerical Analysis and Applied Mathematics, Vol. 2, 2009.

17. Obreja D. et al, *Identification of hydrodynamic coefficients for manoeuvring simulation model of a fishing vessel*, Ocean Engineering 37, 2010.

18. Pacuraru F. et al, *Numerical Simulation of the Flow around a Steerable Propulsion Unit*, 25th IAHR Symposium on Hydraulic Machinery and System, Timisoara, Romania, 2010.

19. Strom-Tejsen, J., *A Digital Computer Technique for Prediction of Standard Maneuvers of Surface Ship, Research and Development Report*, David Taylor Model Basin, Washington, 1965.

Internet Documents:

20. *ABS Guide for Vessel Maneuverability*, Houston, TX, 2006.

21. *BV Rules for the Classification of Steel Ships*, Part B, Paris, 2005.

22. IMO Resolution MSC 137(76), *Standards for Ship Manoeuvrability,* 2002.

APPENDIX 1

The SR and SV series of steering gear

The SR series is suitable for small to medium-sized vessels. The steering gear is designed with integrated frequency controlled pumps.

The pump utilises a reversible hydraulic pump motor together with a frequency converter for changing the speed and the direction of the pump. The design gives smooth starting and stopping of the steering gear, and enables a precise analogue control system. The pump engines are mounted directly on the rudder actuator, which lessens the need for piping work on board a vessel.

Steering gear

Typical applications:

Suitable for vessels such as:
- Work boats
- Fishing vessels
- Offshore supply vessels
- Smaller cargo vessels
- Smaller passenger vessels
- Yachts

Unique technical solutions minimize noise and vibration levels.

The pump engines are mounted directly on the rudder actuator.

Benefits of the SR series
- Low noise level
- Low power consumption
- Low heat generation
- Excellent positioning precision

Red indicates pressurised oil. Green indicates excess oil.

The compact and simple design lessens the weight and is quick and easy to install.

TYPE	Max. stock dia. (mm)	Max. working torque (kNm)	Max. rudder angle	Weight approx. kg	Max. radial load (kN)	Max. axial load (kN)
SR 562L-FCP	140	16	2 x 61.0	400	175	104
SR 562-FCP	160	40	2 x 61.0	400	175	104
SR 622-FCP	200	70	2 x 72.0	620	400	200
SR 642-FCP	240	110	2 x 72.0	920	600	250
SR 662-FCP	280	170	2 x 72.0	1800	700	354
SR 722-FCP	340	275	2 x 74.0	2750	855	370
SR 723-FCP	340	412	2 x 44.0	2800	855	370
SV 430-2-FCP	340	430	2 x 72º	3430	1400	500
SV 650-3-FCP	360	650	2 x 46º	3430	1400	500

5

APPENDIX 2

TURNING CIRCLE MANOEUVER

STABILITY CRITERION C= .0001755458
SLOPE [(deg/sec)/deg]=   -.33513

TURNING CIRCLE PARAMETERS
```
rudder angle [deg]................        5.0
advance  -90 deg- [m]..........      260.6
transfer -90 deg- [m]...........     -207.6
max advance [m].................     260.7
tactical diameter [m]..........      425.4
time for change  90 deg [sec]...    61.2
time for change 180 deg [sec]...   115.6
max transfer [m]................     -425.4
steady turning radius [m].......     213.0
steady drift angle [deg]........      -1.4
final speed [kn]................      11.95
```

TURNING CIRCLE PARAMETERS
```
rudder angle [deg].............       -5.0
advance  -90 deg- [m]..........      260.6
 transfer -90 deg- [m]..........     207.6
max advance [m].................     260.7
tactical diameter [m]...........     425.4
time for change  90 deg [sec]...    61.2
time for change 180 deg [sec]...   115.6
 max transfer [m]................     425.4
steady turning radius [m].......     213.0
steady drift angle [deg]........       1.4
final speed [kn]................      11.95
```

TURNING CIRCLE PARAMETERS
```
rudder angle [deg].............       10.0
advance  -90 deg- [m]..........      157.8
 transfer -90 deg- [m]...........    -103.4
max advance [m].................     157.9
tactical diameter [m]..........      217.1
time for change  90 deg [sec]...    34.8
time for change 180 deg [sec]...    62.9
max transfer [m]................     -217.2
 steady turning radius [m].......    109.1
 steady drift angle [deg]........     -2.7
 final speed [kn]................     11.85
```

TURNING CIRCLE PARAMETERS
```
rudder angle [deg].............      -10.0
advance  -90 deg- [m]..........      157.8
transfer -90 deg- [m]...........     103.4
max advance [m].................     157.9
tactical diameter [m]..........      217.1
time for change  90 deg [sec]...    34.8
time for change 180 deg [sec]...    62.9
max transfer [m]................     217.2
steady turning radius [m].......     109.1
steady drift angle [deg]........       2.7
final speed [kn]................      11.85
```

TURNING CIRCLE PARAMETERS
```
rudder angle [deg].............       15.0
advance  -90 deg- [m]..........      124.5
transfer -90 deg- [m]...........     -70.5
max advance [m].................     124.6
tactical diameter [m]..........      149.5
time for change  90 deg [sec]...    26.3
time for change 180 deg [sec]...    45.7
max transfer [m]................     -149.6
steady turning radius [m].......     75.4
steady drift angle [deg]........      -3.9
final speed [kn]................      11.74
```

TURNING CIRCLE PARAMETERS
```
rudder angle [deg].............      -15.0
advance  -90 deg- [m]..........      124.5
transfer -90 deg- [m]...........     70.5
max advance [m].................     124.6
tactical diameter [m]..........      149.5
time for change  90 deg [sec]...    26.3
time for change 180 deg [sec]...    45.7
max transfer [m]................     149.6
steady turning radius [m].......     75.4
steady drift angle [deg]........       3.9
final speed [kn]................      11.74
```

TURNING CIRCLE PARAMETERS
rudder angle [deg].............   20.0
advance -90 deg- [m]..........   107.8
transfer -90 deg- [m]...........   -55.1
max advance [m].................   108.0
tactical diameter [m]...........   116.7
time for change 90 deg [sec]...   22.2
time for change 180 deg [sec]...   37.2
max transfer [m]................   -116.9
steady turning radius [m].......   58.7
steady drift angle [deg]........   -5.0
final speed [kn]................   11.62

TURNING CIRCLE PARAMETERS
rudder angle [deg].............   30.0
advance -90 deg- [m]..........   90.8
transfer -90 deg- [m]...........   -39.5
max advance [m].................   91.1
tactical diameter [m]...........   84.9
time for change 90 deg [sec]...   18.1
time for change 180 deg [sec]...   29.0
max transfer [m]................   -85.2
steady turning radius [m].......   42.5
steady drift angle [deg]........   -7.1
final speed [kn]................   9.32

TURNING CIRCLE PARAMETERS
rudder angle [deg].............   -20.0
advance -90 deg- [m]..........   107.8
transfer -90 deg- [m]...........   55.1
max advance [m].................   108.0
tactical diameter [m]...........   116.7
time for change 90 deg [sec]...   22.2
time for change 180 deg [sec]...   37.2
max transfer [m]................   116.9
steady turning radius [m].......   58.7
steady drift angle [deg].......   5.0
final speed [kn]................   11.62

TURNING CIRCLE PARAMETERS
rudder angle [deg].............   -30.0
advance -90 deg- [m]..........   90.8
transfer -90 deg- [m]...........   39.5
max advance [m].................   91.1
tactical diameter [m]...........   84.9
time for change 90 deg [sec]...   18.1
time for change 180 deg [sec]...   29.0
max transfer [m]................   85.2
steady turning radius [m].......   42.5
steady drift angle [deg]........   7.1
final speed [kn]................   9.32

TURNING CIRCLE PARAMETERS
rudder angle [deg].............   25.0
advance -90 deg- [m]..........   97.7
transfer -90 deg- [m]...........   -46.2
max advance [m].................   97.9
tactical diameter [m]...........   97.6
time for change 90 deg [sec]...   19.8
time for change 180 deg [sec]...   32.3
max transfer [m]................   -97.8
steady turning radius [m].......   48.9
steady drift angle [deg]........   -6.1
final speed [kn]................   10.99

TURNING CIRCLE PARAMETERS
rudder angle [deg].............   35.0
advance -90 deg- [m]..........   85.9
transfer -90 deg- [m]...........   -34.8
max advance [m].................   86.2
tactical diameter [m]...........   75.9
time for change 90 deg [sec]...   16.9
time for change 180 deg [sec]...   26.8
max transfer [m]................   -76.1
steady turning radius [m].......   37.7
steady drift angle [deg]........   -8.1
final speed [kn]................   7.09

TURNING CIRCLE PARAMETERS
rudder angle [deg].............   -25.0
advance -90 deg- [m]..........   97.7
transfer -90 deg- [m]...........   46.2
max advance [m].................   97.9
tactical diameter [m]...........   97.6
time for change 90 deg [sec]...   19.8
time for change 180 deg [sec]...   32.3
max transfer [m]................   97.8
steady turning radius [m].......   48.9
steady drift angle [deg]........   6.1
final speed [kn]................   10.99

TURNING CIRCLE PARAMETERS
rudder angle [deg].............   -35.0
advance -90 deg- [m]..........   85.9
transfer -90 deg- [m]...........   34.8
max advance [m].................   86.2
tactical diameter [m]...........   75.9
time for change 90 deg [sec]...   16.9
time for change 180 deg [sec]...   26.8
max transfer [m]................   76.1
steady turning radius [m].......   37.7
steady drift angle [deg]........   8.1
final speed [kn]................   7.09

10°/10° ZIG-ZAG MANOEUVER

TIME	RUDDER ANGLE	ADVANCE	TRANSFER	SPEED	HEADING ANGLE	OMEG	DRIFT
[SEC]	[DEG]	[M]	[M]	[KNOTS]	[DEG]	[DEG/SEC]	[DEG]
.0	.0	.0	.0	12.00	.0	.000	.0
1.0	-10.0	6.2	.0	12.00	.0	.0	.3
2.0	-10.0	12.3	-.1	11.99	.2	.286	.7
3.0	-10.0	18.5	-.1	11.99	.6	.517	1.1
4.0	-10.0	24.7	-.1	11.99	1.3	.775	1.4
5.0	-10.0	30.8	-.1	11.99	2.2	1.048	1.7
6.0	-10.0	37.0	.0	11.99	3.4	1.324	2.0
7.0	-10.0	43.2	.2	11.98	4.9	1.595	2.2
8.0	-10.0	49.3	.6	11.98	6.6	1.854	2.4
9.0	-10.0	55.5	1.2	11.98	8.6	2.096	2.6
10.0	-5.5	61.6	1.9	11.98	10.8	2.306	2.6
11.0	9.5	67.7	3.0	11.97	13.2	2.320	2.2
12.0	10.0	73.7	4.3	11.96	15.4	2.128	1.5
13.0	10.0	79.6	5.9	11.96	17.4	1.829	.8
14.0	10.0	85.4	7.8	11.95	19.0	1.454	.1
15.0	10.0	91.2	9.9	11.95	20.2	1.031	-.4
16.0	10.0	97.0	12.2	11.95	21.0	.580	-.9
17.0	10.0	102.6	14.5	11.95	21.3	.120	-1.4
18.0	10.0	108.3	16.9	11.94	21.2	-.335	-1.8
19.0	10.0	114.0	19.3	11.94	20.6	-.773	-2.1
20.0	10.0	119.6	21.6	11.94	19.6	-1.186	-2.4
21.0	10.0	125.4	23.9	11.94	18.2	-1.567	-2.6
22.0	10.0	131.1	26.0	11.94	16.5	-1.912	-2.8
23.0	10.0	137.0	27.9	11.94	14.4	-2.218	-2.9
24.0	10.0	142.9	29.6	11.94	12.0	-2.485	-3.0
25.0	10.0	148.8	31.1	11.94	9.4	-2.713	-3.1
26.0	10.0	154.9	32.2	11.93	6.6	-2.905	-3.1
27.0	10.0	160.9	33.1	11.93	3.6	-3.062	-3.1
28.0	10.0	167.0	33.6	11.93	.5	-3.188	-3.1
29.0	10.0	173.2	33.8	11.93	-2.8	-3.286	-3.1
30.0	10.0	179.3	33.7	11.92	-6.1	-3.359	-3.1
31.0	10.0	185.4	33.1	11.92	-9.5	-3.411	-3.1
32.0	-2.0	191.5	32.2	11.92	-12.9	-3.373	-2.8
33.0	-10.0	197.5	30.9	11.91	-16.1	-3.101	-2.0
34.0	-10.0	203.4	29.2	11.90	-19.0	-2.702	-1.2
35.0	-10.0	209.1	27.2	11.89	-21.5	-2.228	-.5
36.0	-10.0	214.8	24.8	11.89	-23.4	-1.707	.2
37.0	-10.0	220.3	22.3	11.89	-24.8	-1.163	.8
38.0	-10.0	225.8	19.5	11.89	-25.7	-.615	1.3
39.0	-10.0	231.2	16.7	11.89	-26.0	-.078	1.7
40.0	-10.0	236.6	13.9	11.89	-25.8	.435	2.1
41.0	-10.0	242.0	11.0	11.89	-25.1	.916	2.4
42.0	-10.0	247.5	8.2	11.89	-23.9	1.357	2.7
43.0	-10.0	253.0	5.6	11.89	-22.4	1.754	2.9
44.0	-10.0	258.6	3.0	11.89	-20.4	2.105	3.0
45.0	-10.0	264.2	.7	11.89	-18.1	2.410	3.1
46.0	-10.0	270.0	-1.4	11.89	-15.6	2.669	3.2
47.0	-10.0	275.8	-3.2	11.88	-12.8	2.886	3.2
48.0	-10.0	281.7	-4.7	11.88	-9.8	3.063	3.2
49.0	-10.0	287.7	-5.9	11.88	-6.7	3.203	3.2
50.0	-10.0	293.8	-6.8	11.88	-3.4	3.311	3.2
51.0	-10.0	299.9	-7.3	11.88	.0	3.391	3.2

SPIRAL MANOEUVER

RUDDER ANGLE [DEG]	RATE OF HEADING [DEG/SEC]	TIME OF STEADY [SEC]	SPEED [KNOTS]	DRIFT ANGLE [DEG]	TURNING RADIUS [M]
25.0	-6.621	72.6	10.99	-6.1	48.9
20.0	-5.422	18.6	10.91	-4.9	59.3
15.0	-4.224	18.9	10.93	-3.8	76.3
10.0	-2.920	19.9	11.03	-2.6	111.3
9.0	-2.731	10.8	11.08	-2.4	119.6
8.0	-2.453	13.4	11.16	-2.1	134.1
7.0	-2.173	13.5	11.23	-1.9	152.4
6.0	-1.886	13.7	11.31	-1.6	176.7
5.0	-1.591	13.9	11.38	-1.3	210.9
4.0	-1.288	14.1	11.45	-1.1	262.2
3.0	-.977	14.3	11.52	-.8	347.4
2.0	-.662	14.4	11.58	-.5	515.9
1.0	-.341	14.5	11.64	-.2	1007.1
.0	-.015	14.6	11.69	.0	22512.4
-1.0	.312	14.6	11.74	.3	1108.3
-2.0	.641	14.6	11.77	.6	541.1
-3.0	.970	14.5	11.80	.9	358.7
-4.0	1.298	14.4	11.83	1.1	268.6
-5.0	1.623	14.3	11.84	1.4	215.0
-6.0	1.945	14.2	11.85	1.7	179.5
-7.0	2.262	14.0	11.85	1.9	154.4
-8.0	2.573	13.8	11.85	2.2	135.7
-9.0	2.878	13.6	11.84	2.5	121.2
-10.0	3.176	13.3	11.82	2.7	109.7
-15.0	4.652	18.4	11.74	4.0	74.4
-20.0	5.865	16.6	11.60	5.2	58.3
-25.0	6.620	49.6	10.99	6.1	48.9
-20.0	5.422	18.6	10.91	4.9	59.3
-15.0	4.224	18.9	10.93	3.8	76.3
-10.0	2.920	19.9	11.03	2.6	111.3
-9.0	2.731	10.8	11.08	2.4	119.6
-8.0	2.453	13.4	11.16	2.1	134.1
-7.0	2.173	13.5	11.23	1.9	152.4
-6.0	1.886	13.7	11.31	1.6	176.7
-5.0	1.591	13.9	11.38	1.3	210.9
-4.0	1.288	14.1	11.45	1.1	262.2
-3.0	.977	14.3	11.52	.8	347.4
-2.0	.662	14.4	11.58	.5	515.9
-1.0	.341	14.5	11.64	.2	1007.1
.0	.015	14.6	11.69	.0	22513.6
1.0	-.312	14.6	11.74	-.3	1108.3
2.0	-.641	14.6	11.77	-.6	541.1
3.0	-.970	14.5	11.80	-.9	358.7
4.0	-1.298	14.4	11.83	-1.1	268.6
5.0	-1.623	14.3	11.84	-1.4	215.0
6.0	-1.945	14.2	11.85	-1.7	179.5
7.0	-2.262	14.0	11.85	-1.9	154.4
8.0	-2.573	13.8	11.85	-2.2	135.7
9.0	-2.878	13.6	11.84	-2.5	121.2
10.0	-3.176	13.3	11.82	-2.7	109.7
15.0	-4.652	18.4	11.74	-4.0	74.4
20.0	-5.865	16.6	11.60	-5.2	58.3
25.0	-6.620	49.6	10.99	-6.1	48.9